GENERAL CIRCULATION OF THE E-REGION

by

Leonard S. Fedor

B.S., San Diego State College
(1961)

SUBMITTED IN PARTIAL FULFILLMENT
OF THE REQUIREMENTS FOR THE
DEGREE OF MASTER OF
SCIENCE
at the
MASSACHUSETTS INSTITUTE OF
TECHNOLOGY
September, 1964

Signature of Author .....
Department of Meteorology, August 24, 1964

Certified by .....
Thesis Supervisor

Accepted by .....
Chairman, Departmental Committee
on Graduate Students

GENERAL CIRCULATION OF THE E-REGION

by

Leonard S. Fedor

Submitted to the Department of Meteorology on August 24, 1964 in partial fulfillment of the requirement for the degree of Master of Science.

ABSTRACT

Ionospheric sounders may be used to determine the motions in the upper atmosphere by monitoring the reflected waves at three spaced receivers. The correlation method of determining the motions in the ionosphere is presented in detail. The data from fifteen sounders is used to formulate a preliminary picture of the atmospheric general circulation in the region from 95 km to 115 km.

The diurnal variations of the wind at selected stations are shown for various seasons. The data is arranged according to distribution for each hour and a mean value is given for each hour.

Height profiles of the zonal wind showing the seasonal variation are given at four-hour intervals. A height profile of the prevailing component of the zonal wind is determined from two sets of profiles. The height profile of the tidal variations is also shown. Zonal and meridional prevailing winds are shown in hemispheric maps for both summer and winter.

Thesis Supervisor: Reginald E. Newell

Title: Assistant Professor of Meteorology

TABLE OF CONTENTS

LIST OF ILLUSTRATIONS

LIST OF TABLES

CHAPTER I. INTRODUCTION

A. General Circulation

Initial studies of the general circulation of the atmosphere have been concerned with the troposphere, where the weather systems form. As data became available the studies were extended to include the stratosphere. It is natural to continue the general circulation investigations into the upper atmosphere. Physicists have been determining the motions in the ionosphere for many years at various stations. It is the purpose of this thesis to use the more recent data to obtain a picture of the circulation in the region from 95 km to 115 km.

A survey article by Murgatroyd (1957) proposed a model for the zonal motions in the upper atmosphere (up to 100 km) using measurements made by a variety of methods. For the high altitudes these methods include the use of noctilucent clouds, ionized meteor trails, ejection of sodium from rockets, radio propagation, and others. The results of Murgatroyd's study are given in Figure 1. Above 80 km the results were obtained from the data of nine stations and include data from both hemispheres. Kochanski (1963) proposed models of the general circulation at 80 km and 100 km based mainly on the meteor trail measurements at Jodrell Bank and Adelaide. Such a model necessarily suffers

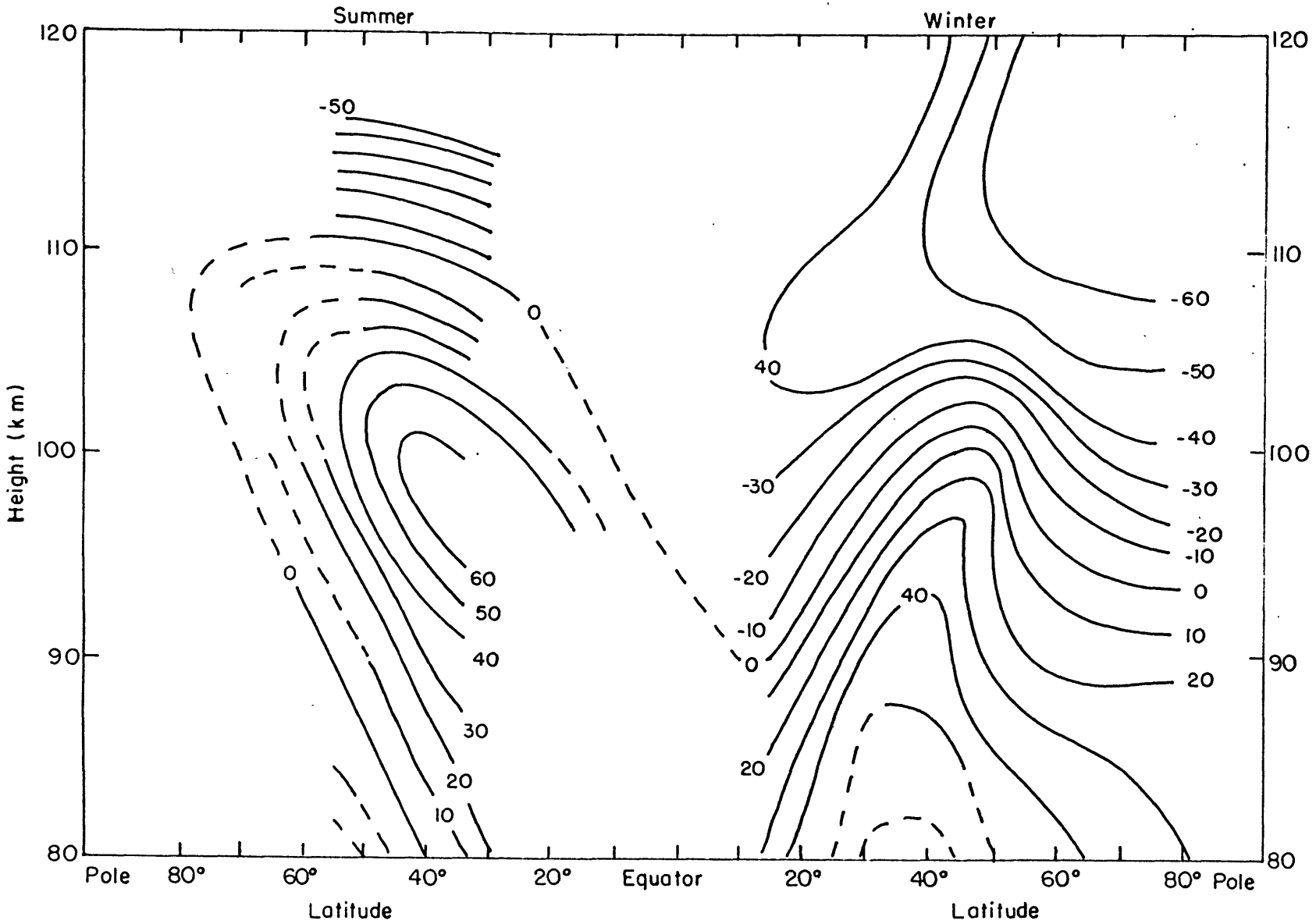

Figure 1: Observed Zonal Wind Component After Murgatroyd (1957)
(westerly components positive, m/sec)

for its lack of observations and number of stations. However, there has been information gained from the data at the individual meteor wind stations. For example, this data shows that internal gravity waves are present (Hines, 1960) and the Jodrell Bank data shows strong tidal components.

A source of much information in the studies of the general circulation at lower altitudes has been the separation of the motions into harmonic components (see, for example, Teweles, 1963). Four groupings of the resultant waves are made; the zonal flow (n = 0), long or planetary waves (n = 1 to 4), cyclone waves (n = 5 to 8), and short waves (n = 9 to 15). In the troposphere the cyclone waves provide the largest energy contribution to the zonal flow (Teweles, 1963), while in the stratosphere the planetary waves contribute the most energy to the zonal flow (Teweles, 1963). In particular, at 100 mb, eddies of wave number 1 and 2 contribute the bulk of the energy to the zonal flow. There is energy exchanged among the eddies of different wave number. The eddy of wave number 3 receives the most energy from the other eddies. Charney and Drazin (1961) considered the vertical propagation of planetary-scale waves. The damping of these waves with altitude is dependent upon the magnitude of the zonal winds in the stratosphere. They concluded that these waves probably could not be propagated above the stratosphere, except

possibly in the spring after the breakdown of the polar night jet, and for a short time in the autumn. Hines (1963) points out that in the winter when the transmission coefficient increases (he determines from Charney and Drazin that the transmission coefficient for a horizontal wavelength of 10^4 km is 10^{-3} in the winter) more than enough energy needed to support prevailing motions can be propagated to 95 km. Hines' calculations were approximations but they point out that planetary-scale motions propagated from below may be a source of energy for the motions in the upper atmosphere.

Internal gravity waves generated in the troposphere may propagate into the ionosphere. Gossard (1962) discussed the generation of internal gravity waves in connection with tropospheric weather. Jones (1963) proposes that internal gravity waves may be generated as secondary waves resulting from the interaction of the tides with geographic undulations. Hines (1960, 1963) has shown that the lower ionosphere is a permissible region for the existence of these waves. His discussion included experimental evidence of their existence in this region. The waves should not be in evidence much above 100 km because of the increasing importance of molecular viscosity (Jones, 1963).

The influence of the tides in the lower ionosphere is well documented. The data from meteor trail measurements at Jodrell Bank (53°N) show that there is a prevailing wind of about 15 m/sec, with a 24-hour tidal component of about 10 m/sec, and a 12-hour tidal component of about 20 m/sec (Greenhow and Neufeld, 1961). Meteor trail measurements at Adelaide (35°S) show that the 24-hour tidal component is directed northward at 1730 LT (local time) with a magnitude of 27 m/sec and it is directed eastward at 0930 LT with a magnitude of 25 m/sec. The 12-hour tidal component at Adelaide is directed northward at 0000 LT with a magnitude of 20 m/sec in the summer and northward at 0530 LT with a magnitude of 5 m/sec in the winter; the 12-hour tidal component is directed eastward at 0720 LT with a magnitude of 12 m/sec. Radio waves reflected from the ionosphere at Brisbane (27°S) show a 24-hour tidal component with a magnitude of 7 m/sec. The 12-hour tidal component at Brisbane is directed northward at 0930 LT with a magnitude of 10 m/sec in the summer and at 0230 LT with a magnitude of 15 m/sec in the winter; it is directed eastward at 0840 LT with a magnitude of 8 m/sec (Burke and Jenkinson, 1957). The observations at Freiburg (51°N) were analyzed according to the distribution in the percentage of times each value occurs (Harnischmacher, 1963). The data was arranged to occur with both solar time and lunar time.

Harnischmacher then found that the solar and lunar phase shifts of the 12-hour tidal component were quite similar. On the average both go through north at 0300 hours and 1500 hours solar or lunar time. He concluded that gravitational forces were the cause of the solar and lunar 12-hour terms. Harnischmacher defines the term engagement to describe the importance and concentration of the distribution maximum. An engagement of 100% would exist for a delta-function distribution, an engagement of 0% would indicate that no preference can be found for the distribution. In solar time the engagement is 25% for the prevailing component, 3% for the 24-hour tidal component, and 25% for the 12-hour tidal component. In lunar time the engagement is 5% for the prevailing component, 9% for the 24-tidal component, and 15% for the 12-hour tidal component.

B. Detection of Motions by Radio Methods

The measurements used in this thesis are all derived from the fading of radio waves reflected from the ionosphere. It is important to know what relation the measurements have to the actual winds at ionospheric heights.

Radio waves transmitted from the ground interact with the free electrons in the ionosphere resulting in the waves being reflected back to the ground. The reflection coefficient is dependent upon the frequency of the waves, electron density, the magnitude and direction of the earth's magnetic field, and the electron-neutral particle collision frequency (see, for example, Ratcliffe, 1959a). Depending upon the time of day and angle of incidence very low frequency (3 kc/s to 30 kc/s) and low frequency (30 kc/s to 300 kc/s) radio waves are reflected from the D-region (below 95 km) and the lower E-region. Medium frequency (300 kc/s to 3 mc/s) radio waves are reflected in the lower E-region. In the D-region the collision frequency is high so that waves reflected here are strongly absorbed. The collision frequency is considerably reduced in the E-region but waves reflected here will suffer some absorption in passing through the D-region. Since the electron density varies throughout the day the radio waves will be reflected at different heights during the day.

At any particular frequency the ionosphere does not behave as a perfect reflector. The direction of propagation bends as the waves traverse the medium until they emerge from the bottom

of the ionosphere. When the time of travel is known and the free-space velocity is assumed an apparent reflection height results (Ratcliffe, 1959a). Uncertainty of this height in relation to the true height is about 10 km (Briggs, 1960) and will depend upon the frequency and the angle of incidence.

The reflected signal is variable in amplitude and phase. This is true because the electron density is irregular, the electrons having a tendency to form "clouds". The radio waves will be scattered from these irregularities and form a diffraction pattern. The reflected signal received at the ground will vary with time if an unchanging diffraction pattern moves with a steady drift, if random changes occur within the diffraction pattern, or if there is a combination of steady drift and random changes (Briggs, et.al., 1950; Bowhill, 1956a). Determination of the velocities of drift will be discussed in detail in succeeding paragraphs. An extensive study of the relationship between the diffraction pattern at the ground and the diffraction pattern at the diffracting screen has been made by Bowhill (1956b). In terms of wavelength the higher frequency waves give the appearance that the screen is a very long distance from the ground. The structure size (to be defined) and the fading speed of the pattern at the ground have a one-to-one correspondence with the pattern at the screen. For long waves (VLF and LF) the

relation between the pattern at the screen and the pattern at the ground is not simple but it is determinable. Fooks (1962) shows that the irregularities have their greatest effect on the reflected signal when they are just below the height of reflection. This agrees with experiment results (Jones, 1958).

The relationship between the motions determined by radio methods and the neutral wind is still not clearly understood. Electrodynamics may play an important role in determining the motions at the altitudes considered here. From a summary article by Ratcliffe (1959b) electromagnetic effects are negligible in the D-region and the motion of the electrons is identical to the neutral wind. In the E-region the winds and the electric fields (set up by the winds and by polarization effects) have equal effect on the ionization drifts. The exact height where the electric-field effect becomes important is not known. Jones (1958) has compared the results from the radio wave fading technique with the meteor trails technique and concluded that the ionization irregularities move with the neutral wind up to 110 km.

E-region sounders determine the motions of densely ionized electron clouds (sporadic E) at night. Axford (1963) proposes a model which shows that the sporadic E may be formed by the

motion of electrons along the earth's magnetic field lines. The motion of electrons along the field lines may be caused by neutral wind shears set up by internal gravity waves (Hines, 1960). The vertical movement of the internal gravity waves can cause a vertical transport of these clouds (Axford, 1963). Gossard and Paulson (1964) have proposed that electron cloud projections extend into the D-region causing the rapid phase changes "seen" by ionospheric sounders. These projections may remain for some time before attachment and recombination processes dissipates them. The projections may separate into smaller clouds before they finally disappear. This may be why the ratio of random velocity to drift velocity (to be defined) in the D-region (Sales and Bowhill, 1962) is greater than that in the E-region (Fooks and Jones, 1961).

CHAPTER II. CALCULATION OF THE MOTIONS

A. Introduction

The motions in the ionosphere may be determined from radio waves that have been reflected from the ionosphere and received at three spaced receivers. The methods of determining the motions are presented here. There are three methods presently being used by various workers. The time-delay method (see, for example, Sales, 1960) has been called the spaced receiver or Mitra method after its originator. The method devised by Briggs, Phillips, and Shinn (1950) uses statistical functions and is called the correlation method. Yerg (1959) has proposed a statistical method that gives results that are similar to those given by the correlation method. The correlation method with modifications by Phillips and Spencer (1955) and by Sales and Bowhill (1962) is presented in this chapter. The limit of the time-delay method is shown.

B. The Method of Briggs, Phillips, and Shinn

1. The Space-Time Ellipse

Consider a two-dimensional diagram where the coordinates are space and time as in Figure 2.

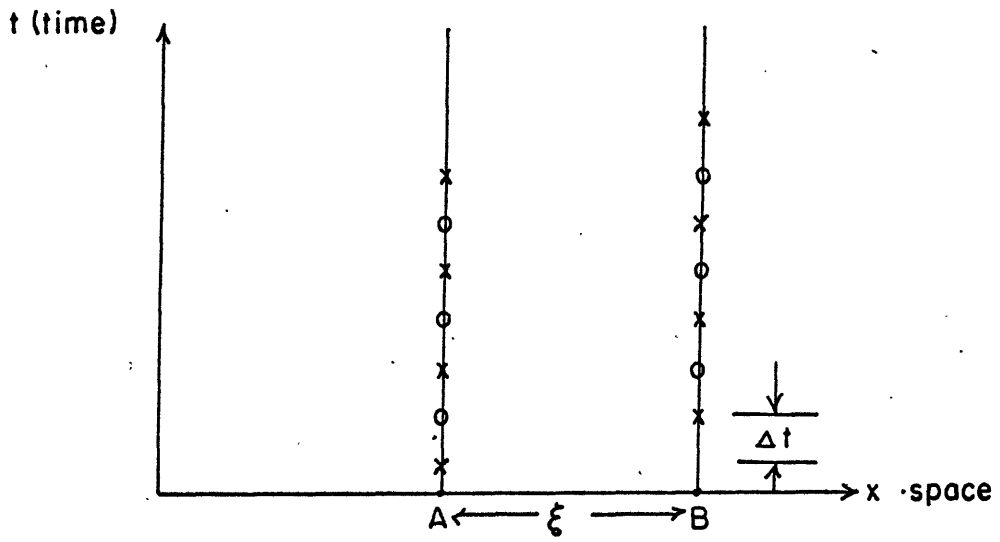

Figure 2. Space-Time Plot of a Sine Wave Moving Along the x-axis.

Suppose that a receiver has been placed at A and another at B on the x-axis, at a distance, ξ, apart. If a sine wave travels along the x-axis its temporal record at A would be indicated by the maxima and minima (crosses and circles) along the line parallel to the t-axis passing through A in Figure 2. The same sine wave would arrive at B but its time record is displaced by a time, Δt, the time it takes the sine wave to travel from A to B. Therefore, knowing ξ it is possible to determine the speed at which the sine wave is traveling along the x-axis, i.e., $\xi/\Delta t$.

If, instead of a simple sine wave, the received signals were a diffraction pattern of radio waves that resulted from the reflection of the waves from the ionosphere, then a similar space-time plot may be made. In order to obtain a more complete picture consider that there are an infinite number of receivers situated along the x-axis. The space-time plot then might appear as in Figure 3.

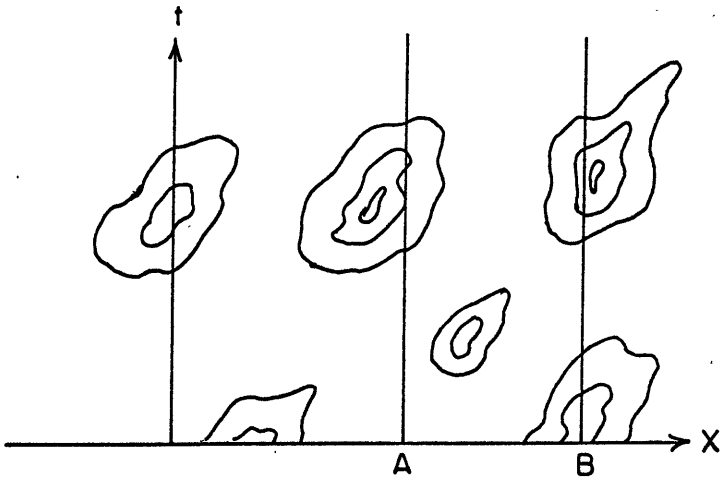

Figure 3. Space-Time Plot of Random Signal Moving Along Positive x-axis.

The closed contours are isolines of amplitude and are shown sloping corresponding to the time delay of the signal as it travels from A to B as in Figure 2. The contours of the diffraction pattern are shown irregular since the ionospheric diffracting screen causing the pattern will be irregular. The exact nature of the diffraction pattern cannot be determined since it is impossible to have an infinite number of receivers and impractical to have more than a few.

This is as far as the Mitra method carries the analysis. Three receivers are set up to form a triangle. The temporal records of a pair of receivers are compared for similar maxima. The time displacements determined over a length of the record, usually about fifteen minutes, are then averaged to give a fading time. Knowing the distance between the two receivers gives a component of the drift velocity in the direction of the line joining them. A similar procedure is made using a second pair of receivers of the triangle. The two components are added vectorially to find the drift velocity. The errors possible with this method will soon become apparent.

Consider a two-dimensional correlation function defined such that, $\rho(\xi,0)$ is the spatial auto-correlation function and $\rho(0,\tau)$ is the temporal auto-correlation function. There

is experimental evidence that $\rho(\xi,0)$ and $\rho(0,\tau)$ have similar shapes (Bowhill, 1956a). The cross-correlation function is $\rho(\xi_o,\tau)$ where ξ_o is the spatial separation between two receivers. The three-dimensional picture of the correlation function would be a surface whose maximum value occurs at zero time lag and zero space lag, given by $\rho(0,0) = 1$. Considering that the correlation function is fairly well behaved near the origin ($\xi = 0$, $\tau = 0$), to a first approximation an isopleth will have the form of an ellipse. An isopleth, ρ_o, of the correlation function is shown in Figure 4. The slope of the ellipse is due to the time required for an event to move from one point to the next. The inverse of the slope of the major axis (line 00') is the drift velocity component in the x-direction, $\Delta x/\Delta t$.

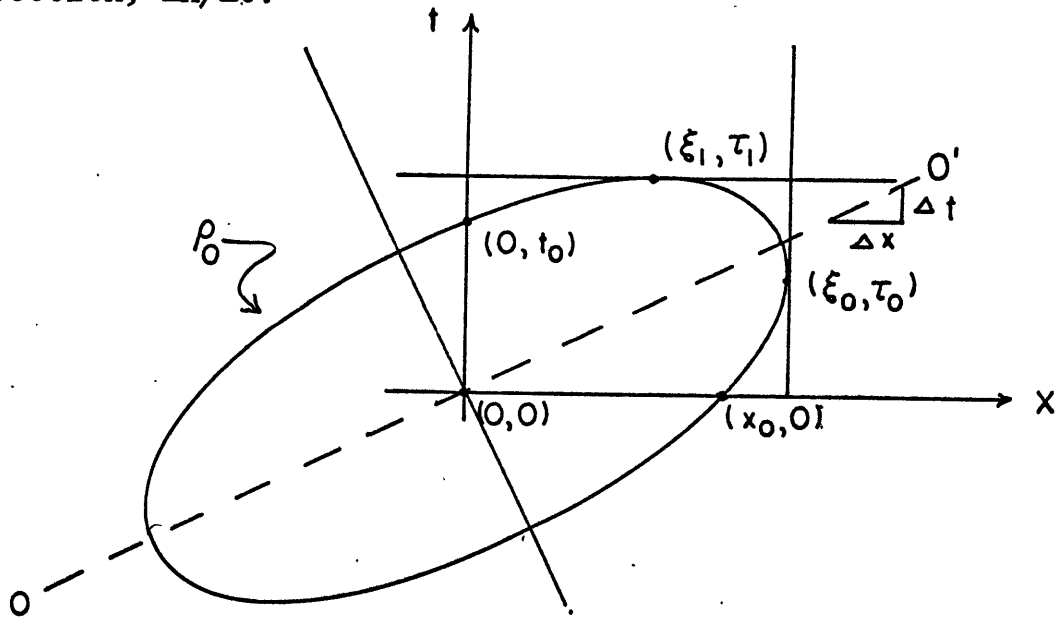

Figure 4. Space-Time Plot of a Contour of the Correlation Function.

2. Velocity Definitions

The preceding discussion has been limited to the effect a stable diffraction pattern has on a space-time plot. If the diffraction pattern changes form as it drifts the velocity of drift cannot be found simply, as by the Mitra method. These changes of form will be called random changes. In effect it will induce a random component (random velocity, to be defined) on the drift velocity. It will be assumed that the random velocity and the drift velocity do not change during the length of a time record, i.e., the record is statistically stationary. The record is assumed to be short with respect to long period changes such as tidal oscillations. Lee (1962) has made an analysis for a vertical ionospheric sounder at a frequency of 300 kc/s and determined that a record of fourteen minutes with 84 scaling points gave satisfactory results. This was a compromise between a long record less subject to sampling errors and a short record that will give better resolution of the movements.

The following definitions will be used to describe the motions of the diffraction pattern (Briggs, et.al., 1950).

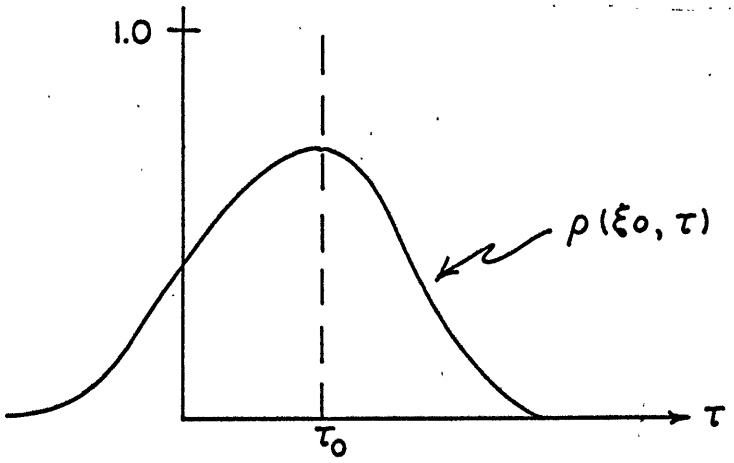

Figure 5. Temporal Cross-Correlation Function Between Two Receivers Separated by the Distance ξ_o.

a. Apparent Drift Velocity (V')

This is the velocity obtained when the records of two receivers, separated by a known distance, ξ_o, are examined for the best cross-correlation. If Figure 5 is the cross-correlation function for the two receivers then the time lag for maximum correlation is τ_o. Therefore

$$V' = \xi_o/\tau_o \qquad (1)$$

This is identical to the velocity obtained by the time-delay method.

b. Fading Velocity (V_c')

This is the ratio of the space shift to the time shift needed to produce the same change in value of the received signal. If for a time lag, t_o, the temporal correlation is ρ_o, then one finds the space lag, x_o, such that $\rho(x_o,0) = \rho_o = \rho(0,t_o)$, then

$$V_c' = x_o/t_o \tag{2}$$

The fading velocity is the overall drift velocity, that is, its components include the drift velocity and the randomness of the diffraction pattern.

c. Drift Velocity (V)

This is the velocity an observor would have to move at in order to experience the minimum amount of fading of the signal. For a given time displacement, τ_1, one finds the spatial displacement that will give the maximum value of the spatial correlation function. From Figure 6

$$V = \xi_1/\tau_1 \tag{3}$$

The ξ-axis is parallel to the x-axis.

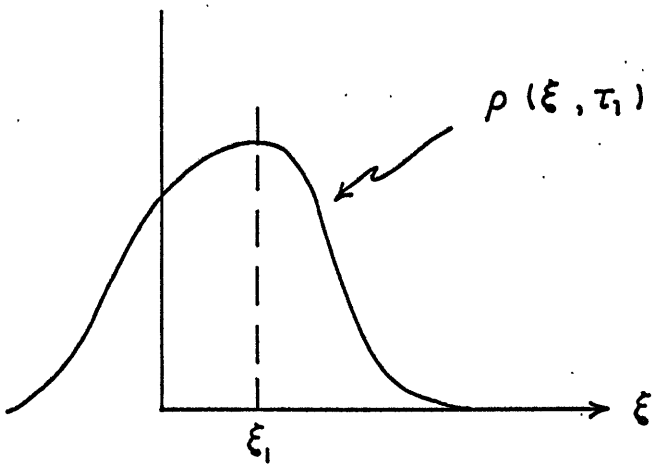

Figure 6. Space Cross-Correlation Function Between Two Receivers Separated by the Time τ_1.

d. Characteristic Velocity (V_c)

This is the fading velocity (V_c') found by the observer moving with a velocity V. Since τ_1 may be chosen such that $\rho(\xi_1, \tau_1) = \rho_o = \rho(V\tau_1, \tau_1)$, then, $\rho(x_o,0) = \rho(\xi_1,\tau_1)$. Therefore

$$V_c = x_o/\tau_1 \qquad (4)$$

The fading velocity (V_c') and the apparent drift velocity (V') are easily found from the auto- and cross-correlation functions. But it is impractical to obtain the function shown in Figure 6, since it would require an infinite number of

receivers. Therefore, connecting equations must be found in order to determine the drift velocity (V) of the pattern and the characteristic velocity (V_c) which is a measure of the randomness of the pattern.

3. The Connecting Equations

By suitable choice of x_o, t_o, ξ_o, and τ_1 the points $(0,t_o)$, (ξ_o,τ_o), and $\xi_1,\tau_1)$ may be located on the ρ_o ellipse, a contour of the correlation surface. These points are shown in Figure 4. The general equation for an ellipse is

$$A\xi^2 + 2B\xi\tau + C\tau^2 = 1 \tag{5}$$

A, B, and C may be found from Figure 3. At the point $(0,t_o)$ equation (5) becomes

$$C = 1/t_o^2 \tag{6}$$

The ellipse has a vertical tangent at the point (ξ_o,τ_o). Therefore $\frac{d\xi}{d\tau} = 0$ at (ξ_o,τ_o). So that proper substitutions at the point (ξ_o,τ_o) gives

$$B = -\tau_o/\xi_o t_o^2 \tag{7}$$

and

$$A = (t_o^2 + \tau_o^2)/t_o^2\xi_o^2 \tag{8}$$

A, B, and C may also be found using the points $(x_o,0)$ and (ξ_1,τ_1) where there is a horizontal tangent such that, $\frac{d\tau}{d\xi} = 0$ at (ξ_1,τ_1). This procedure gives

$$A = 1/x_o^2 \tag{9}$$

$$B = -\xi_1/x_o^2\tau_1 \tag{10}$$

$$C = (x_o^2 + \xi_1^2)/x_o^2\tau_1^2 \tag{11}$$

Rearranging equations (9) and (10)

$$x_o^2 = 1/A \tag{12}$$

$$\tau_1 = -\xi_1 A/B \tag{13}$$

Combining equations (11), (12), and (13)

$$\xi_1^2 = B^2/A(AC-B^2) \tag{14}$$

then

$$\tau_1^2 = A/(AC-B^2) \tag{15}$$

dividing equation (12) by equation (15)

$$(x_o^2/\tau_1^2) = (C/A) - (B^2/A^2) \tag{16}$$

but from equation (4), $V_c = x_o/\tau_1$. And from equations (6) and (9), $C/A = x_o^2/t_o^2 = (V_c')^2$ by equation (2). From equation (13) and equation (3) $B^2/A^2 = V^2$. Therefore equation (16) may now be written

$$(V_c')^2 = V^2 + V_c^2 \tag{17}*$$

Combining equations (6) and (7) and making use of equation (1) gives $\xi_o/\tau_o = -C/B = V'$. Therefore

$$VV' = (-B/A)(-C/B) = C/A = (V_c')^2 \tag{18}*$$

4. Structure Size

So far the discussion has been concerned with the motion of a one-dimensional diffraction pattern resulting from the reflection of radio waves from the ionosphere. It is important to define a quantity that will describe the extent of the ionospheric

irregularities. The structure size may be defined as the distance, or time, where the correlation function falls to some arbitrary value. Bowhill (1956a) used a value of 0.61 ($e^{-\frac{1}{2}}$) while Fooks and Jones used 0.50. Let the time lag where the auto-correlation function falls to 0.50 be called the fading period and be designated by b, i.e., $\rho(0,b) = 0.50$. Then the structure size, d, is given by $\rho(d,0) = \rho(0,b) = 0.50$. The fading velocity is defined by equation (2). Therefore

$$V_c' = d/b \tag{19}$$

The value of the correlation function $\rho(\xi_o,\tau)$ at $\tau = 0$, where ξ_o is the separation between two receivers, will give one point on the spatial correlation function. Then choose a time lag, τ_2, such that $\rho(0,\tau_2) = \rho(\xi_o,0)$. This assumes that the temporal and spatial correlation functions have similar shapes. Then

$$d = (\xi_o/\tau_2)b \tag{20}$$

C. The Velocities in a Two-Dimensional Space

1. Isotropy and Anisotropy

Suppose that the diffraction pattern is frozen in time. A central point is arbitrarily chosen and the spatial correlation function is determined. If the structure size is found for each direction and is found to be constant, independent of direction, the diffraction pattern is said to be statistically isotropic. If the equations given in Part B are used to determine the velocities in two dimensions, isotropy is assumed. This is essentially the Briggs, Phillips, and Shinn method. If the pattern deviates from this defined isotropy it is an anisotropic pattern. Phillips and Spencer (1955) made the modifications that will include anisotropic patterns. It will be assumed that space lags are sufficiently close to the origin of the spatial correlation function so that, to a first approximation, isopleths will be ellipses. This means that receiver separations must be sufficiently small. It has been determined that the best separation is about one wavelength of the transmitted frequency (Sales, 1960).

2. The V_c' Ellipse

Since only three points are needed to determine the equation of an ellipse, only three receivers are needed to

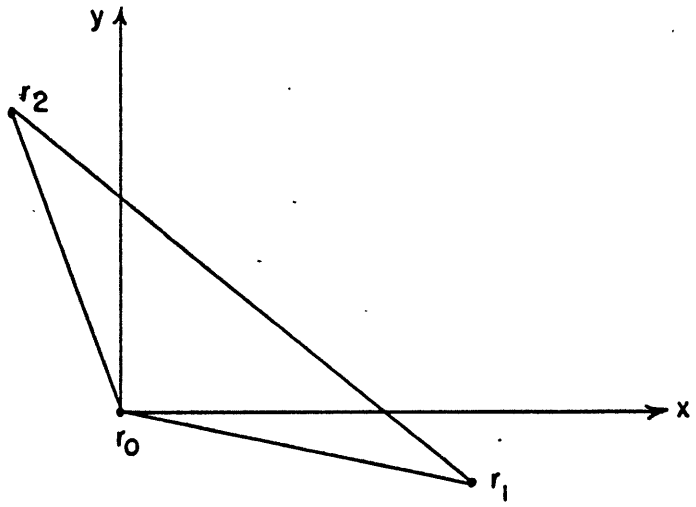

Figure 7. Possible Receiver Locations.

completely describe the extent of the received ionospheric irregularities. One possible triangle of receivers is shown in Figure 7. Considering the records from two of the receivers at a time, a structure size may be determined from each pair of records. Figure 8 shows the three structure sizes obtained with an ellipse drawn through the end points. By dividing each structure size by the fading period a fading velocity for each direction is determined. The resultant ellipse will be called the fading velocity (V_c') ellipse. A general equation for the

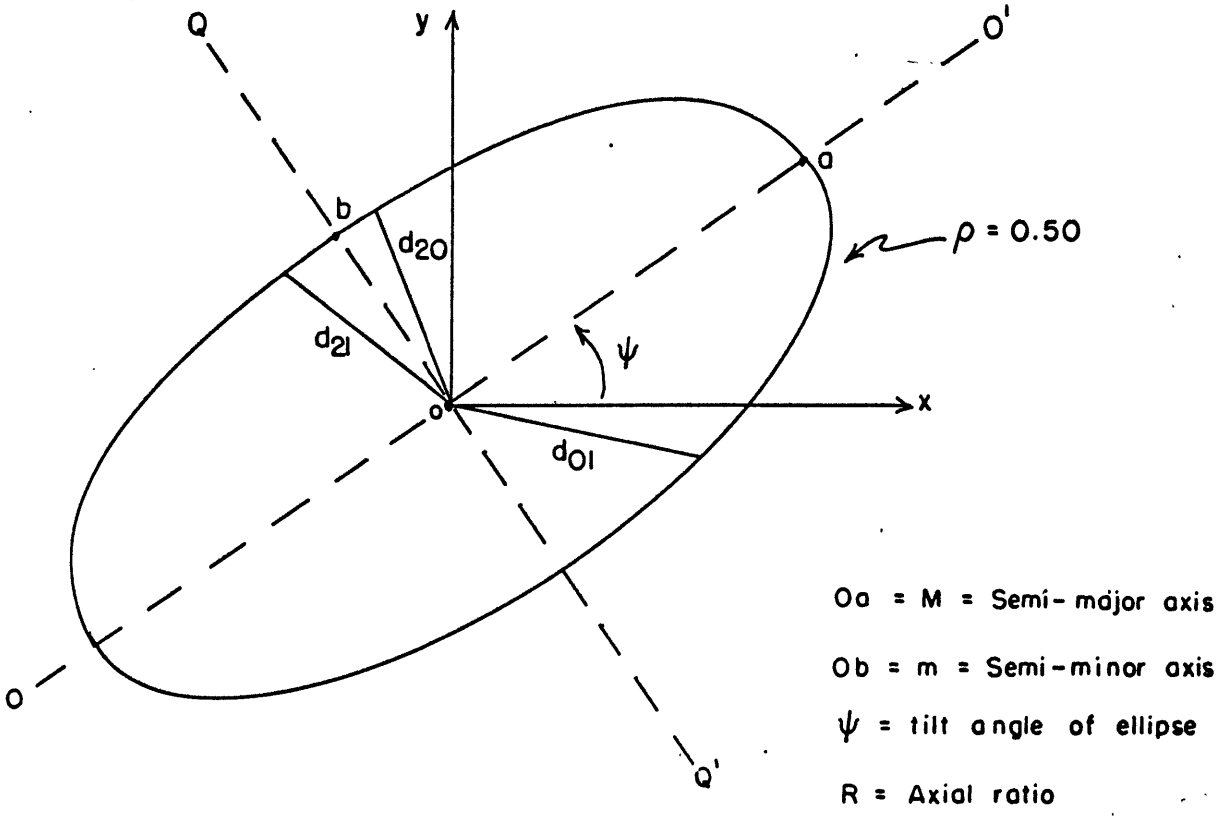

Figure 8. Characteristic Ellipse.

ellipse shown in Figure 8 is $Ax^2 - Bxy + Cy^2 = 1$, where

$$A = (\cos^2\psi/M^2) + (\sin^2\psi/m^2) \tag{21}$$

$$B = (m^{-2} - M^{-2})\sin 2\psi \tag{22}$$

$$C = (\sin^2\psi/M^2) + (\cos^2\psi/m^2) \tag{23}$$

$$\tan 2\psi = B/(C-A) \tag{24}$$

From equations (21), (22), and (23)

$$M^2 = \frac{2}{(A+C) - \left\{B^2 + (A-C)^2\right\}^{\frac{1}{2}}} \tag{25}$$

$$m^2 = \frac{2}{(A+C) + \left\{B^2 + (A-C)^2\right\}^{\frac{1}{2}}} \tag{26}$$

$$R^2 = M^2/m^2 \tag{27}$$

3. Determining the Fading Velocity and Characteristic Velocity in Two Dimensions

Since the fading velocity is dependent on direction a receiver triangle different from the one shown in Figure 7 will result in different values for the drift velocity and characteristic velocity. The following method (Phillips and Spencer) will be used to eliminate the effect of anisotropy. Suppose receivers r_o and r_1 are used to find the apparent drift velocity by equation (1). Then call this velocity V_B'. Similarly, receivers r_o and r_2 will give an apparent drift velocity, V_A'. The resultant of V_A' and V_B' will be called V_D'. The three velocities are shown in Figure 9.

$$\mathrm{Tan}\theta_D = \frac{V_B'\mathrm{Cos}\beta + V_A'\mathrm{Sin}\alpha}{V_A'\mathrm{Cos}\alpha + V_B'\mathrm{Sin}\beta} \tag{28}$$

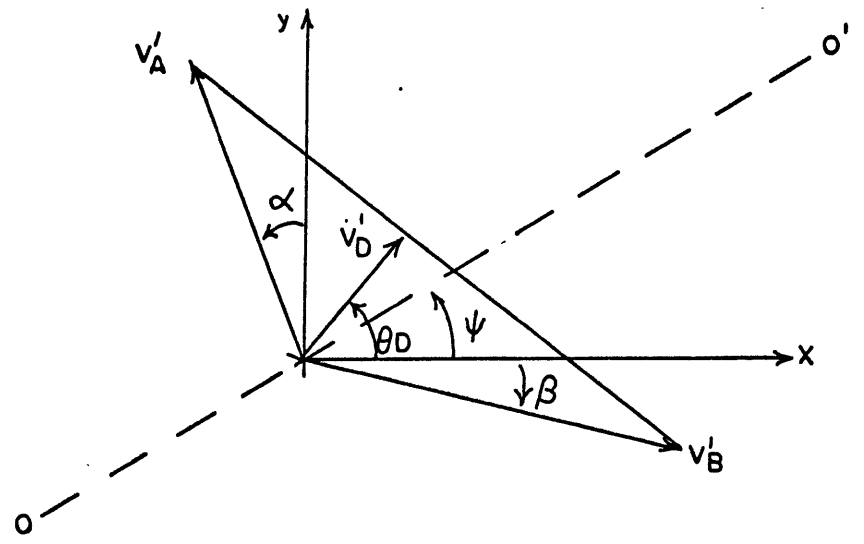

Figure 9. Apparent Drift Velocity - Uncorrected for Anisotropy.

$$V'_D = V'_B\text{Cos}(\theta_D+\beta) = V'_A\text{Sin}(\theta_D-\alpha) \qquad (29)$$

The major axis of the V'_c ellipse shown in Figure 8 lies along the line 00' shown in Figure 9. If all values of V'_c parallel to the major axis are reduced by a factor 1/R, R = axial ratio of the ellipse, the ellipse becomes a circle and the fading velocity is independent of direction. Figure 10 shows V'_A, V'_B, and V'_D transformed to the new coordinate system where all velocity components parallel to the 00' direction have been reduced by 1/R. The subscript T refers to the transformed coordinates. V'_T is the apparent drift velocity in transformed

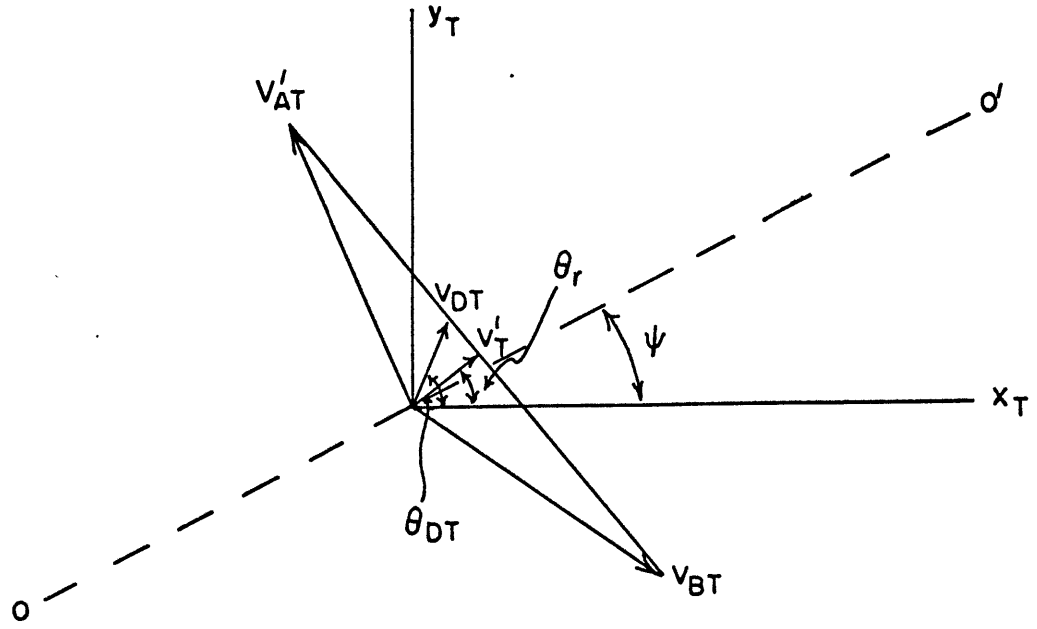

Figure 10. Apparent Drift Velocity - Reduced.

coordinates. Since the pattern is isotropic the same value will always be obtained no matter what the original receiver triangle configuration. Expanding to the original coordinate system from Figure 10 will give Figure 11. Figure 11 is identical to Figure 10 except for the presence of V' and θ. V' is the apparent drift velocity found by considering motion in two dimensions, and by taking into account anisotropy; if the pattern is isotropic than $V' = V'_D$. From the geometry of Figure 11

$$V' = V'_D/\mathrm{Cos}(\theta_D-\theta) \qquad (30)*$$

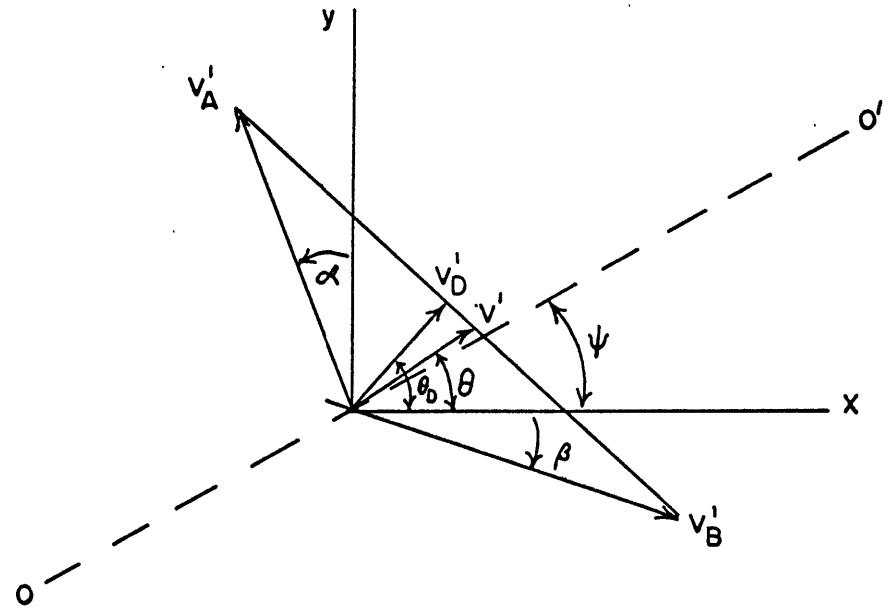

Figure 11. Apparent Drift Velocity - Corrected.

From the geometry of Figure 10

$$V'_T = V'_{DT}\text{Cos}(\theta_{DT}-\theta_T) \tag{31}$$

The relationship between V'_T and V' is

$$V'_T = V'\left\{(1/R^2)\text{Cos}^2(\theta-\psi) + \text{Sin}^2(\theta-\psi)\right\}^{\frac{1}{2}} \tag{32}$$

and between θ and θ_T

$$\mathrm{Tan}(\theta_T-\psi) = R\mathrm{Tan}(\theta-\psi) \tag{33}$$

Similarly

$$V'_{DT} = V'_D\left\{(1/R^2)\mathrm{Cos}^2(\theta_D-\psi) + \mathrm{Sin}^2(\theta_D-\psi)\right\}^{\frac{1}{2}} \tag{34}$$

and

$$\mathrm{Tan}(\theta_{DT}-\psi) = R\mathrm{Tan}(\theta_D-\psi) \tag{35}$$

Combining equations (33) and (35)

$$\mathrm{Cos}(\theta_{DT}-\theta_T) = \frac{1 + R^2\mathrm{Tan}(\theta_D-\psi)\mathrm{Tan}(\theta-\psi)}{\left\{1 + R^2\mathrm{Tan}^2(\theta_D-\psi)\right\}^{\frac{1}{2}}\left\{1 + R^2\mathrm{Tan}^2(\theta-\psi)\right\}^{\frac{1}{2}}} \tag{36}$$

and combining equations (31), (32), and (35)

$$\mathrm{Cos}(\theta_{DT}-\theta_T) = \frac{V'\mathrm{Cos}(\theta-\psi)\left\{1 + R^2\mathrm{Tan}^2(\theta-\psi)\right\}^{\frac{1}{2}}}{V_D\mathrm{Cos}(\theta_D-\psi)\left\{1 + R^2\mathrm{Tan}^2(\theta_D-\psi)\right\}^{\frac{1}{2}}} \tag{37}$$

By combining equations (30), (36), and (37), suitable manipulation gives

$$\mathrm{Tan}(\theta-\psi) = (1/R^2)\mathrm{Tan}(\theta_D-\psi) \qquad (38)^*$$

The fading velocity in the transformed coordinate system is independent of direction. Its magnitude is the length of the semi-minor axis of the fading ellipse. Therefore, its value is

$$V_c' = m\left\{(1/R^2)\mathrm{Cos}^2(\theta-\psi) + \mathrm{Sin}^2(\theta-\psi)\right\}^{-\frac{1}{2}} \qquad (39)^*$$

Equations (17) and (18) now can be used to find the drift velocity (V) and characteristic velocity (V_c). Sales (1960) shows that there must also be a correction made in the determination of the characteristic velocity. If V_c^* is the correct value then

$$V_c^* = \frac{2V_c\left\{1 + R^2\mathrm{Tan}^2(\theta-\psi)\right\}}{(1+R^2)\left\{1 + \mathrm{Tan}^2(\theta-\psi)\right\}} \qquad (40)^*$$

so that equation (17) becomes

$$(V_c')^2 = V^2 + (V_c^*)^2 \qquad (17a)^*$$

It needs to be pointed out that the drift velocity (V) measured at the ground is one-half the ionospheric drift velocity.

4. Concerning a Comparison of the Methods

Yerg (1959) gives the theory for determining the drifts using the total derivatives and partial derivatives of the amplitude of the received signal. Although the method will not be presented here its accuracy is comparable to the Briggs, Phillips, and Shinn (1950) method. The time-delay method uses the apparent drift velocity (V') only in determining the magnitude of the motions. The advantage of this method is that it easily and quickly arrives at a value. It was used by the majority of the workers whose data is used here. In fact, Harnischmacher (1963) has obtained 20,000 values over a period of five years by this method. The correlation method is more accurate but it is more laborious. However, except for determining the points on the fading ellipse (see Figure 3), the analysis can be readily applied to a computer. Fooks and Jones (1961) have compared V' with V for the E and F regions. For the E region V' was greater than V in the majority of cases, with an average value of their ratio of about 1.4. There was no systematic difference between θ and θ_D. However, the majority of values of $(\theta_D-\theta)$ were within $\pm 20^\circ$.

D. Notes About the Stations

The locations of the stations used in the analysis are listed in Table 1. The methods used by each station to determine the winds are noted by T, C, and Y. T is for the time-delay method, C is for the correlation method, and Y is for the Yerg method. The last column in Table 1 shows the number of observations obtained by each station for the listed period. Data was received for only two stations in the southern hemisphere (Johannesburg and Brisbane). Therefore, motions in the southern hemisphere will not be considered in the analysis.

The number of stations reporting data is twice the number available to Murgatroyd (1957) above 95 km. Murgatroyd combined the data from both hemispheres and several different methods of observation. There still remains a major portion of the hemisphere not covered by any observations. Data was made available in varying amounts. The Freiburg data actually covered a period of four years during which time approximately 15,000 observations were made. Individual observations were not given for Freiburg. Instead, results were obtained from distributions of magnitude and phase of the motions for each month. Since this was time consuming only one year's data was used in the analysis. The data at Yuma is limited to three

Table 1 - Stations Used in the Analysis

Station Number	Station Name	Location	Period of Coverage	Type of* Analysis	Total No. of Obs.
1	Yamagawa	130.6°E 31.2°N	7/57-12/60	T	1343
2	Swansea	4.0°W 51.6°N	7/57-6/58	C	137
3	Gorky	44.3°E 56.1°N	8/57-3/60	T	103
4	Irkutsk	104.0°E 52.5°N	4/58-1/60	T	349
5	Ibaden	4.0°E 7.4°N	8/58-12/58	C	244
6	Waltair	83.3°E 17.7°N	6/57-5/60	T	865
7	Tomsk	85.0°E 56.5°N	9/57-6/59	T	128
8	Murmansk	33.0°E 69.0°N	11/58-1/60	T	180
9	Rostov	39.6°E 47.2°N	7/58-12/59	T	456
10	Simeiz	34.0°E 44.6°N	1/58-11/58	T	235
11	Kharkov	36.3°E 50.0°N	8/57-1/60	T	386
12	Mayaguez	66.0°W 18.0°N	2/58-9/58	Y	357
13	Pennsylvania State College	77.9°W 40.8°N	2/61-1/62	C	451
14	Yuma	114.7°W 32.7°N	3/62, 10/62, 2/63	C	94
15	Freiburg	13.3°E 50.9°N	7/60-6/61	T	≈3718

*T = time-delay method Y = Yerg method C = correlation method

months of observations (March and October, 1962; February 1963). Stations reporting data for only part of the day are Yuma, Pennsylvania State College, Ibaden, Gorky, and Simeiz.

The height range for which the data apply is from about 95 km to 115 km. The height of reflection of radio waves was not given for the following stations; Swansea, Ibaden, Freiburg, Mayaguez, Pennsylvania State College, and Yuma. A reflection height may be assigned based on the frequency used at each station and/or the time of day when most of the data was obtained at each station. The height of reflection was assumed to be 95 km at Swansea, Ibaden, Pennsylvania State College, and Yuma. The height of reflection was assumed to be 100 km at Mayaguez and Freiburg. The remaining stations gave a reflection height for each observation.

CHAPTER III. RESULTS

A. Diurnal Wind Variations at Individual Stations

Figures 12a through 22b show the diurnal wind variation at selected stations. Stations that were chosen had ten or more observations at the time indicated, plus a series of such times in a given season. Observations were chosen if they referred to motion in the height range, 95 km through 115 km. The shaded areas indicate those values where there is a concentration of 10% or more of the observations. This procedure is similar to that used by Harnischmacher (1963). Figures 12a through 12d show Harnischmacher's results from five years of data obtained at Freiburg. The magnitude and direction (clockwise from north) of the motion is presented in these figures. The remaining figures in this set have been determined from the observations taken at other stations under the conditions described above.

A summary of the results obtained at Freiburg is presented in Figures 12a through 12d. Harnischmacher (1963) did not determine average values since the distributions sometimes became complicated. Thus, average values would often occur where there is a minimum number of observations. The distribution was limited to every 30° in direction and every 10 m/sec

in magnitude. Figure 12a presents the distributions for spring. A 12-hour variation in direction is well defined. The magnitude shows some variability but no tidal component is evident. The distributions for summer are presented in Figure 12b. The magnitude is very steady and lacks any tidal variations. The summer magnitude is generally smaller in comparison to the spring magnitude. The direction is fairly steady having components towards the east and towards the north. Superimposed on this steady component may be seen a 24-hour tidal component. In the autumn the magnitude is about the same as it is in the summer (Figure 12c). The return of the 12-hour tidal component in direction is shown. Figure 12d presents the distributions for winter. There is a marked increase in magnitude with a wider distribution, which is comparable to the spring distribution. The variations in direction indicate the influence of more than one tidal component.

The diurnal wind distributions determined in this thesis were separated into westerly and southerly components. Mean values at each hour of the day were also determined. A prevailing wind in each season was found by averaging all observations.

Figures 13a through 16b show the diurnal wind variation at Yamagawa for the four seasons. In winter there is a 2 m/sec

prevailing westerly component (Figure 13a). There is a lack of continuity in the distribution resulting from day-to-day variabilities. The concentration of values indicates that these variabilities may have comparable magnitude in either direction. There may be tidal influences but they are not easily discernable. The south-north component for winter is shown in Figure 13b. The prevailing component is northerly with a magnitude of 25 m/sec. Again, there is a variability in the distribution. A strong prevailing westerly component of 37 m/sec may be seen in Figure 14a. The distribution is continuous with a median some 20 m/sec greater than the mean values. Figure 14b shows the diurnal distribution of the south-north component. The distribution is fairly continuous except in the afternoon. The prevailing component is northerly with a 17 m/sec magnitude. A strong 24-hour tidal component may be seen in this figure. During the summer both components have widespread discontinuities (Figures 15a and 15b). The prevailing components are 17 m/sec westerly and 26 m/sec northerly. The mean value variations in both wind components show a strong 12-hour tidal component. In the autumn there is a return to continuous distributions, which is shown by Figures 16a and 16b. The prevailing components are 17 m/sec easterly and 20 m/sec northerly. It is difficult to determine the tidal influence in these figures.

A Fourier analysis of the data from Yamagawa has been made (Aono, Tsukamoto, and Ichinose, 1961). A portion of the results are shown in Table 2. The velocities and times of maximum northward and eastward are given in local time.

Table 2

The 24-, 12-, and 8-Hour Harmonics Obtained By Fourier Analysis (from Aono, et.al., 1961)

	Season	Northward		Eastward	
		Velocity (m/sec)	Time (hours)	Velocity (m/sec)	Time (hours)
24-Hour	Summer	23.4	1236	4.2	1542
Harmonic	Autumn	33.0	1300	21.8	0254
	Spring	13.5	1730	16.5	0400
12-Hour	Summer	25.6	0524	13.6	0924
Harmonic	Autumn	30.9	0418	19.4	0724
	Spring	8.3	0518	13.3	0754
8-Hour	Summer	6.3	0618	2.8	0100
Harmonic	Autumn	1.4	0124	1.8	0254
	Spring	14.0	1400	3.2	0512

Two seasons of data from Waltair were analyzed. The results for summer are shown in Figures 17a and 17b. Both figures show the distribution variability that was in evidence at Yamagawa during the same season. The prevailing wind components are 1 m/sec westerly and 24 m/sec northerly. Tidal motion is present in both figures. The variability of the distribution makes it difficult to determine this tidal influence. Unlike Yamagawa, the data from Waltair for the autumn retains the variability in its distribution (Figures 18a and 18b). However, there is a summer-to-autumn reduction in the magnitude of the tidal effects at Waltair, similar to the summer-to-autumn change at Yamagawa. The prevailing wind components are 14 m/sec easterly and 12 m/sec northerly.

Rostov had only one season (Figures 19a and 19b) with a sufficient number of observations to show diurnal wind variations. A variability of the distribution, similar to that seen at Waltair, is shown for this season. The prevailing winds are 13 m/sec easterly and 14 m/sec northerly. Tidal influences are present in both figures. It is difficult to estimate which tidal components are present because of the limited number of hours represented and the variability of the distribution. The main influences appear to be from the higher order components of the tide.

Two seasons of data from Mayaguez are shown in Figures 20a through 21b. The diurnal wind distributions are for the daytime for both seasons. In each figure the distributions are fairly well concentrated. The prevailing wind components are 5 m/sec westerly and 25 m/sec northerly in the winter; they are 18 m/sec westerly and 16 m/sec northerly in the spring.

A nighttime wind variation for summer at the Pennsylvania State College is shown in Figures 22a and 22b. The prevailing wind components are 11 m/sec westerly and 1 m/sec northerly. Some evidence of tidal effects may be seen in both figures. However, the period of coverage is too short to give a clear picture of the tidal influence.

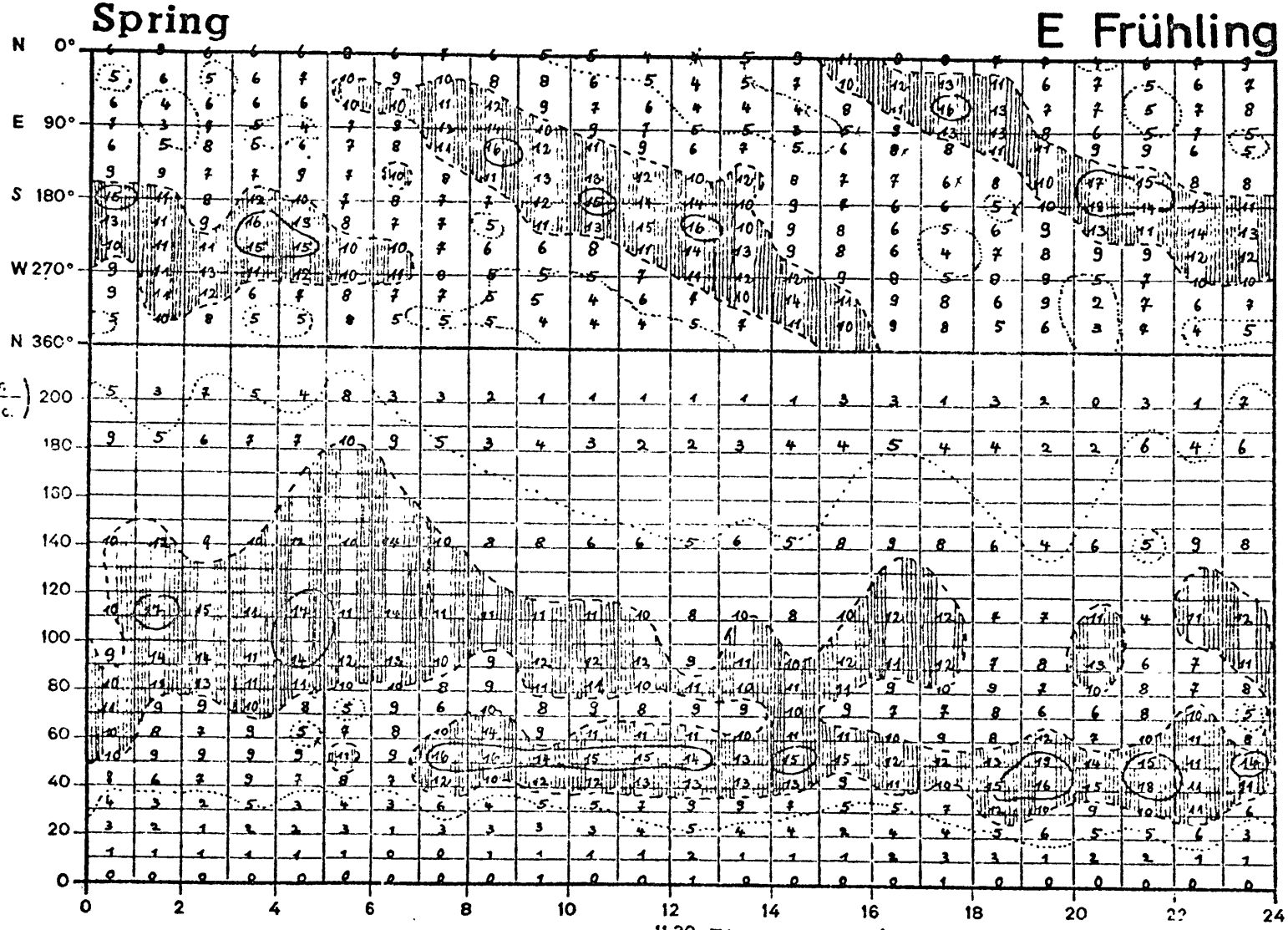

Figure 12a: (After Harnischmacher, 1963)

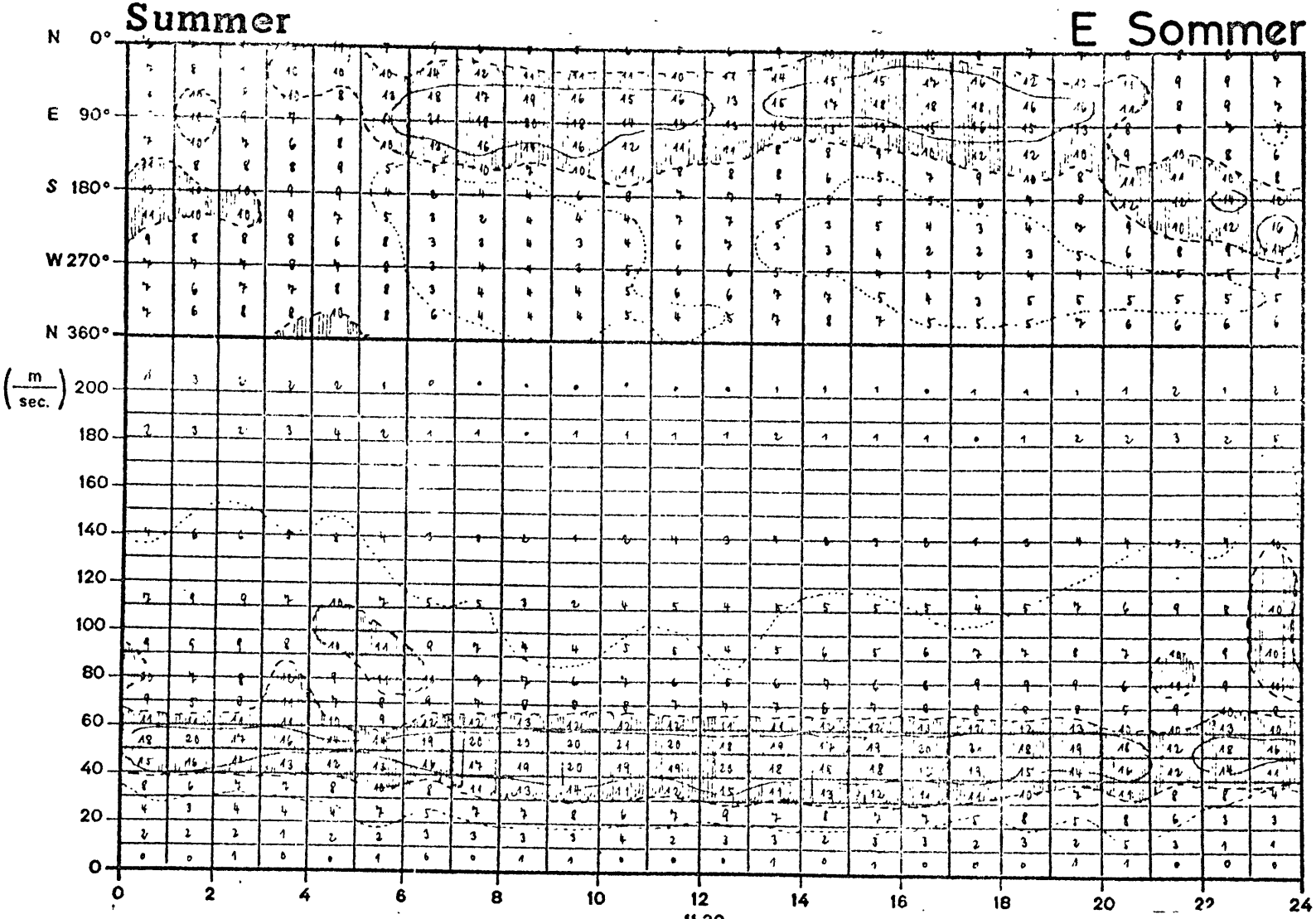

Figure 12b: (After Harnischmacher, 1953)

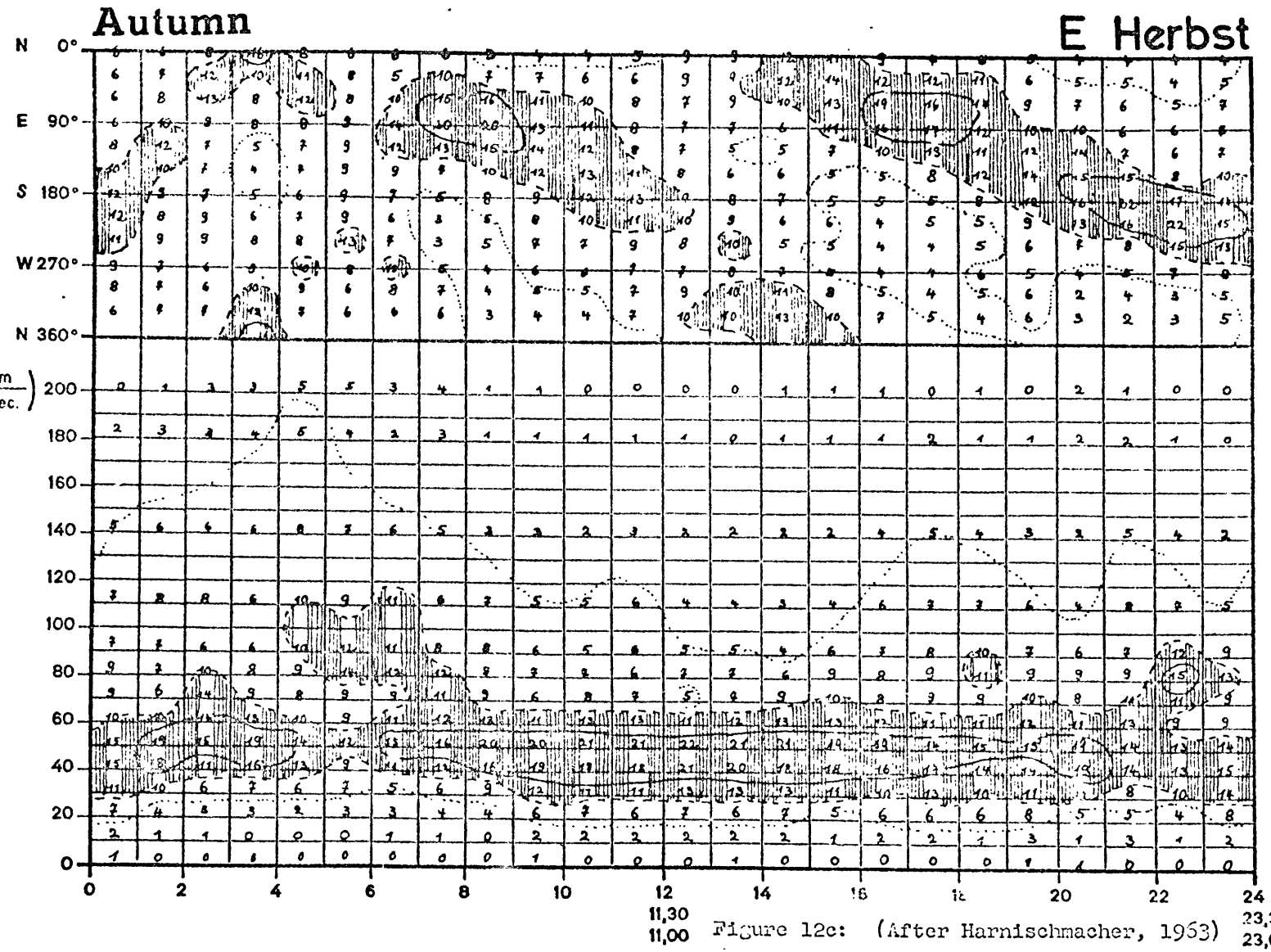

Figure 12c: (After Harnischmacher, 1963)

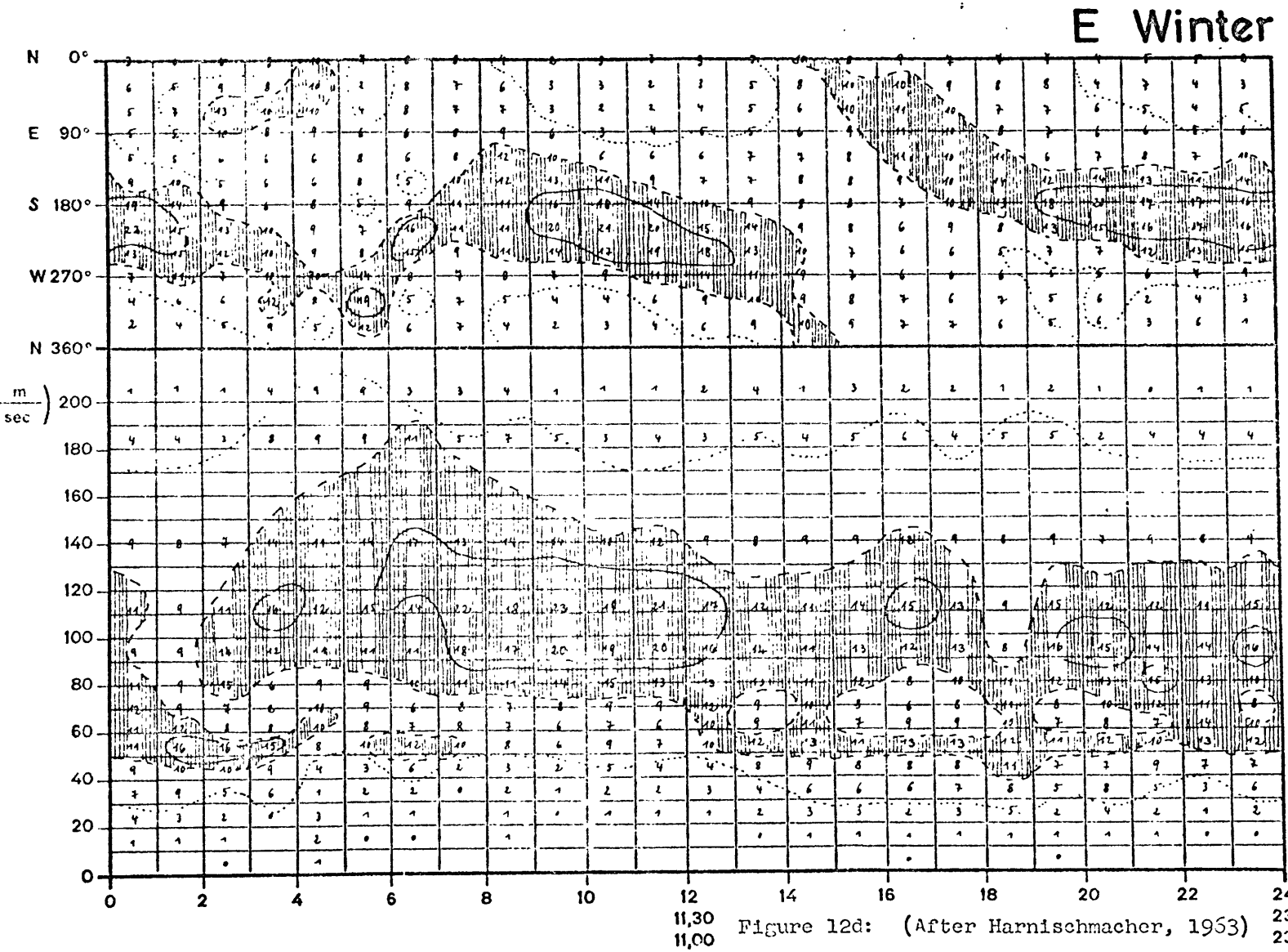

Figure 12d: (After Harnischmacher, 1963)

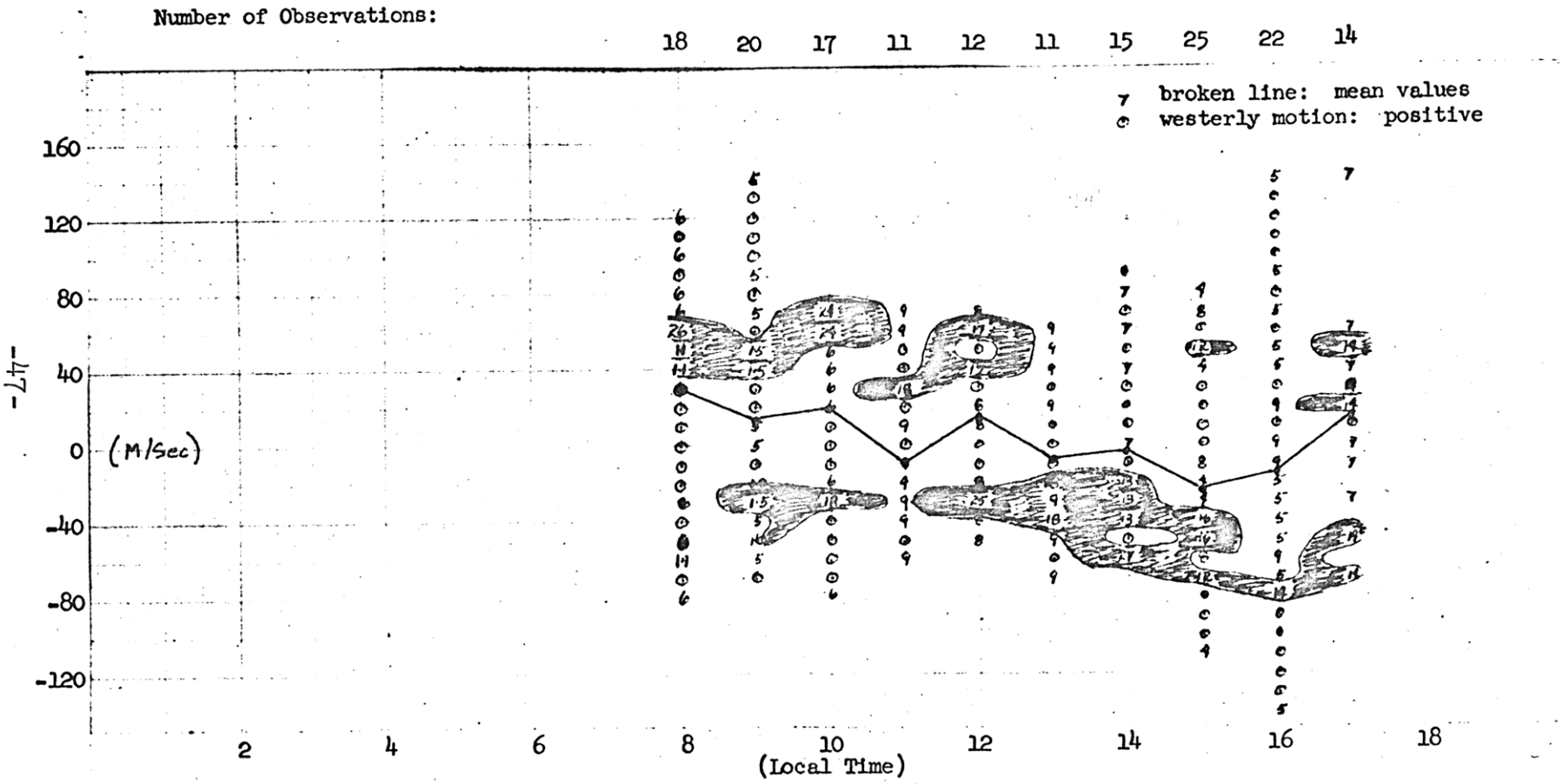

Figure 13a: Diurnal Variation of the West-East Component at Yamagawa (Jan-Feb-Mar)

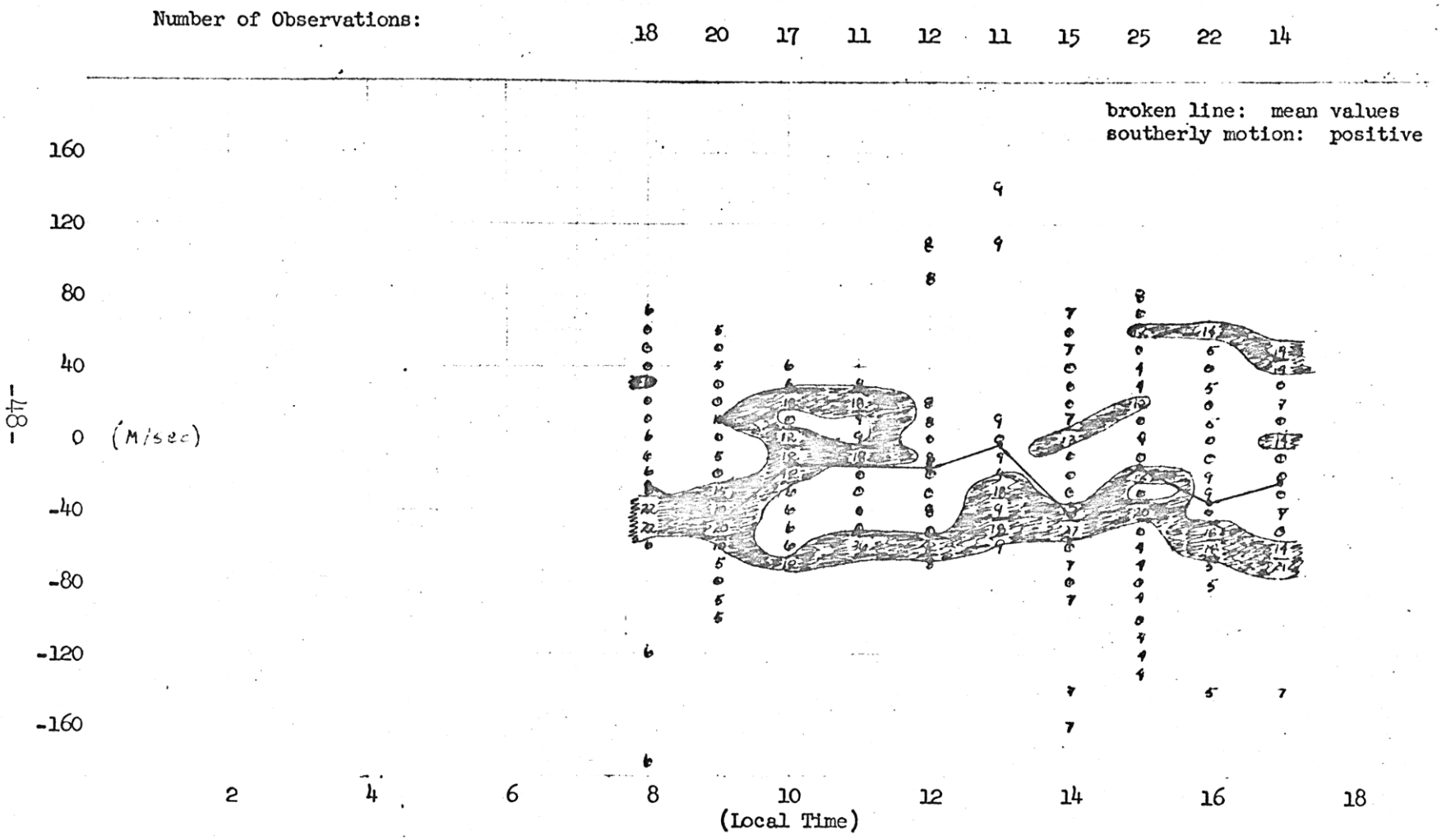

Figure 13b: Diurnal Variation of the South-North Component at Yamagawa (Jan-Feb-Mar)

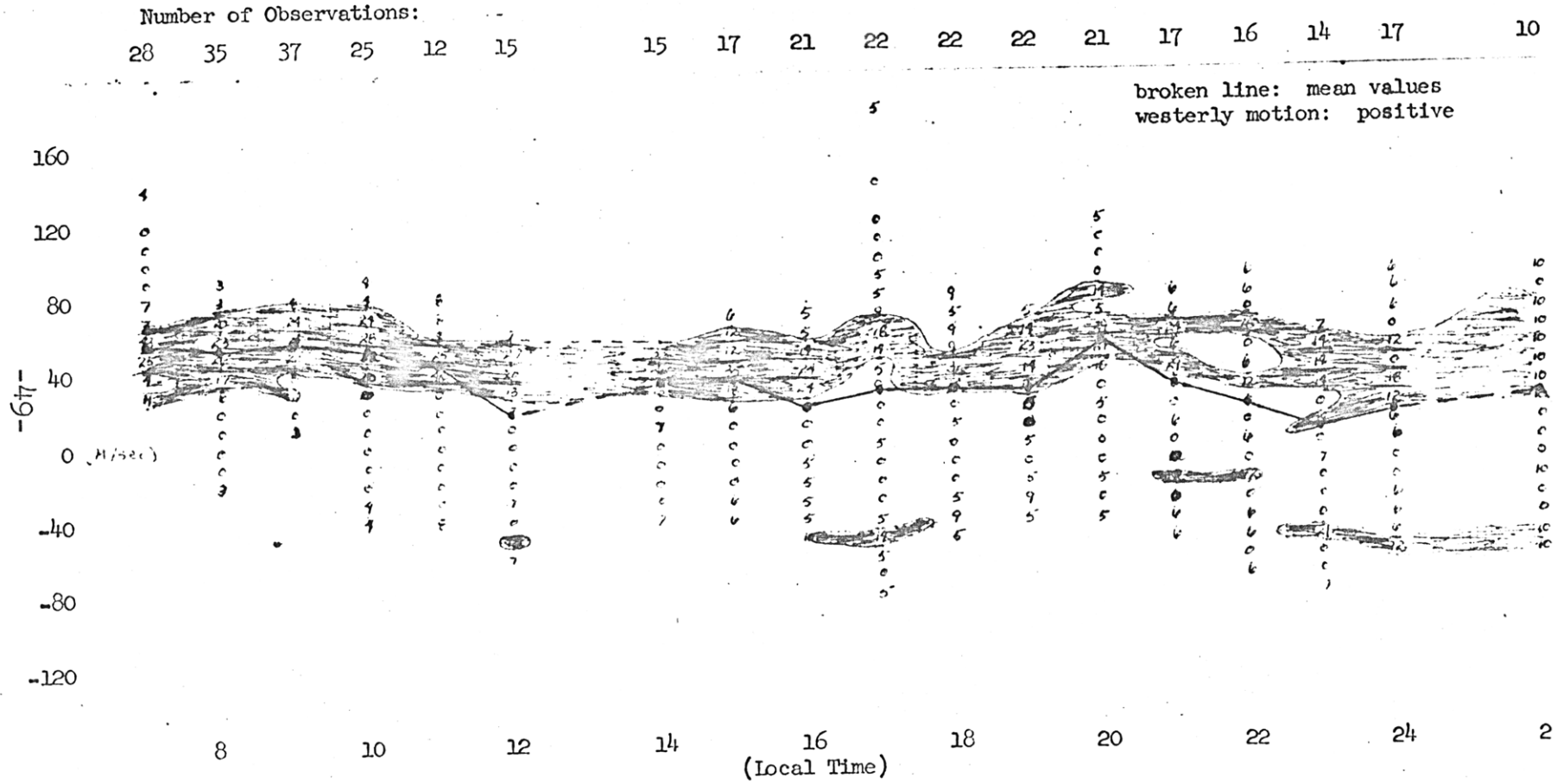

Figure 14a: Diurnal Variation of the West-East Component at Yamagawa (Apr-May-June)

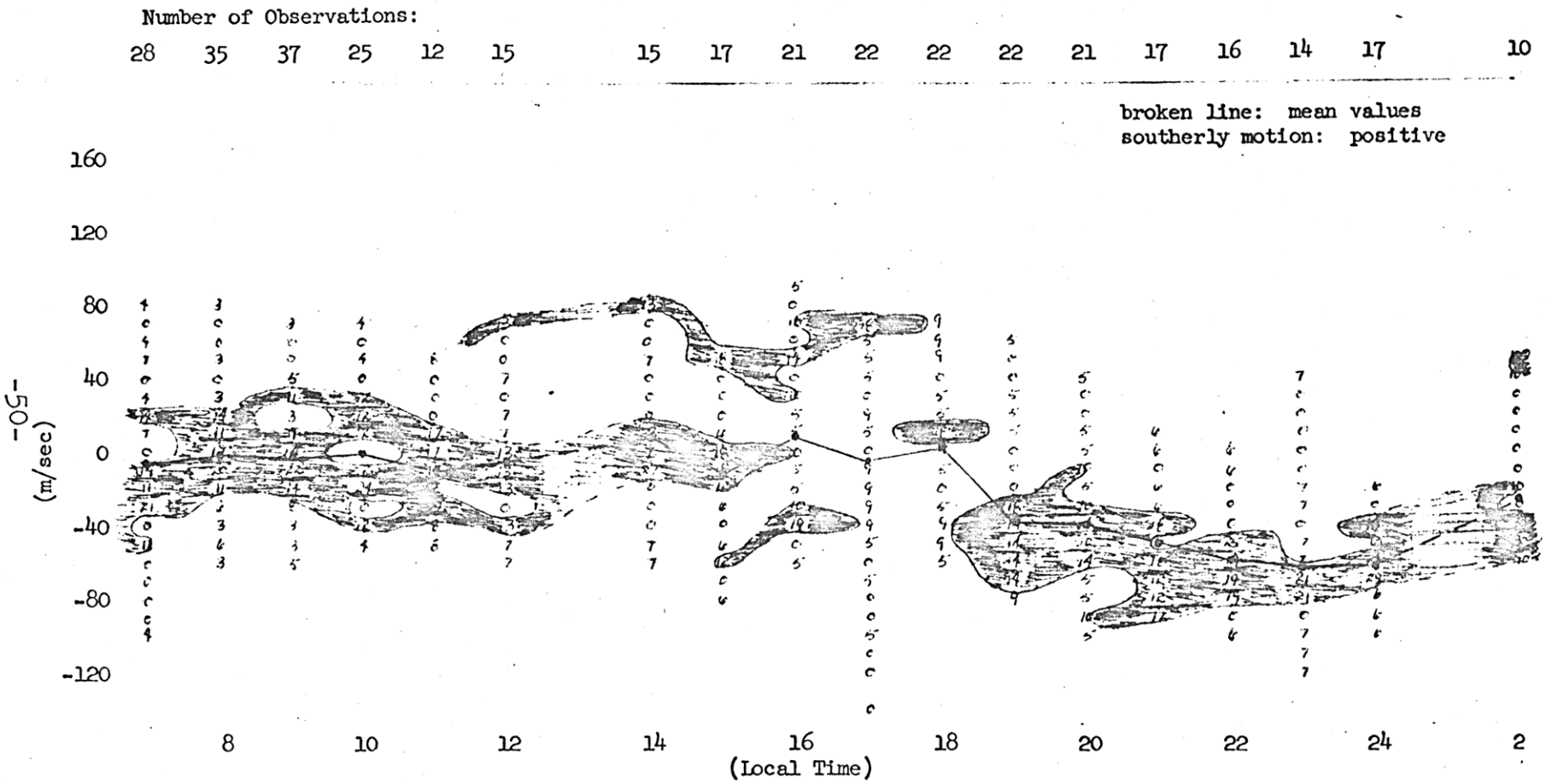

Figure 14b: Diurnal Variation of the South-North Component at Yamagawa (Apr-May-June)

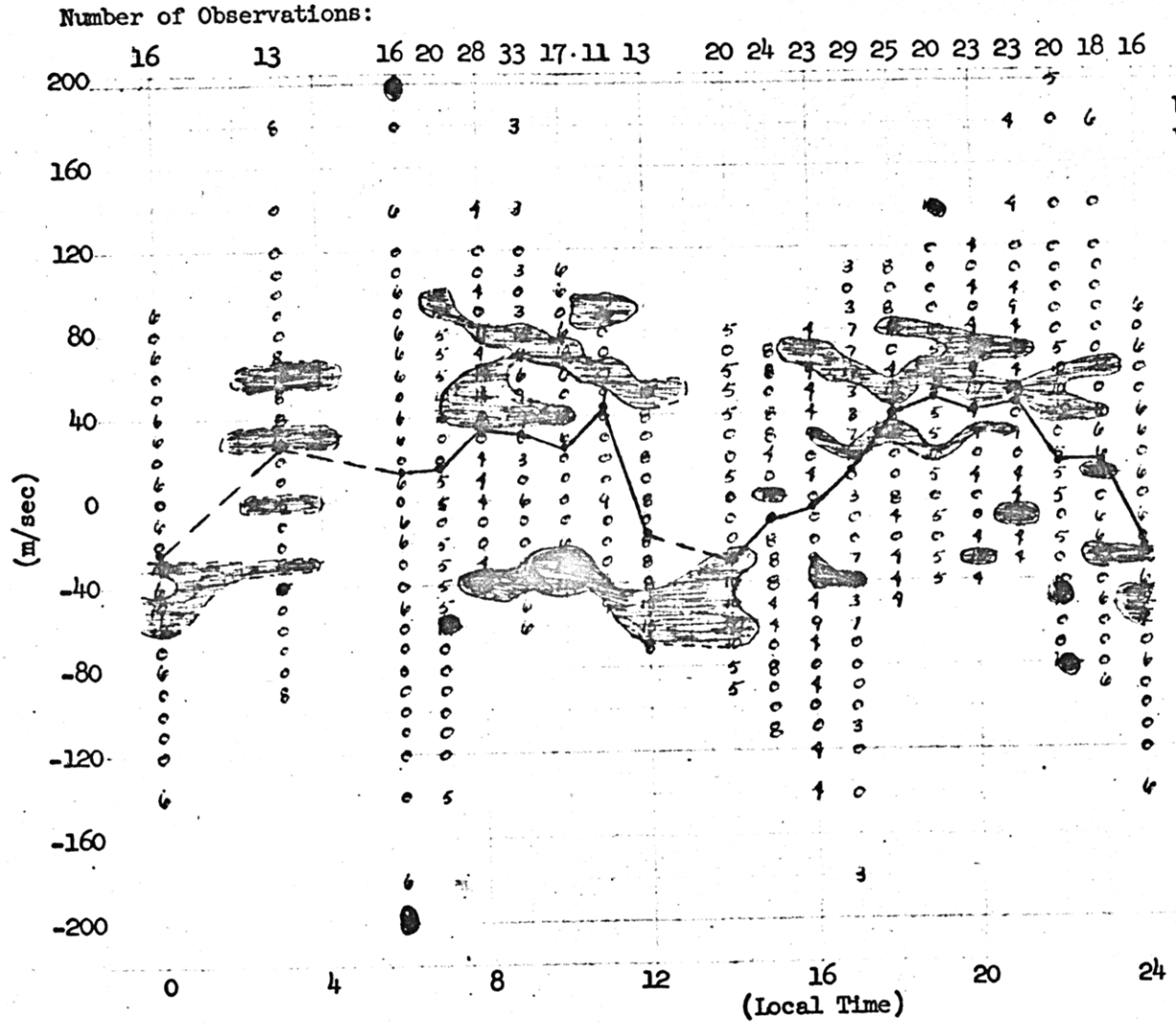

Figure 15a: Diurnal Variation of the West-East Component at Yamagawa (July-Aug-Sept)

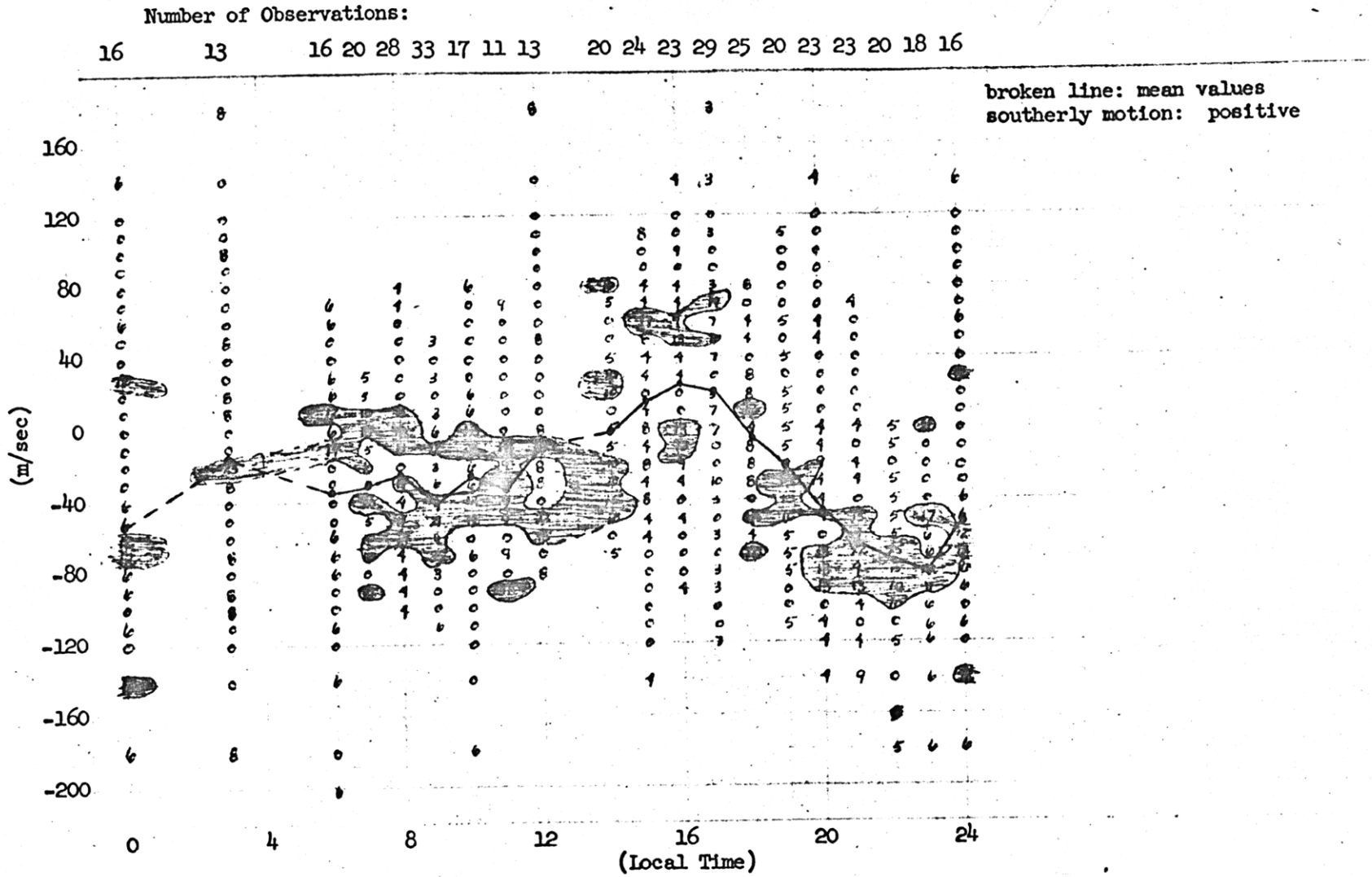

Figure 15b: Diurnal Variation of the South-North Component at Yamagawa (July-Aug-Sept)

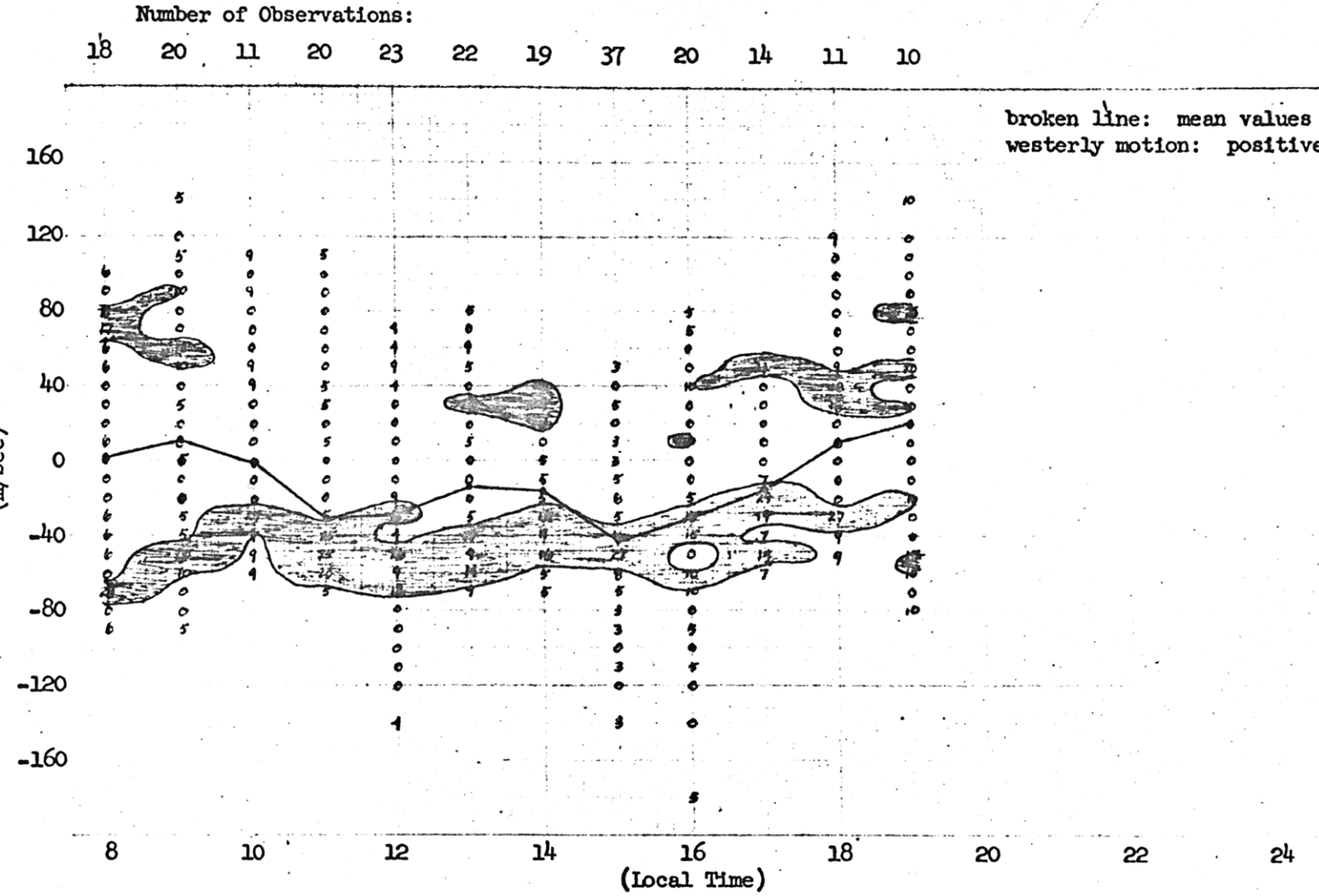

Figure 16a: Diurnal Variation of the West-East Component at Yamagawa (Oct-Nov-Dec)

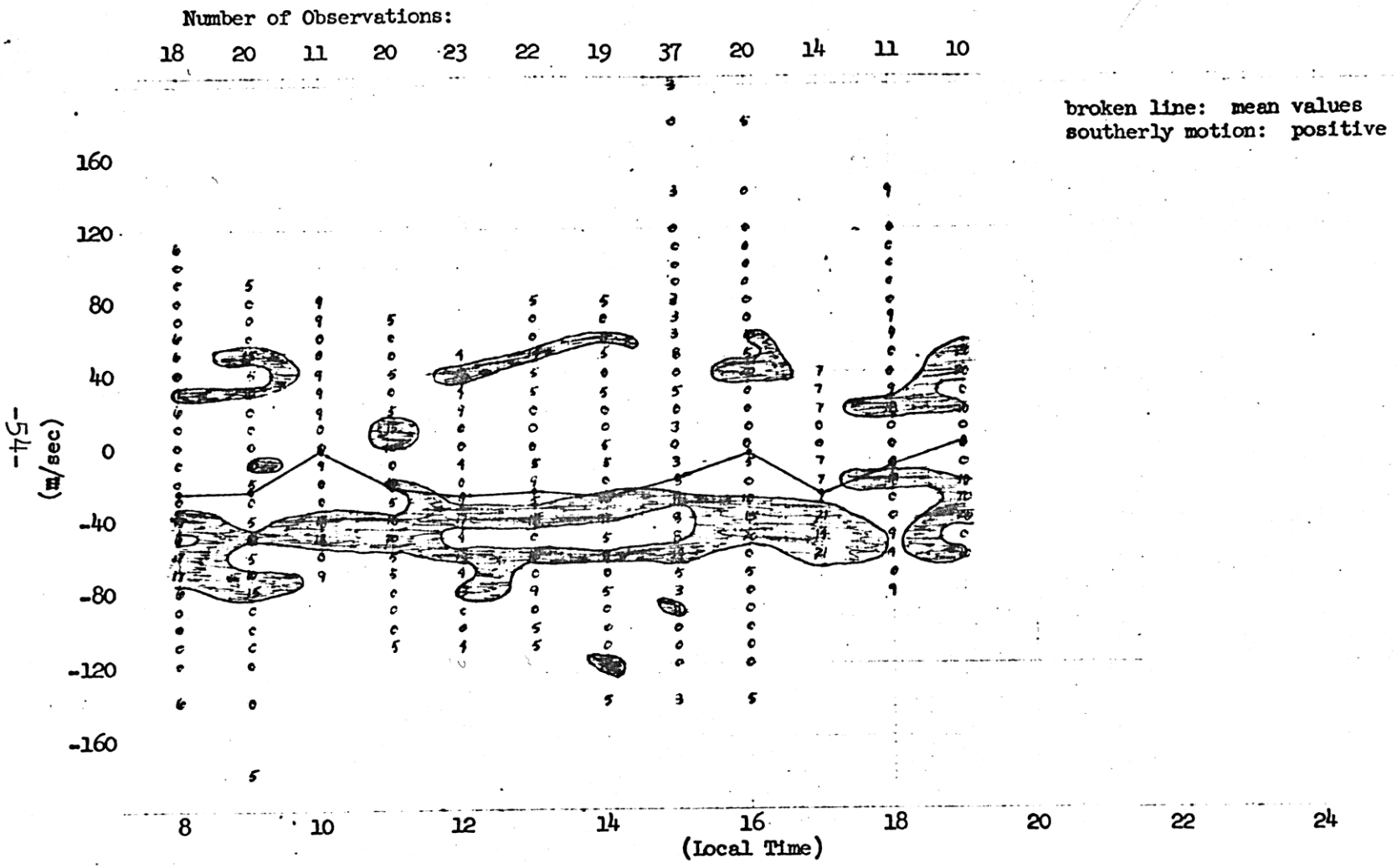

Figure 16b: Diurnal Variation of the South-North Component at Yamagawa (Oct-Nov-Dec)

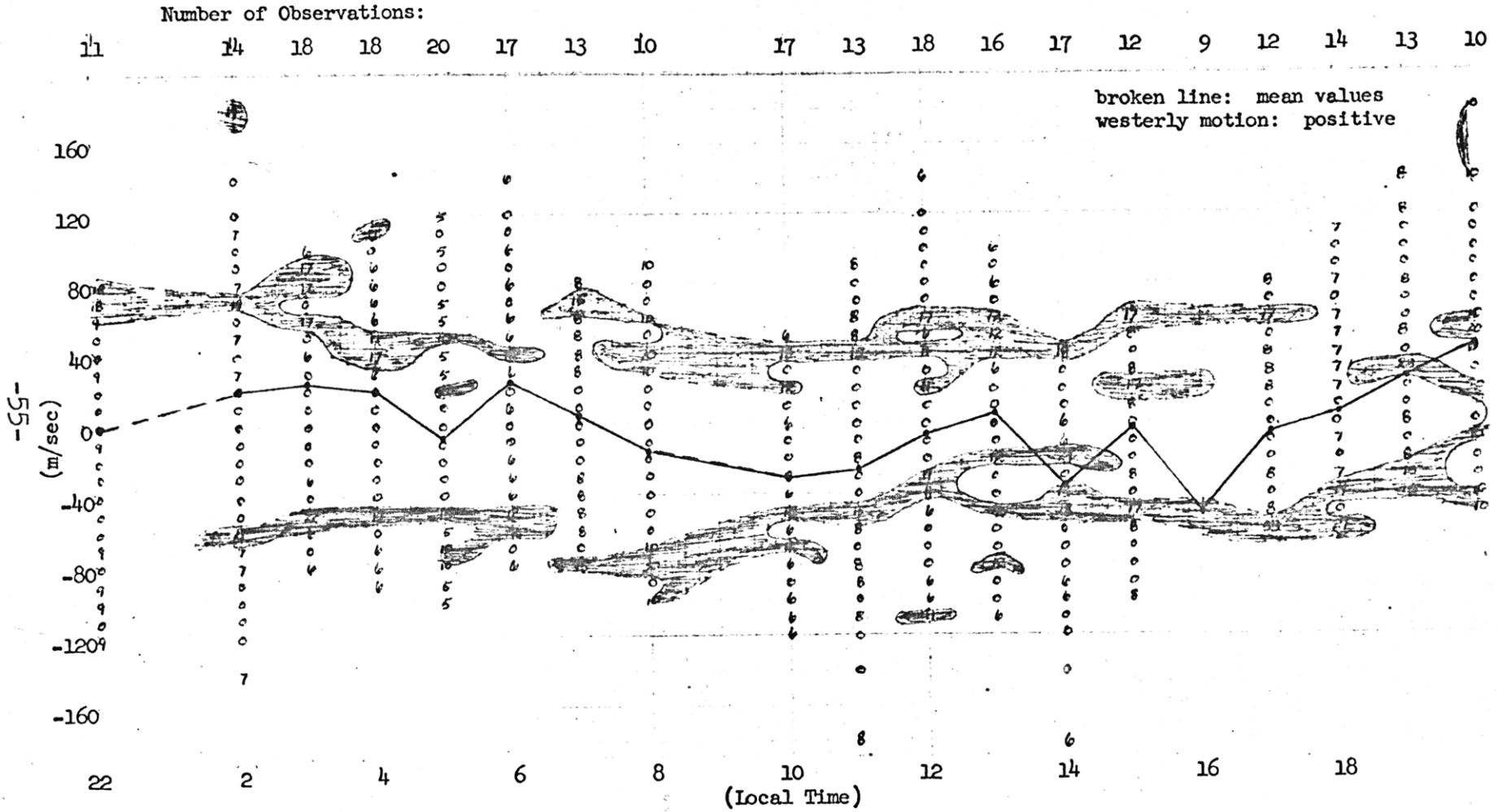

Figure 17a: Diurnal Variation of the West-East Component at Waltair (July-Aug-Sept)

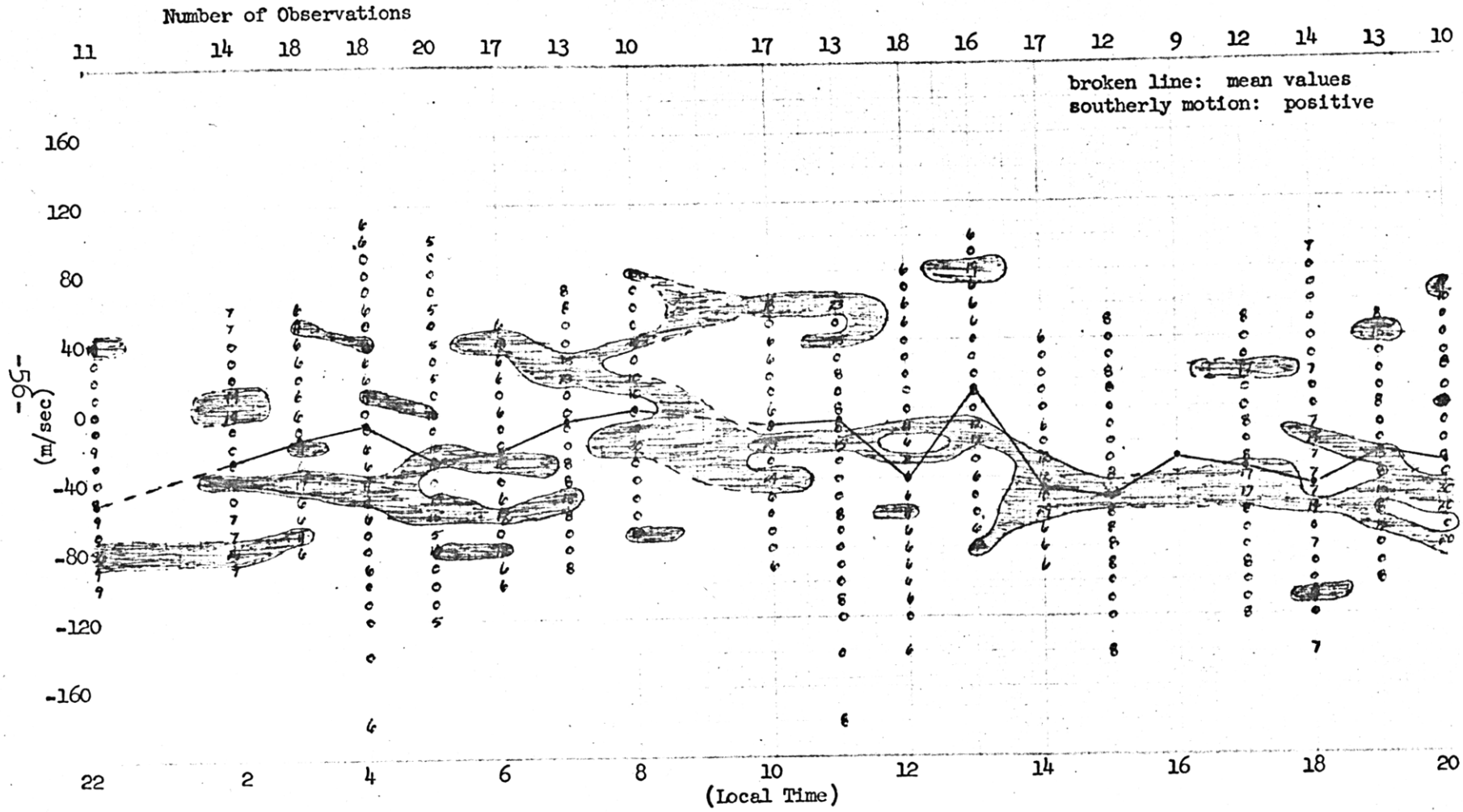

Figure 17b: Diurnal Variation of the South-North Component at Waltair (July-Aug-Sept)

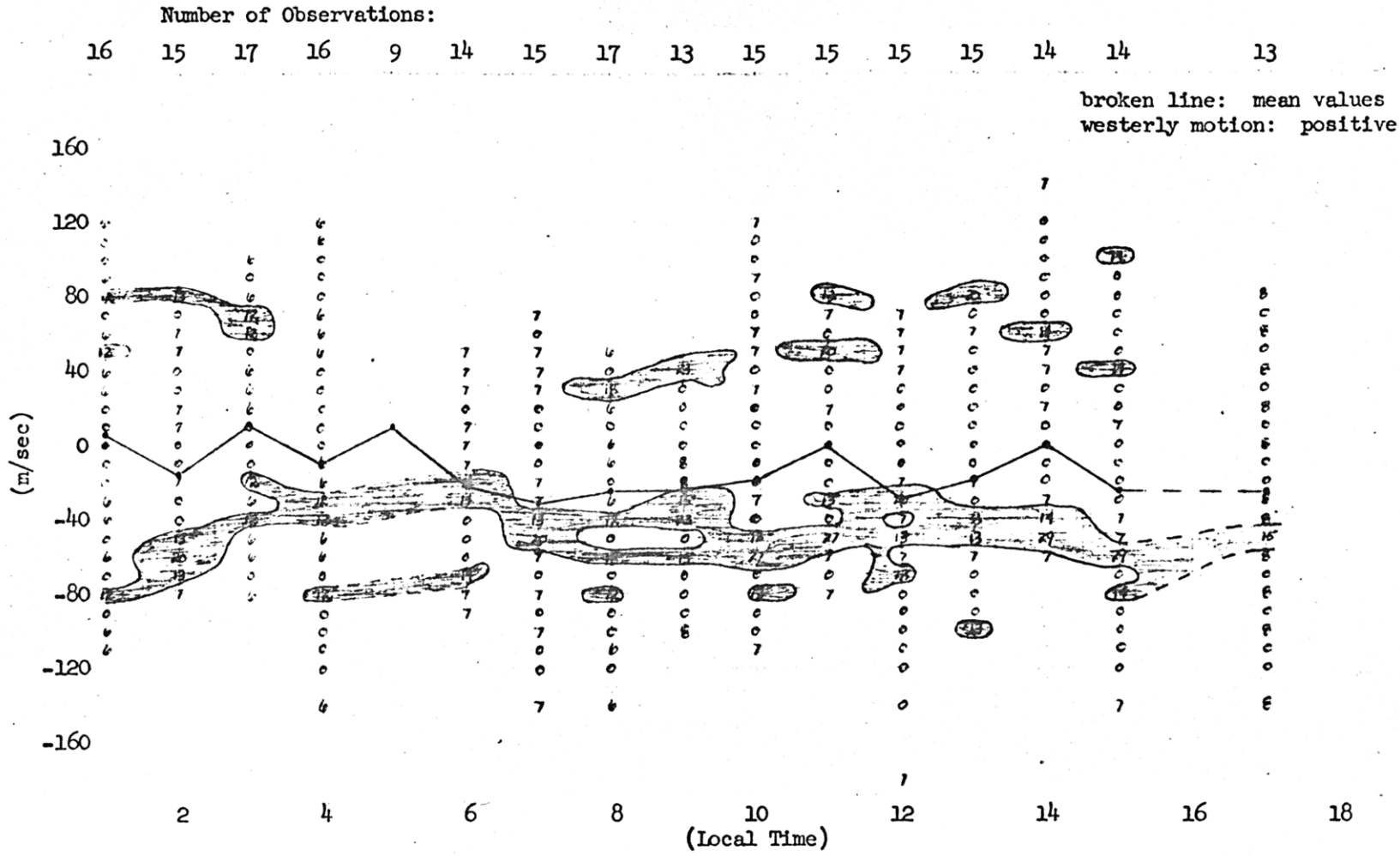

Figure 18a: Diurnal Variation of the West-East Component at Waltair (Oct-Nov-Dec)

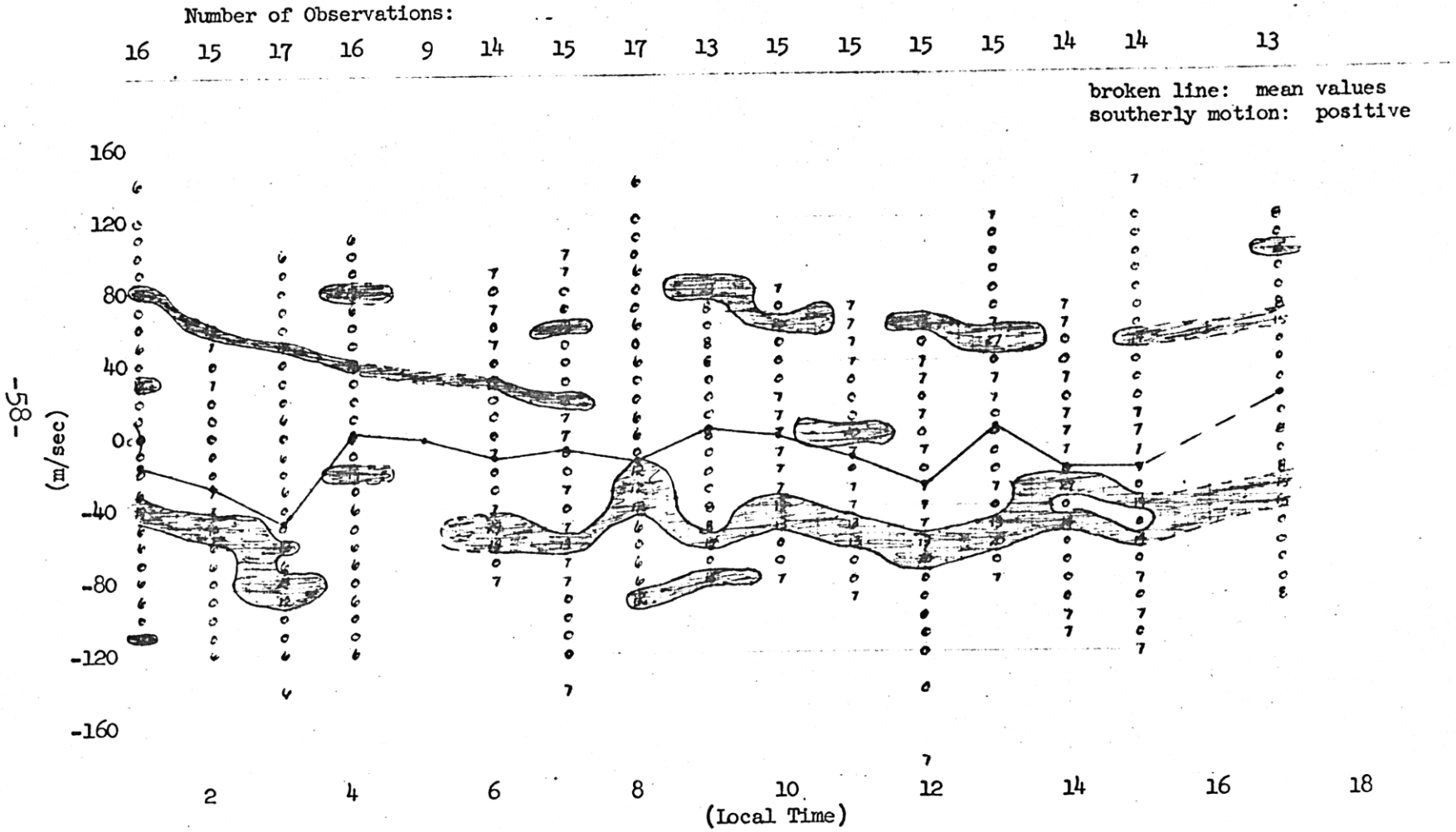

Figure 18b: Diurnal Variation of the South-North Component at Waltair (Oct-Nov-Dec)

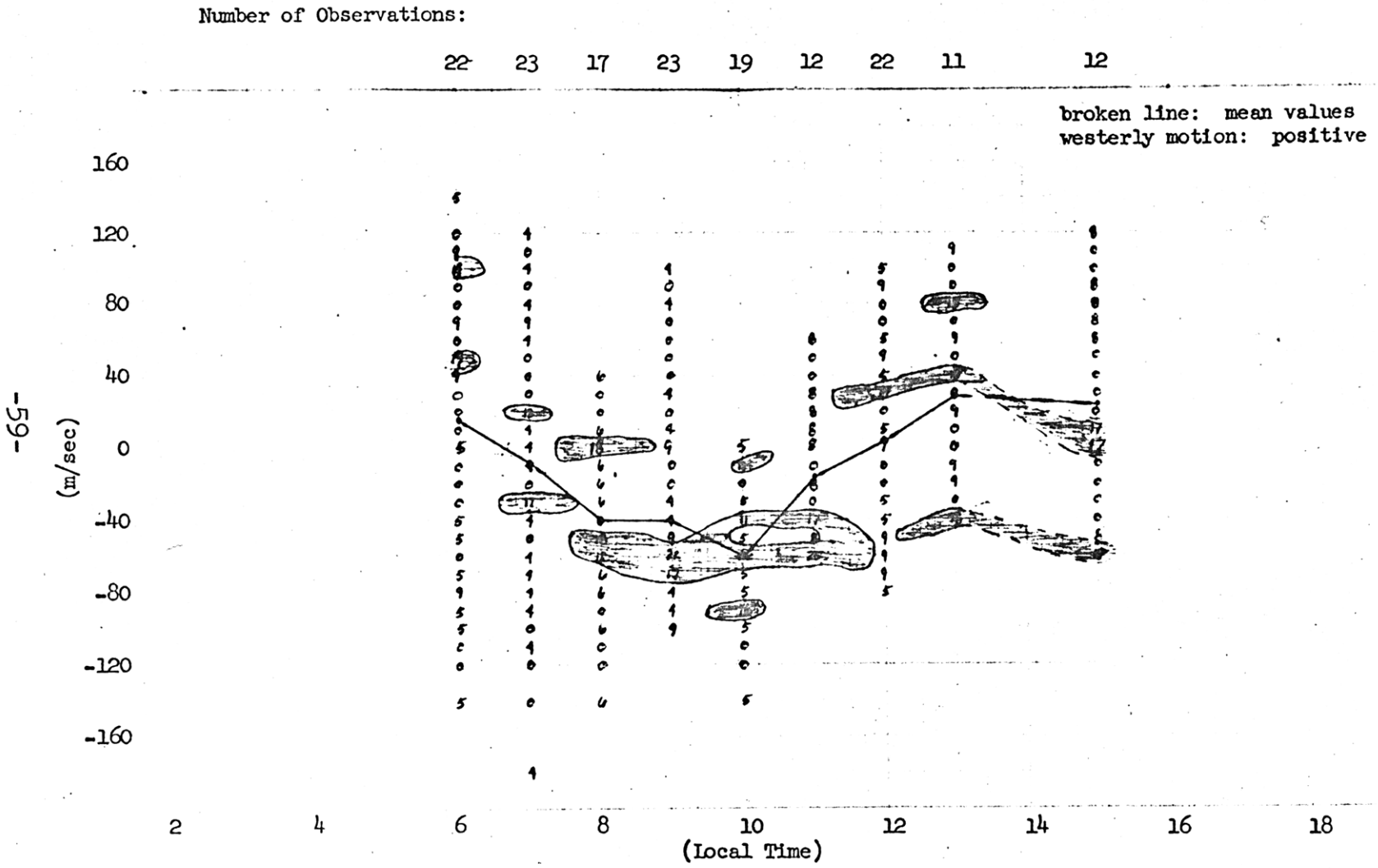

Figure 19a: Diurnal Variation of the West-East Component at Rostov (Oct-Nov-Dec)

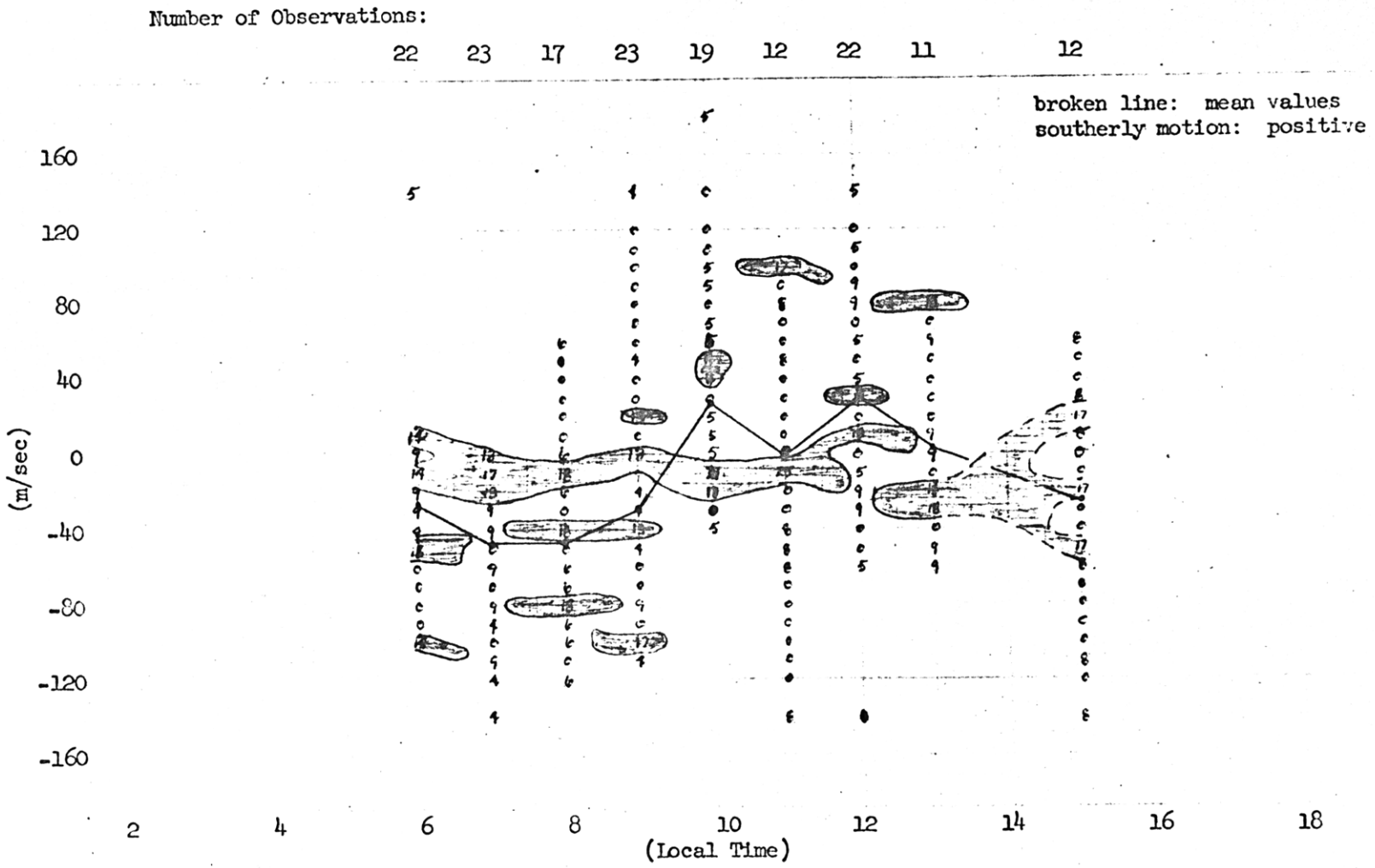

Figure 19b: Diurnal Variation of the South-North Component at Rostov (Oct-Nov-Dec)

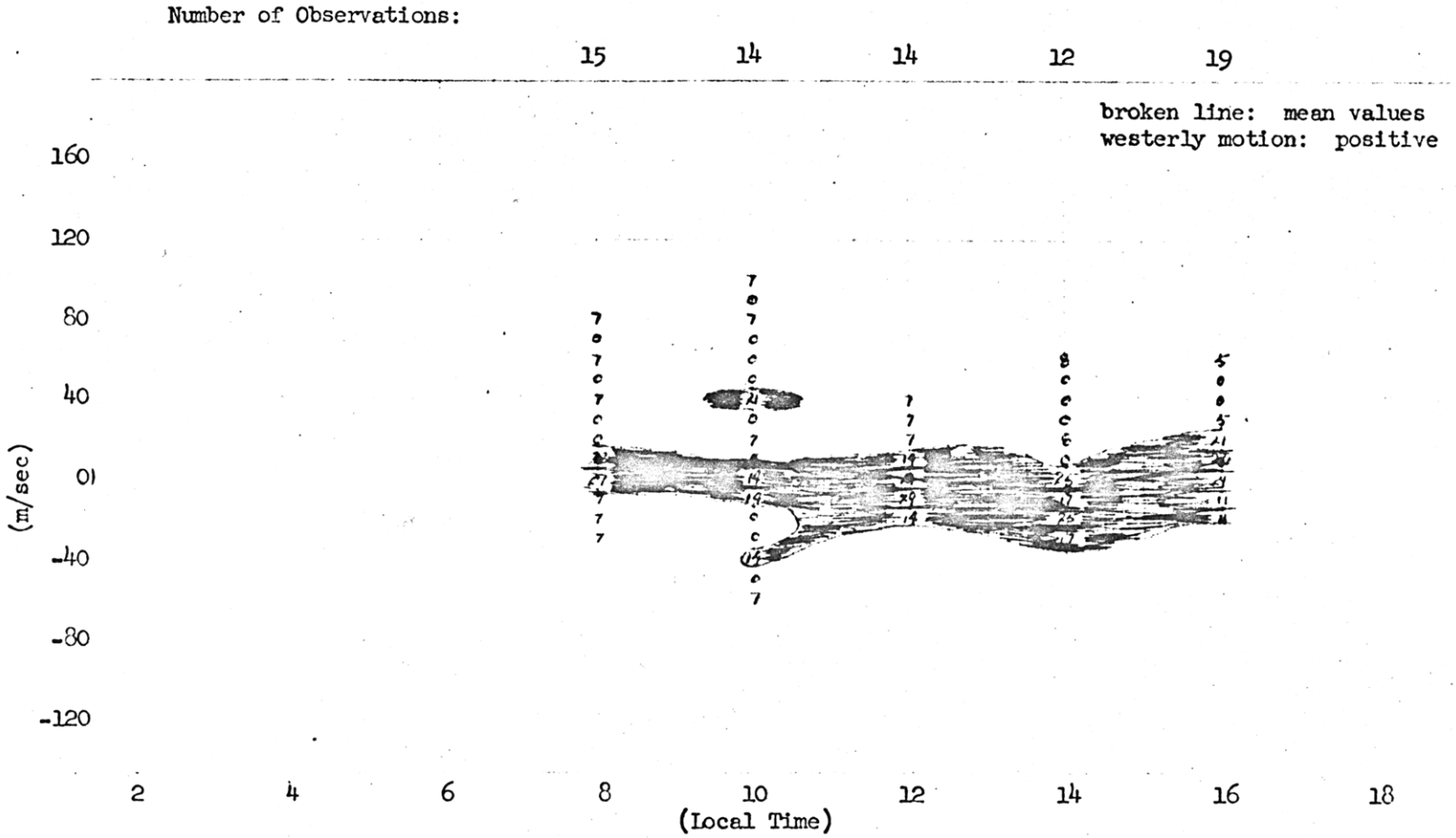

Figure 20a: Diurnal Variation of the West-East Component at Mayaguez (Jan-Feb-Mar)

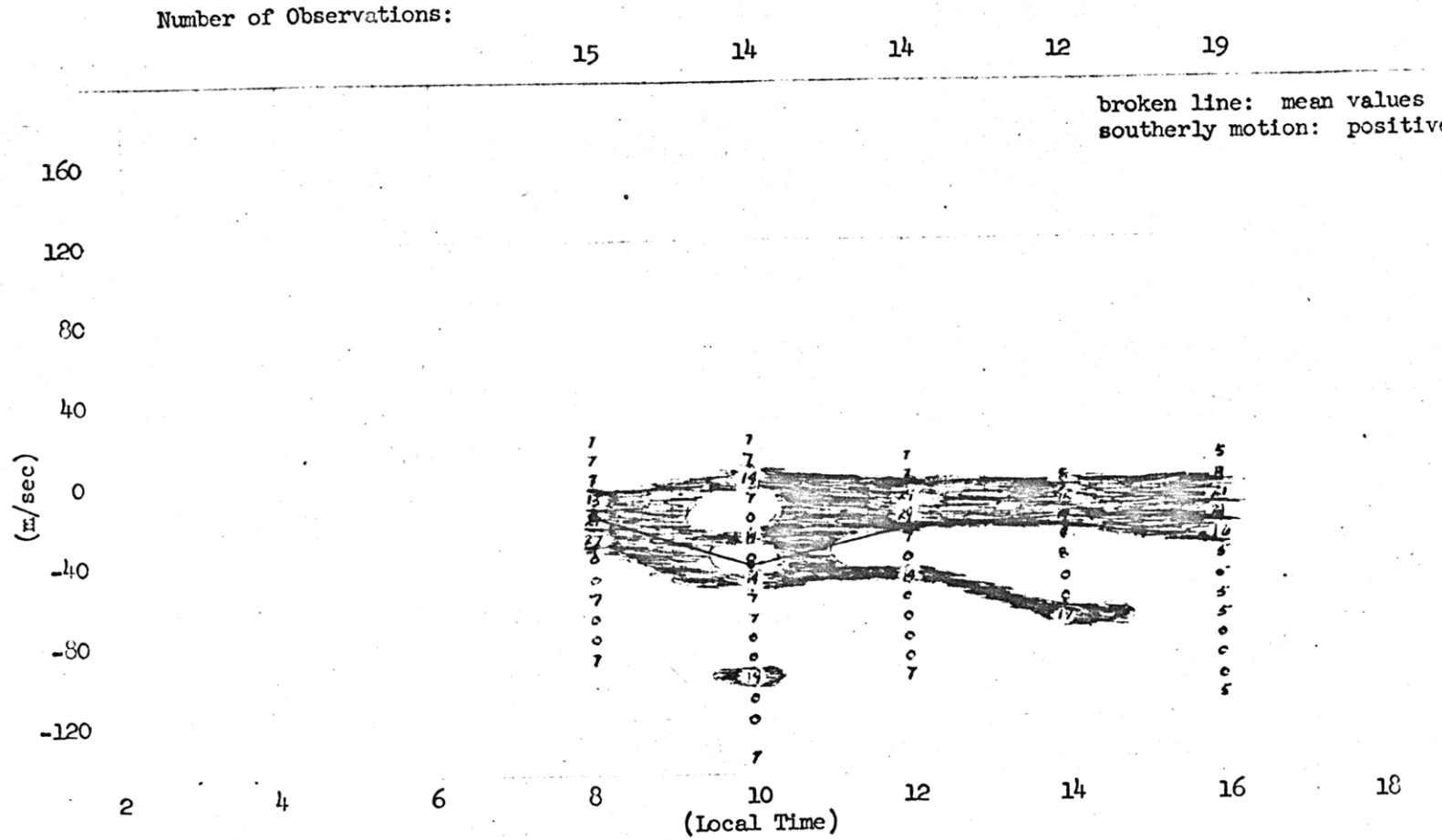

Figure 20b: Diurnal Variation of the South-North Component at Mayaguez (Jan-Feb-Mar)

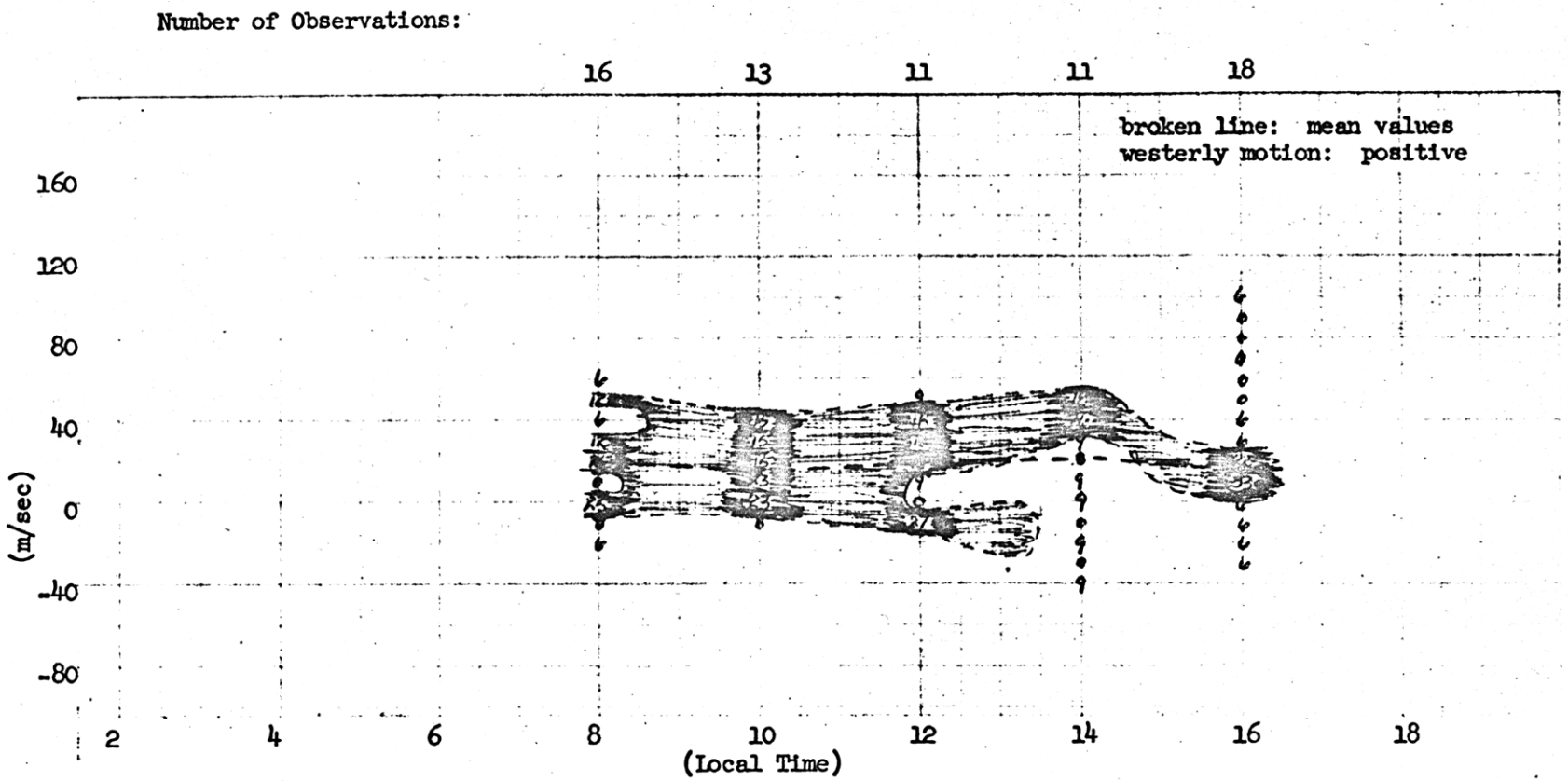

Figure 21a: Diurnal Variation of the West-East Component at Mayaguez (Apr-May-June)

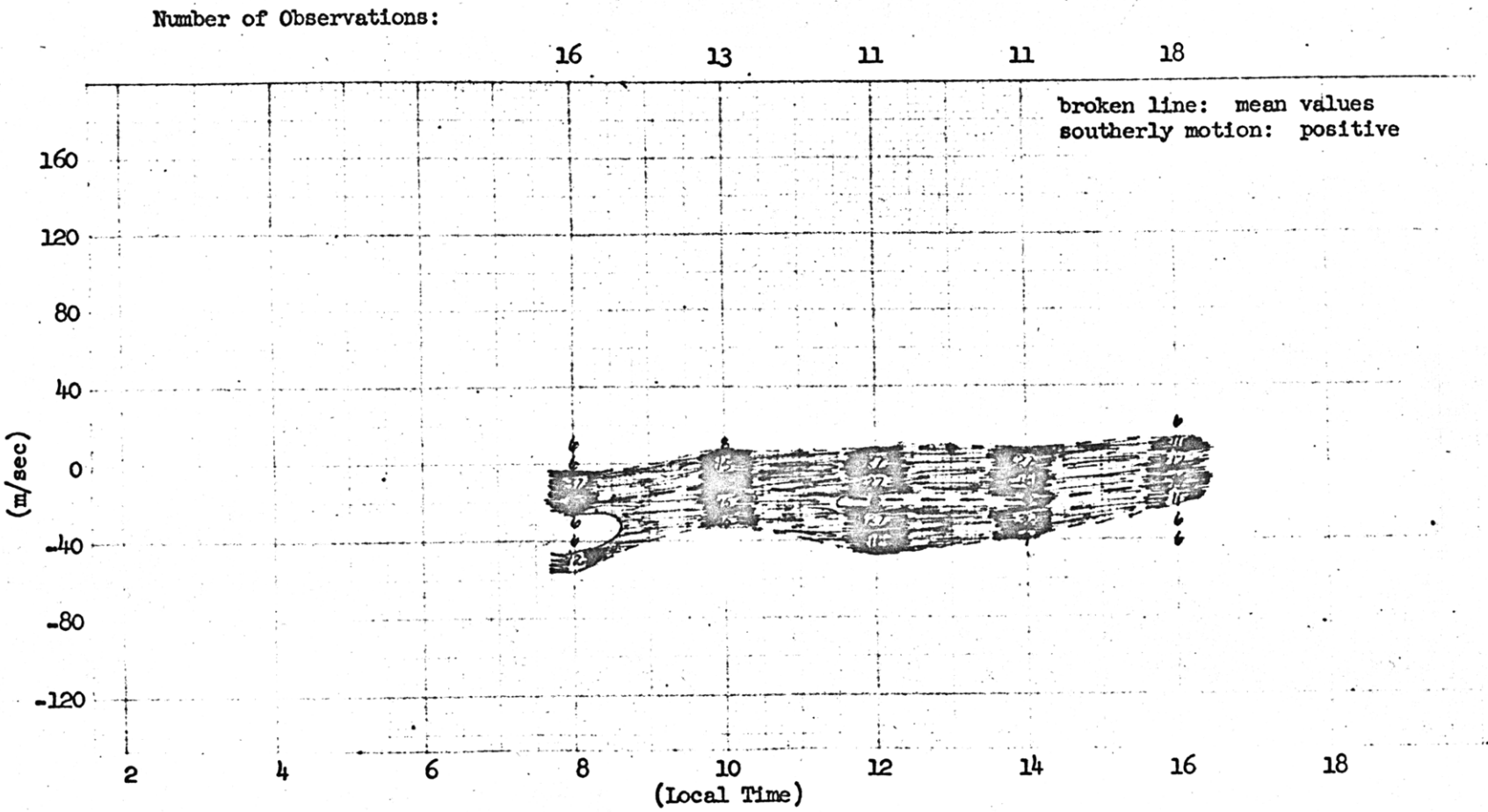

Figure 21b: Diurnal Variation of the South-North Component at Mayaguez (Apr-May-June)

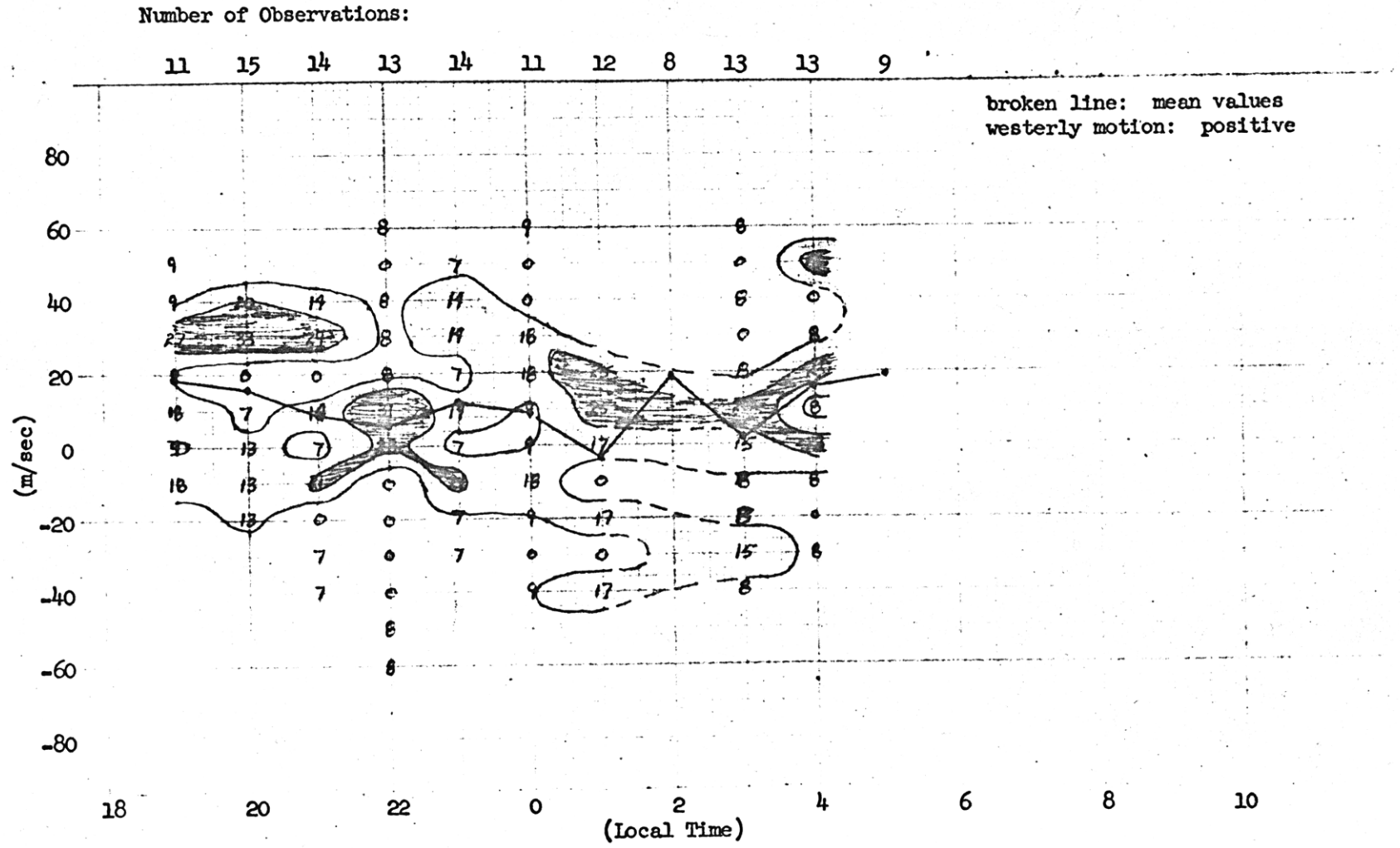

Figure 22a: Diurnal Variation of the West-East Component at the Pennsylvania State College (July-Aug-Sept)

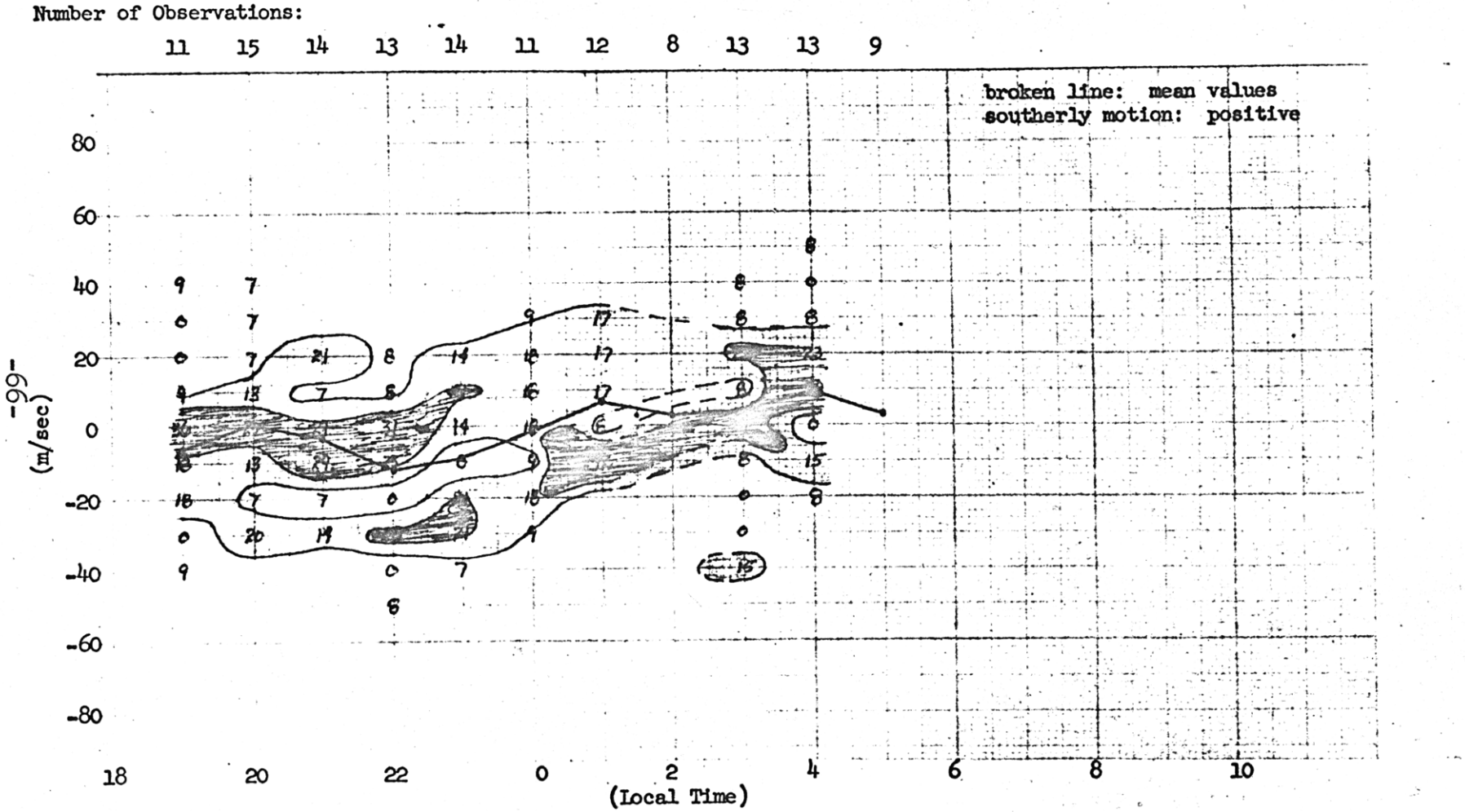

Figure 22b: Diurnal Variation of the South-North Component at the Pennsylvania State College (July-Aug-Sept)

B. Height Profiles of the Zonal Wind

Figures 23a through 23f were obtained by averaging the observations at a particular station over the summer (April through September) and winter (October through March) at the local time of each station. The averaging was accomplished for each height starting at 95 km and continuing for each 5 km up to 115 km. The results were then averaged around every 10°-latitudinal circle. All observations occur between 7° latitude and 70° latitude. Isolines refer to zonal motion in m/sec and are positive for westerlies.

During the morning the motion is generally easterly in the winter and westerly in the summer at 95 km (Figures 23b and 23c). In the afternoon the motion is easterly in both seasons below the 50° latitude (Figures 23d and 23e). In all figures except as shown in Figure 23d, the motion at 100 km and 105 km is independent of season below the 40° latitude. The figures show more variability at 110 km and 115 km with a generally westerly motion in both seasons. This variability should be expected since the number of observations are least at 110 km and 115 km.

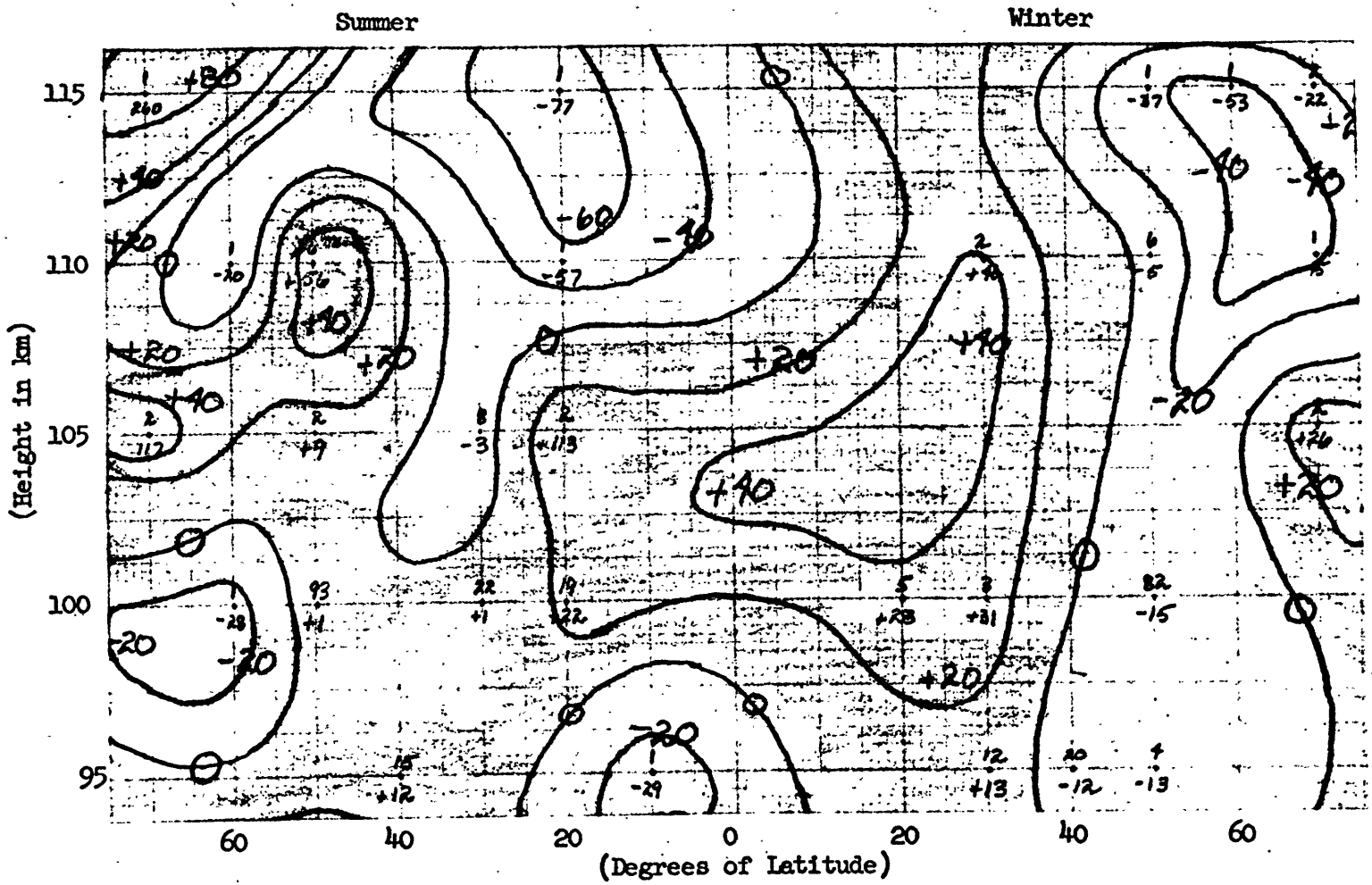

Figure 23a: Height Profile of the Zonal Wind at 0000 Local Time

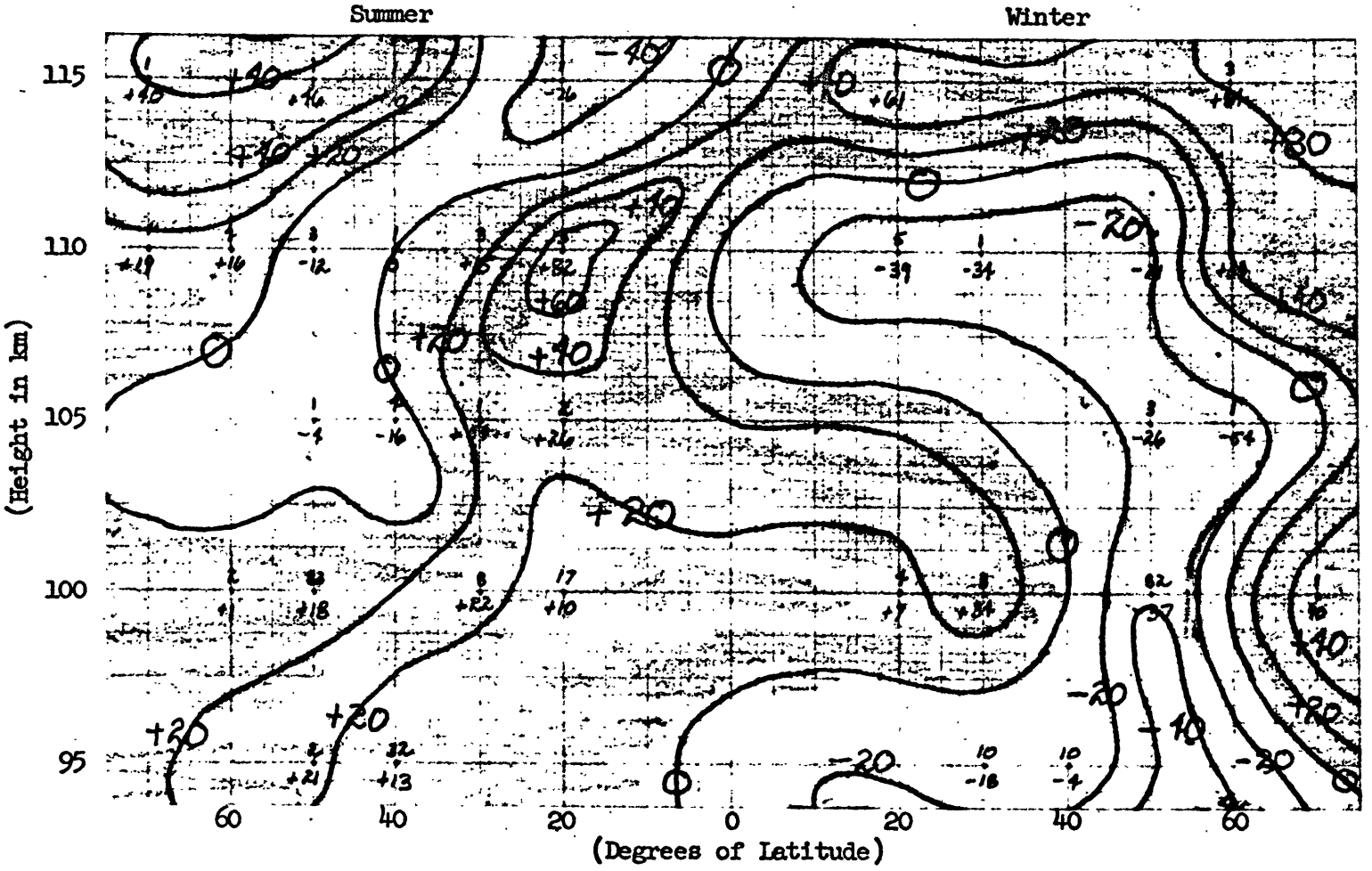

Figure 23b: Height Profile of the Zonal Wind at 0400 Local Time

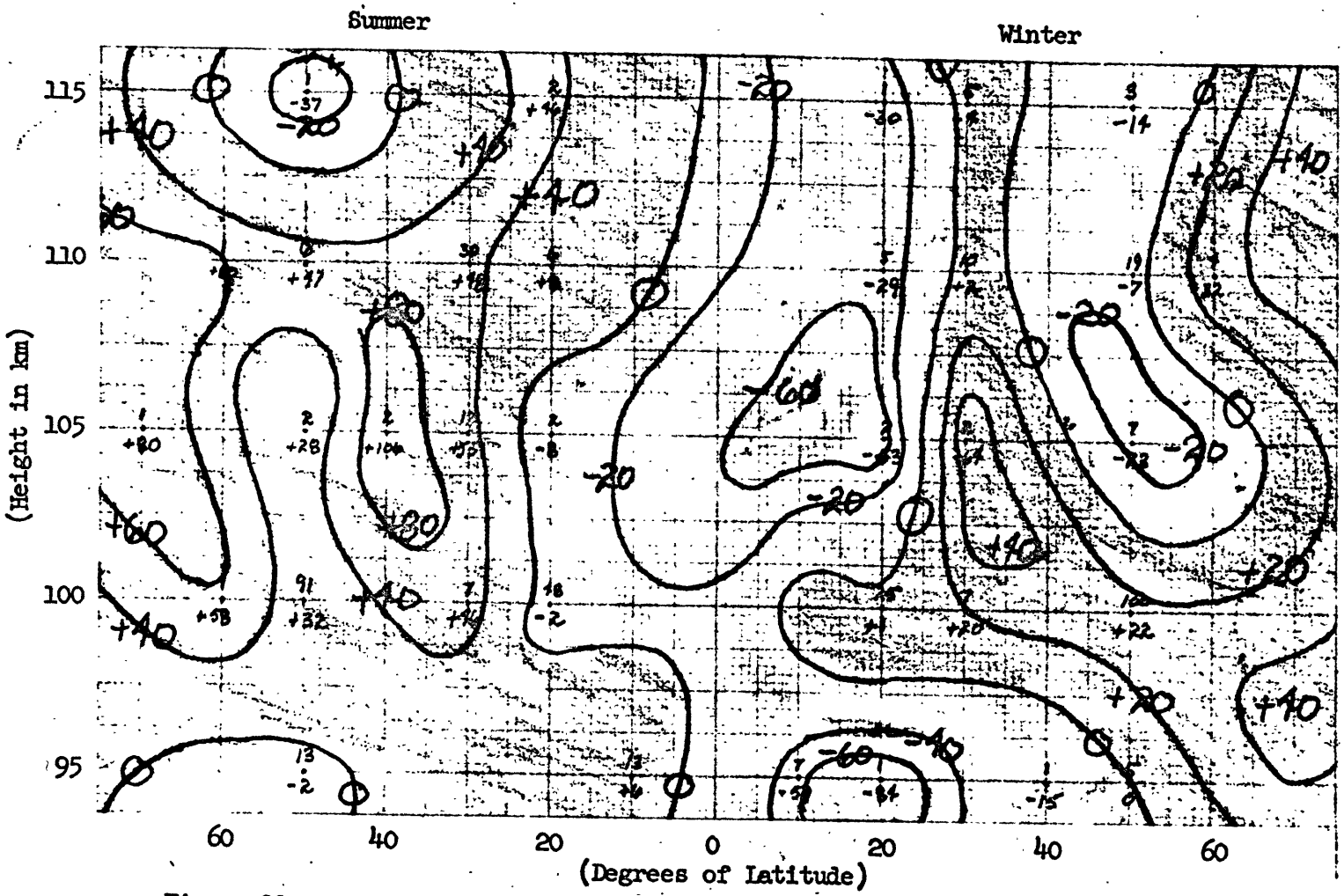

Figure 23c: Height Profile of the Zonal Wind at 0800 Local Time

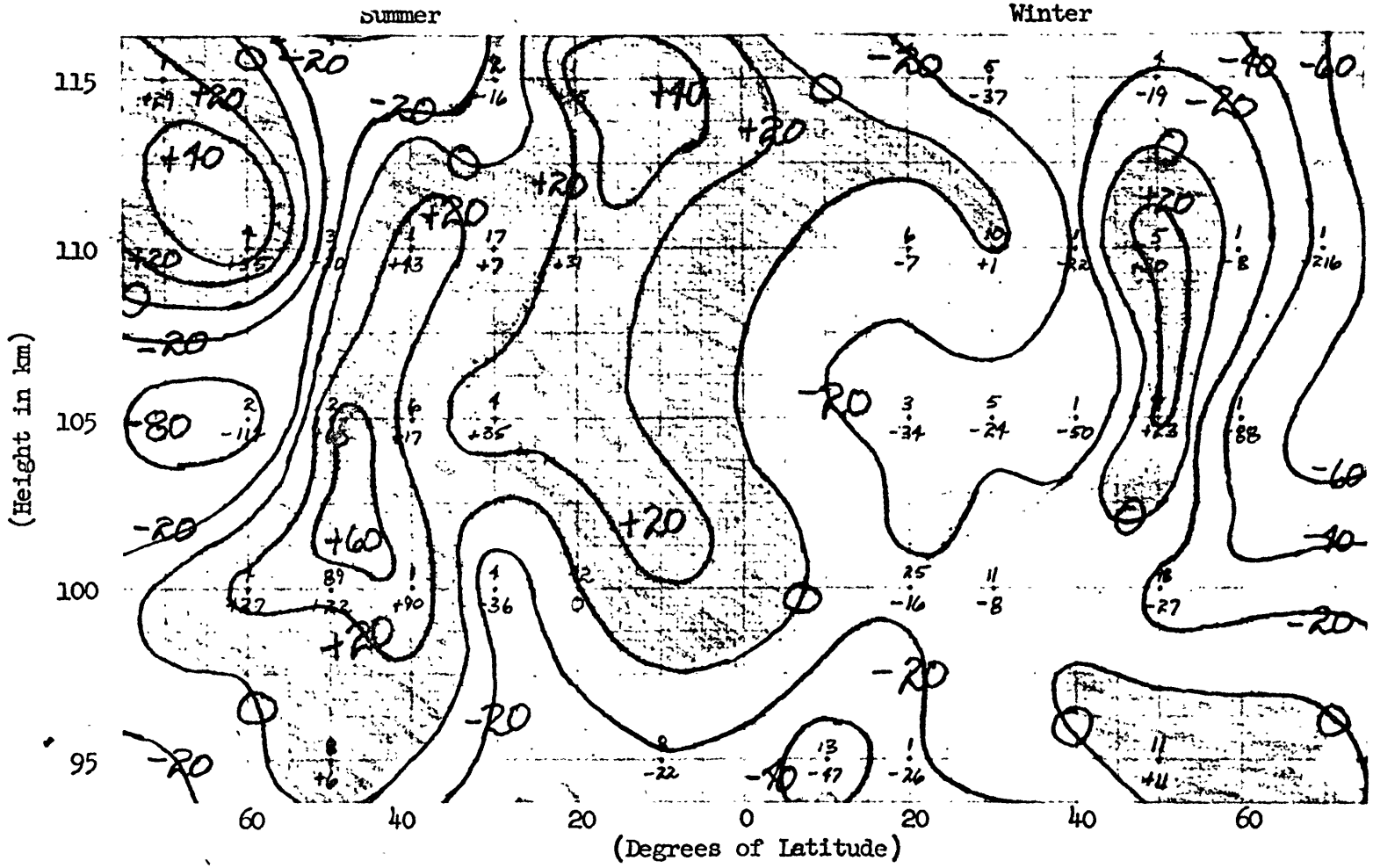

Figure 23d: Height Profile of the Zonal Wind at 1200 Local Time

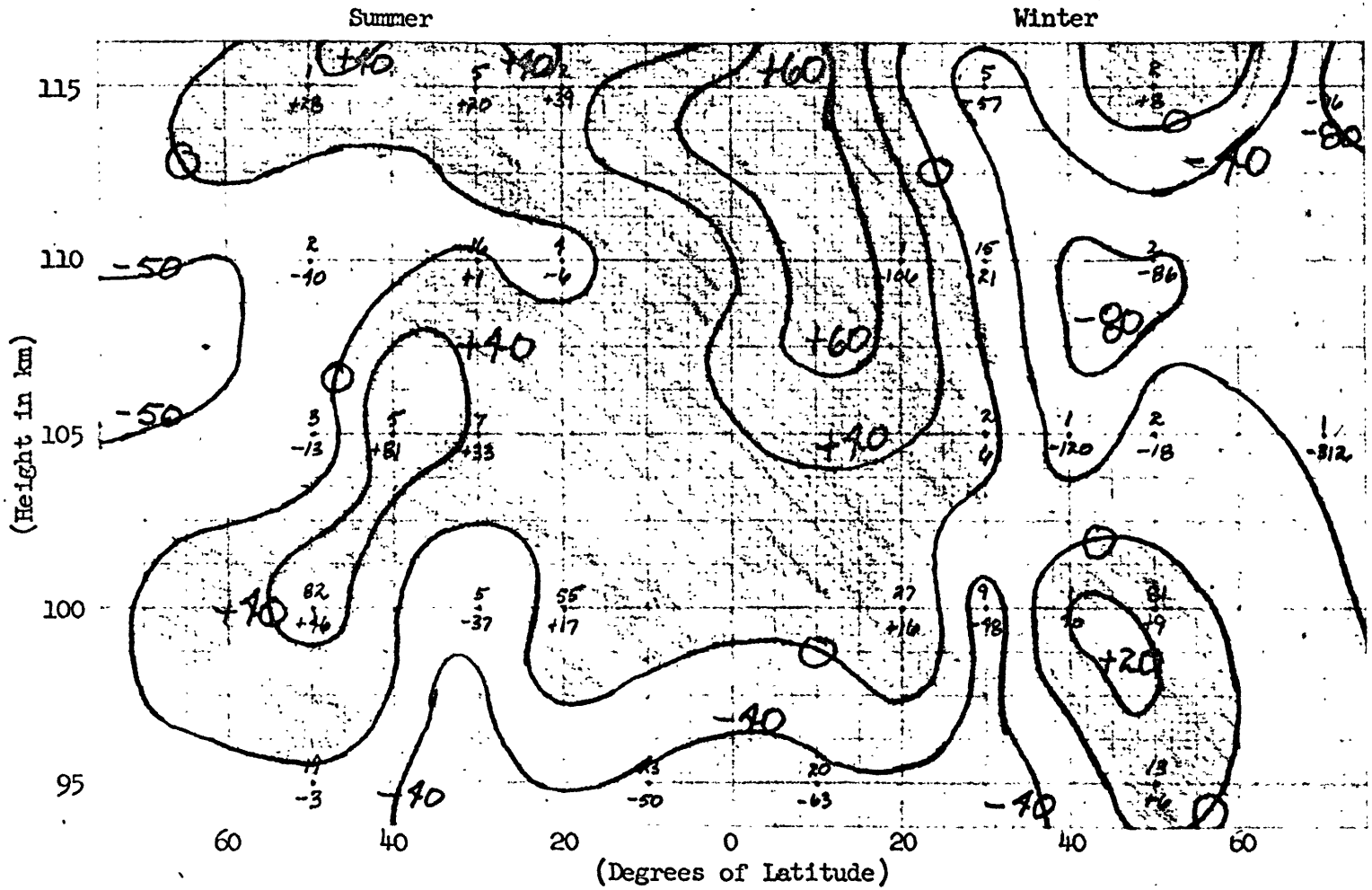

Figure 23e: Height Profile of the Zonal Wind at 1600 Local Time

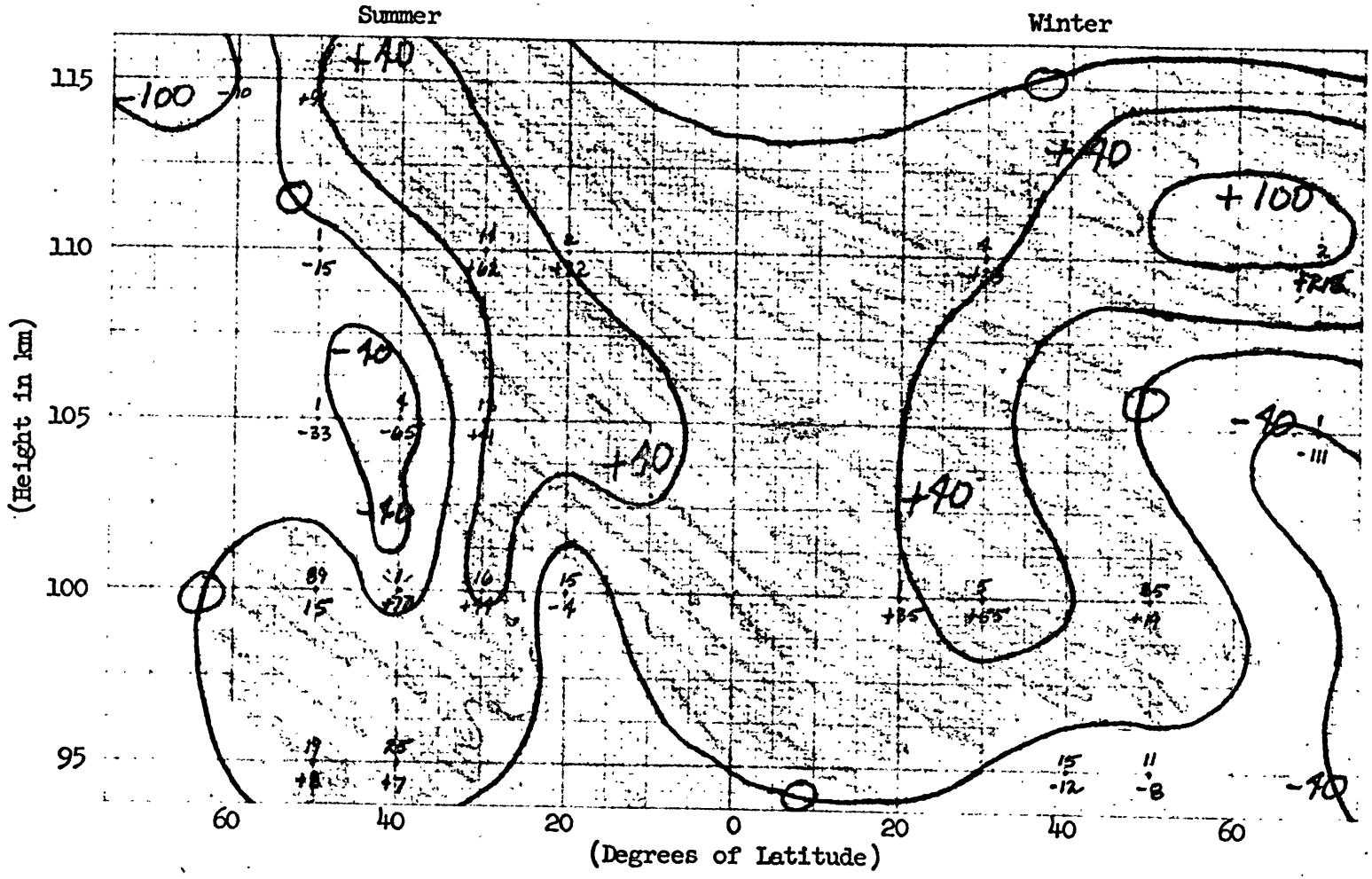

Figure 23f: Height Profile of the Zonal Wind at 2000 Local Time

C. Height Profile of the Prevailing Zonal Wind

A height profile of the zonal winds in the lower E-region is shown in Figure 24a. It was obtained by taking the point-for-point average of Figures 23a through 23f. A set of height profiles was also made from observations grouped according to universal time. The average of these figures is shown in Figure 24b. The two sets of observations were generally dissimilar. The differences between Figures 24a and 24b give an estimate of the error caused by incomplete coverage. The similarities give an estimate of the prevailing zonal wind in the lower E-region. Figure 24a was obtained from 2441 observations and Figure 24b was obtained from 2463 observations.

At 95 km the motion is westerly above 20° latitude in summer. It is easterly at all latitudes in the winter with a maximum at about 20° latitude. The prevailing wind at 100 km between 20° and 50° latitude is westerly in both summer and winter. Maxima of the westerlies occur about 50° latitude in the summer and about 30° latitude in the winter. There is a westerly maximum about 30° latitude in both seasons at 105 km. In winter the motion is easterly above 40° latitude. At 110 km the motion is westerly in summer with a maximum about 40° latitude. It is not clear which zonal motion predominates in winter although it is probably westerly to 40° latitude. The motion is generally westerly in summer and easterly in winter at 115 km.

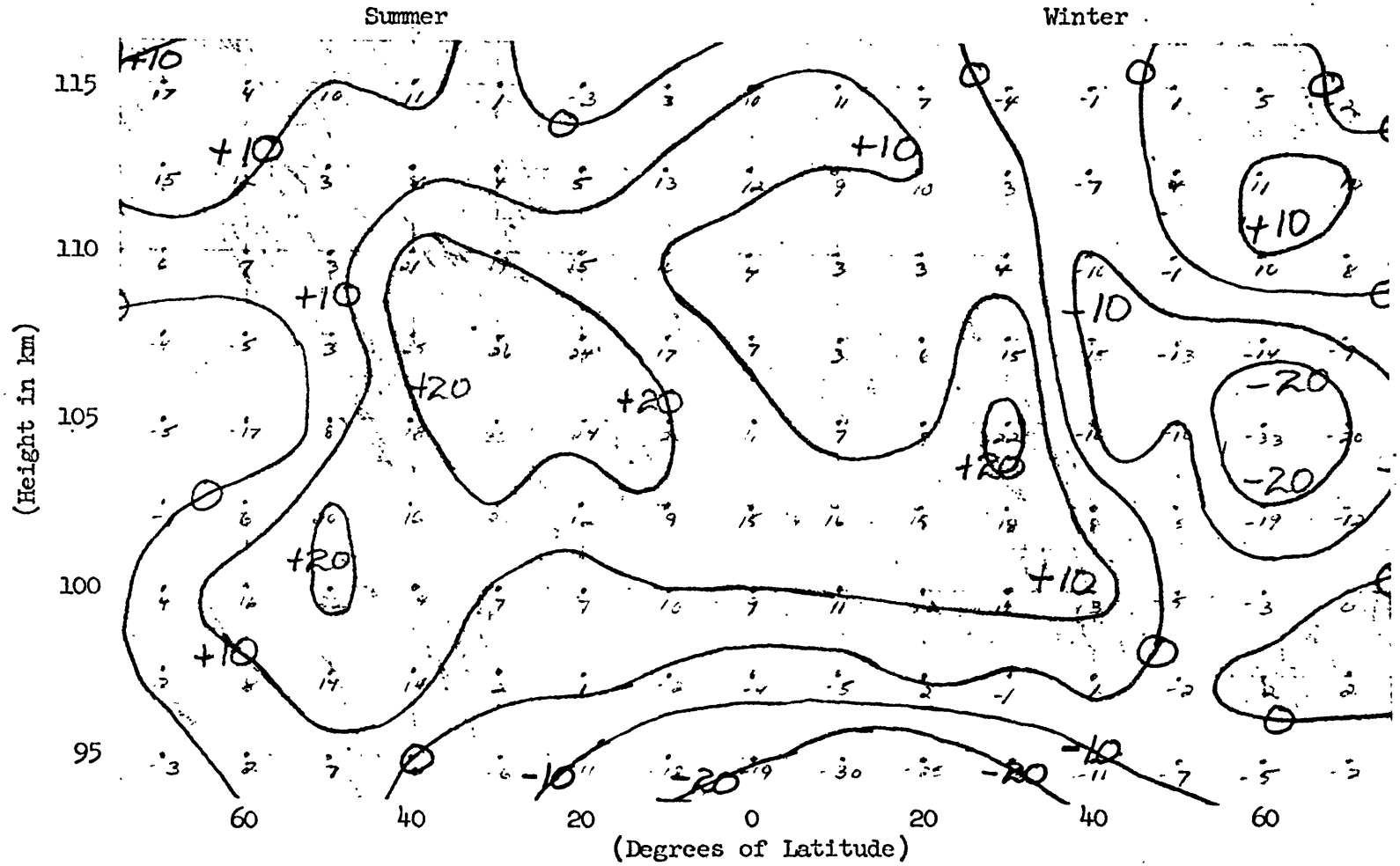

Figure 24a: Height Profile of the Prevailing Zonal Wind

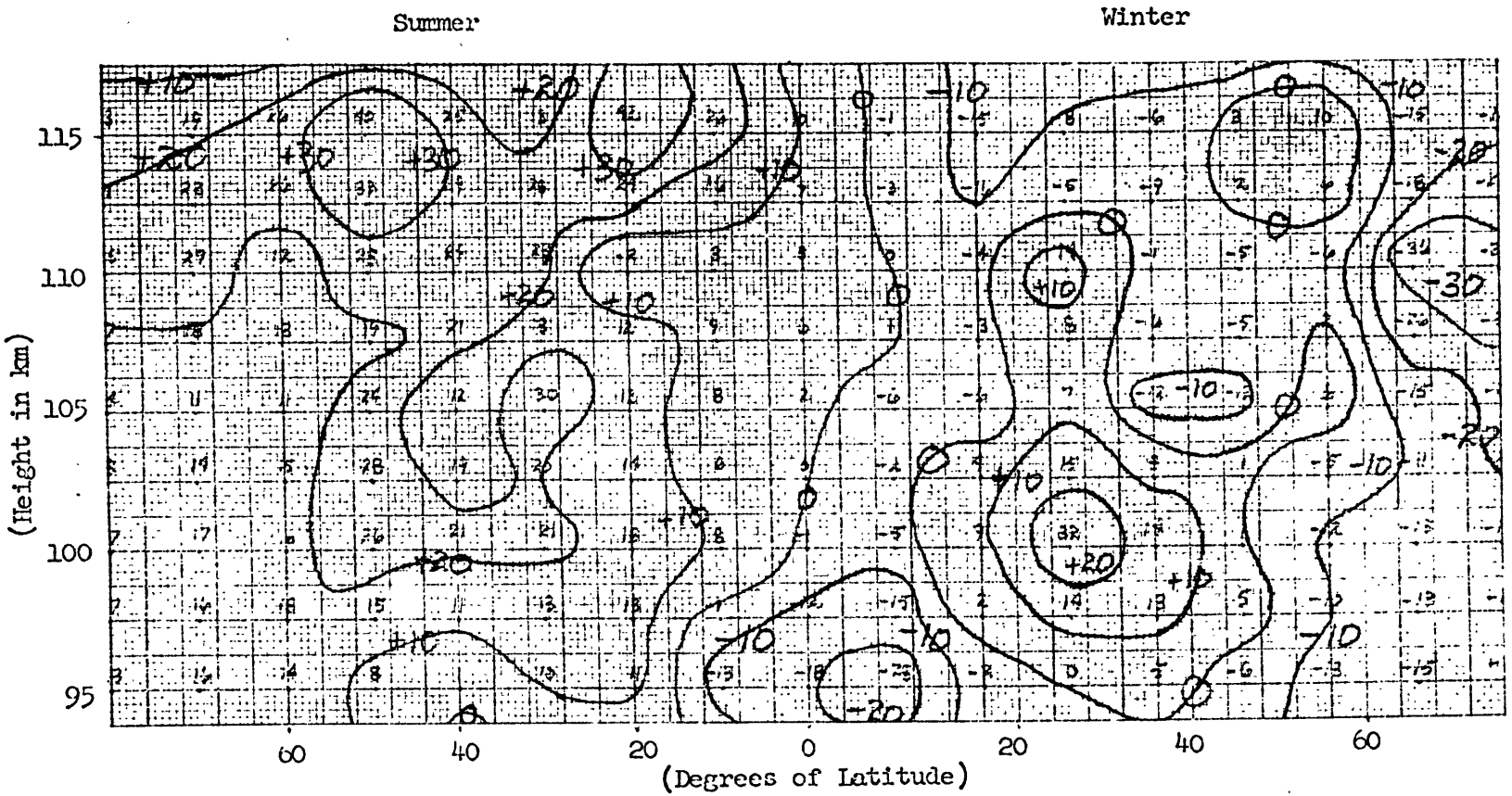

Figure 24b: Height Profile of the Prevailing Zonal Wind

D. Height Profiles of the Zonal Motion Without the Prevailing Component

The prevailing wind (Figure 24a) is subtracted point for point from the total wind (Figures 23a through 23f) to give the diurnal variation of the tidal motion (Figures 25a through 25f). In the summer the large region of easterly motion at 0000 LT (Figure 25a) is considerably reduced in magnitude and scope by 0400 LT (Figure 25b). At 0800 LT (Figure 25c) this region shows strong westerlies. The westerlies are weaker at 1200 LT (Figure 25d) with parts of the region becoming easterly again. At 1600 LT (Figure 25e) the region of westerly motion intensifies but the general shape of the region remains the same. A strong easterly region appears at 2000 LT replacing the westerly region in the previous figure.

Figure 25a shows that the motion is westerly below 40° latitude in the winter. This is basically opposite to the motion in the summer. There is almost a complete reversal in the motion four hours later above 105 km, as shown in Figure 25b. Below 105 km the easterly region intensifies. At 0800 LT (Figure 25c) the motion is strong easterly below 30° latitude. By 1200 LT (Figure 25d) the motion is almost entirely easterly and of lessened intensity. Figure 25e shows that easterly motion again becomes intensified with a strong westerly motion appearing at low latitudes above 100 km. The motion is almost entirely westerly in Figure 25f.

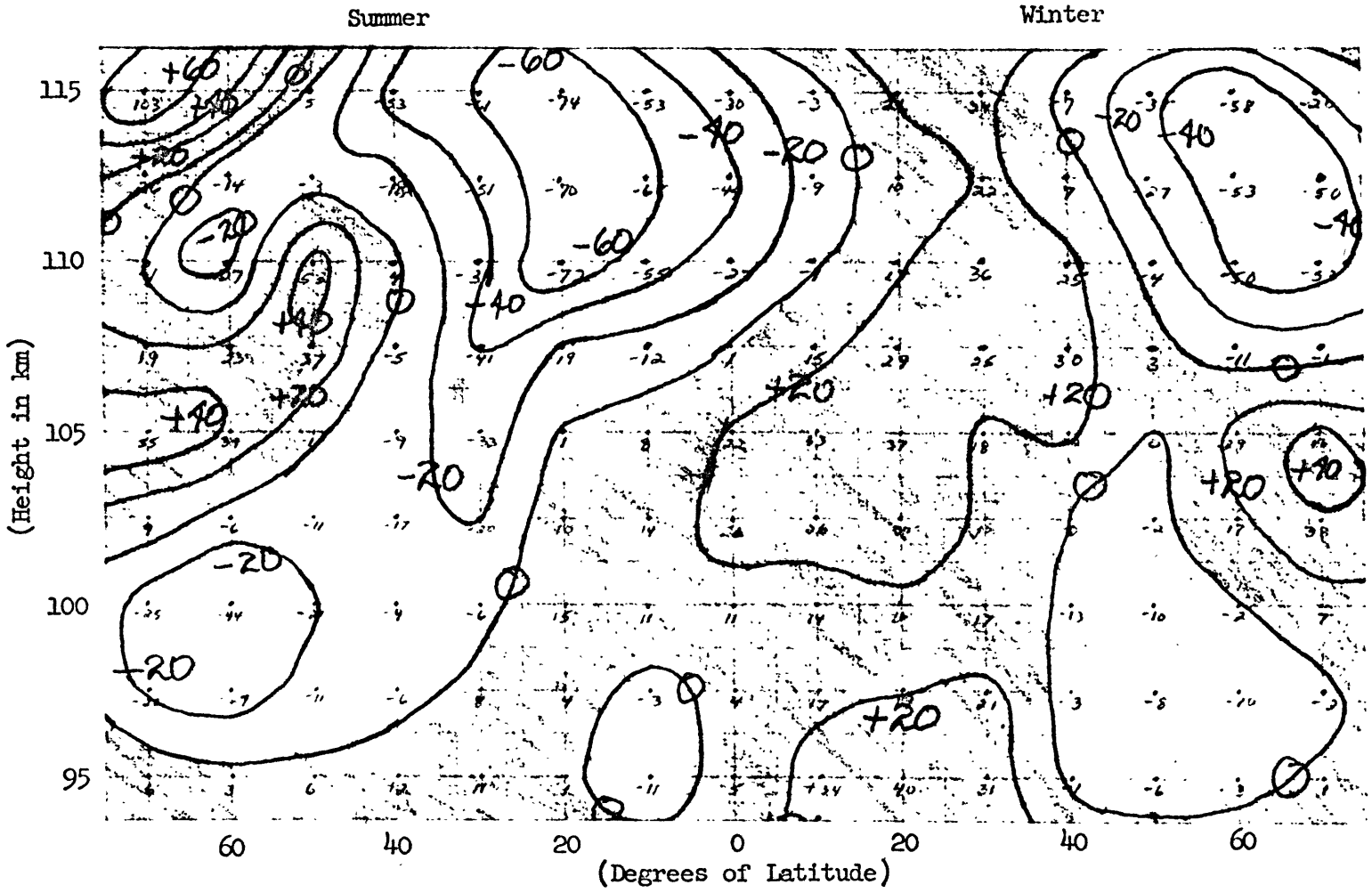

Figure 25a: Height Profile of the Zonal Wind Without the Prevailing Component at 0000 Local Time

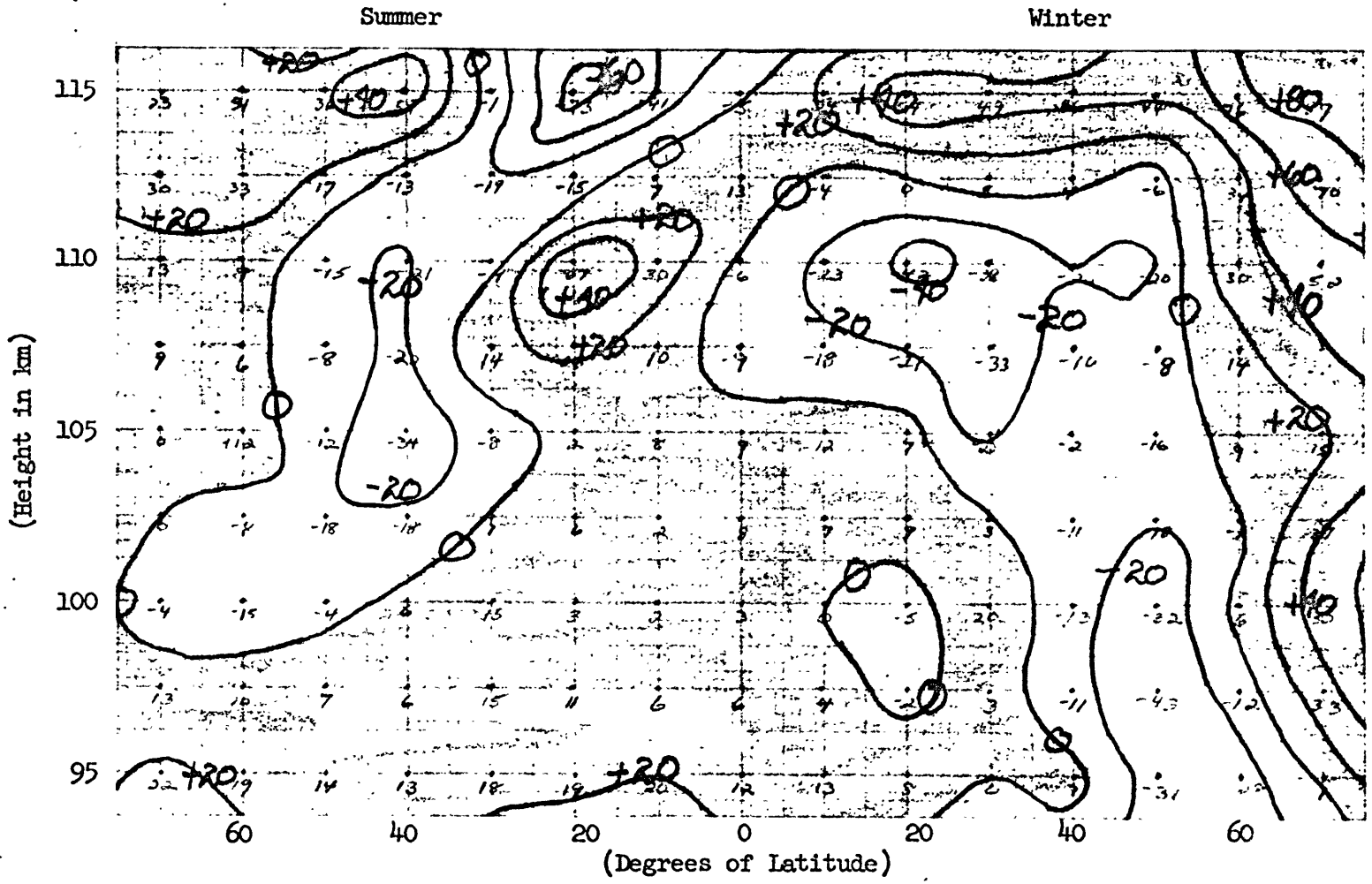

Figure 25b: Height Profile of the Zonal Wind Without the Prevailing Component at 0400 Local Time

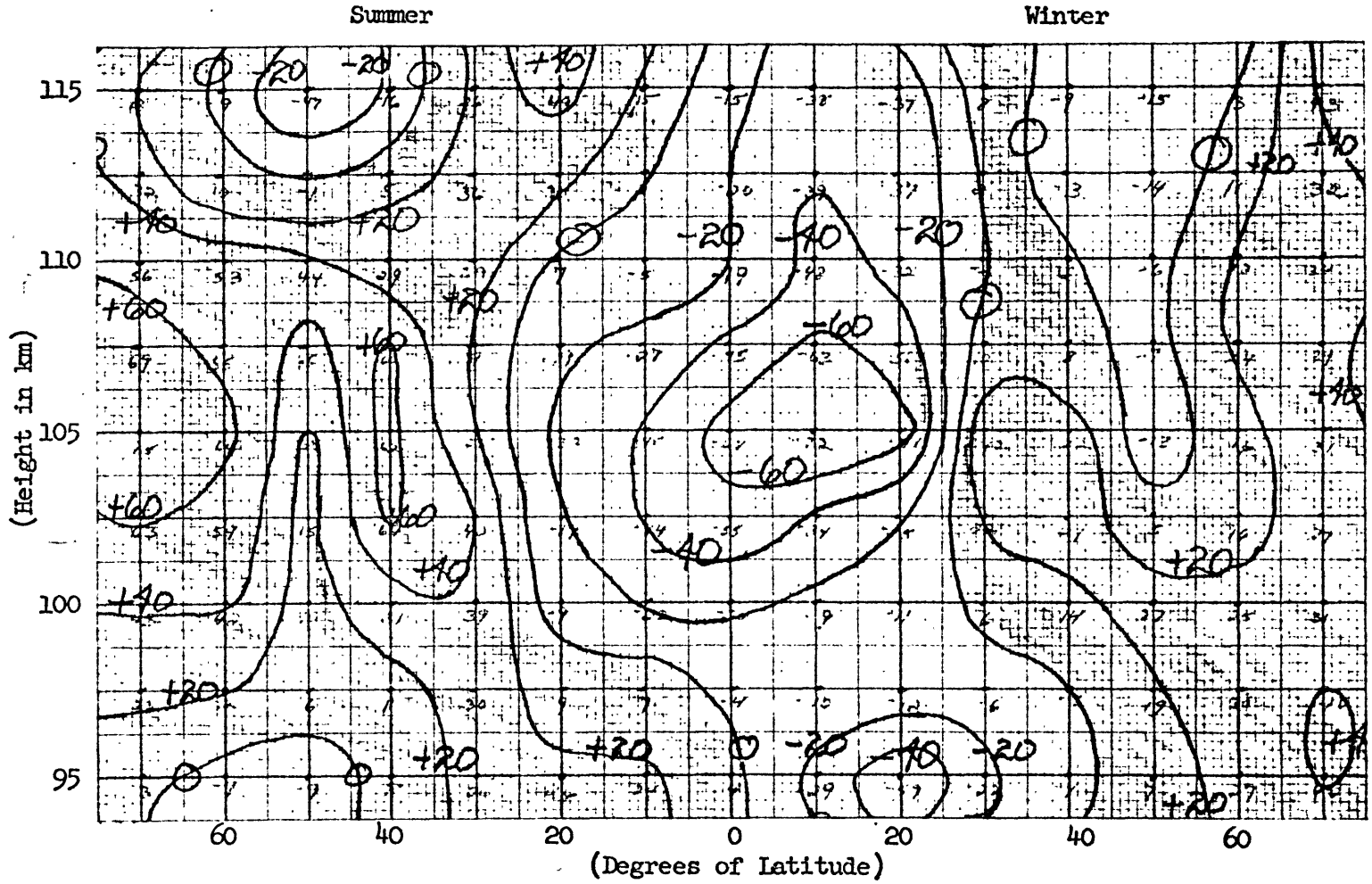

Figure 25c: Height Profile of the Zonal Wind Without the Prevailing Component at 0800 Local Time

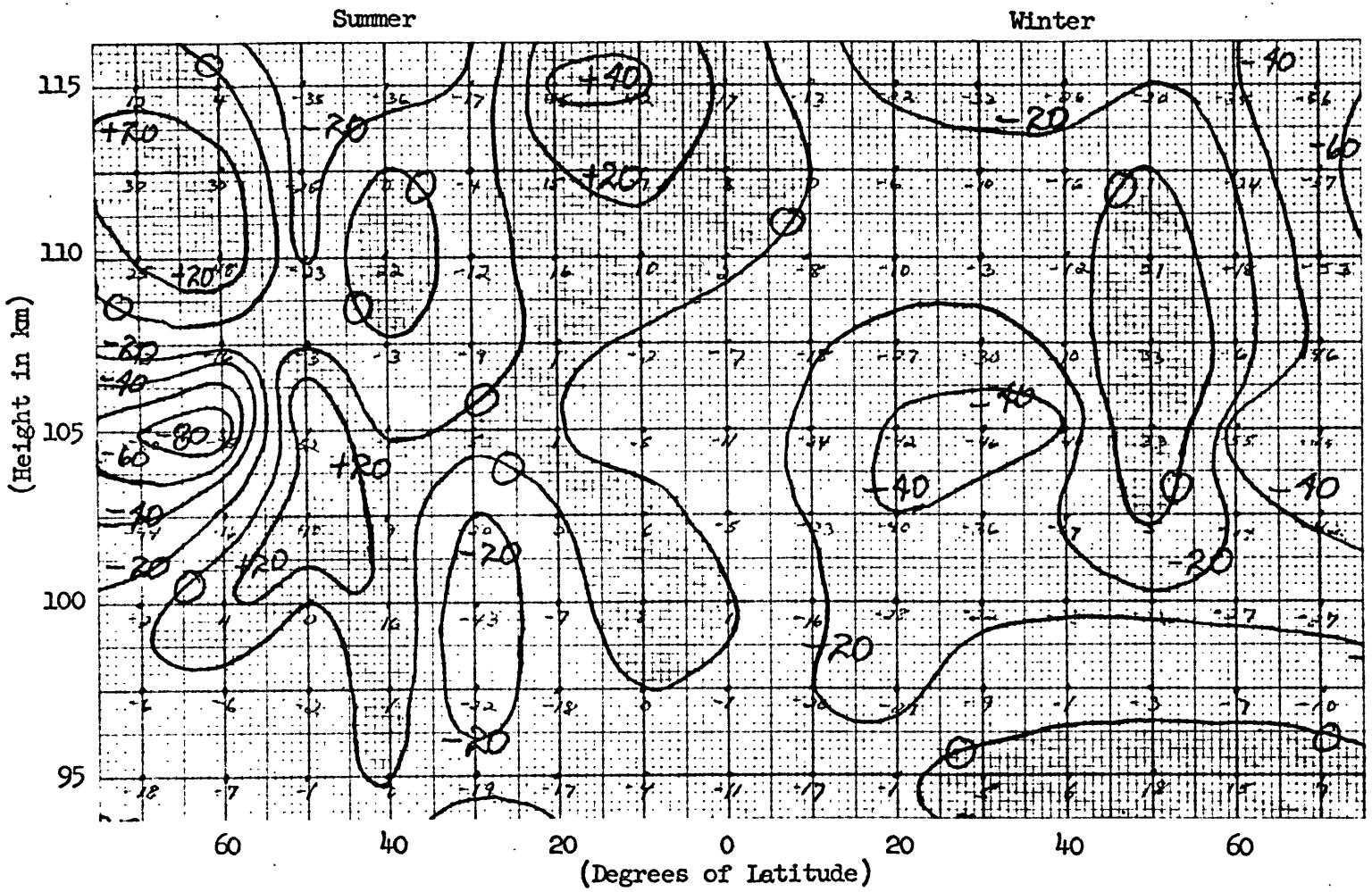

Figure 25d: Height Profile of the Zonal Wind Without the Prevailing Component at 1200 Local Time

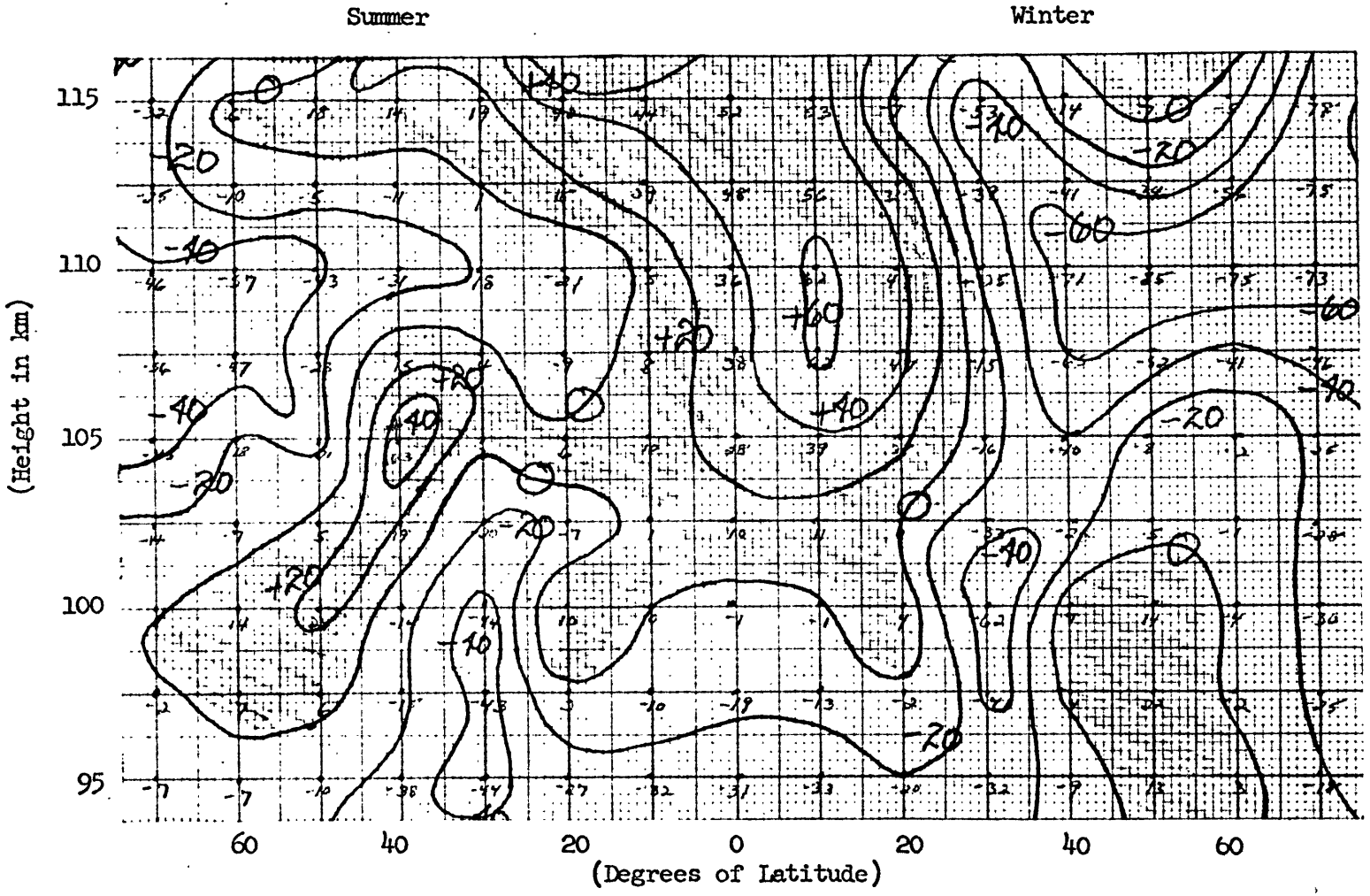

Figure 25e: Height Profile of the Zonal Wind Without the Prevailing Component at 1600 Local Time

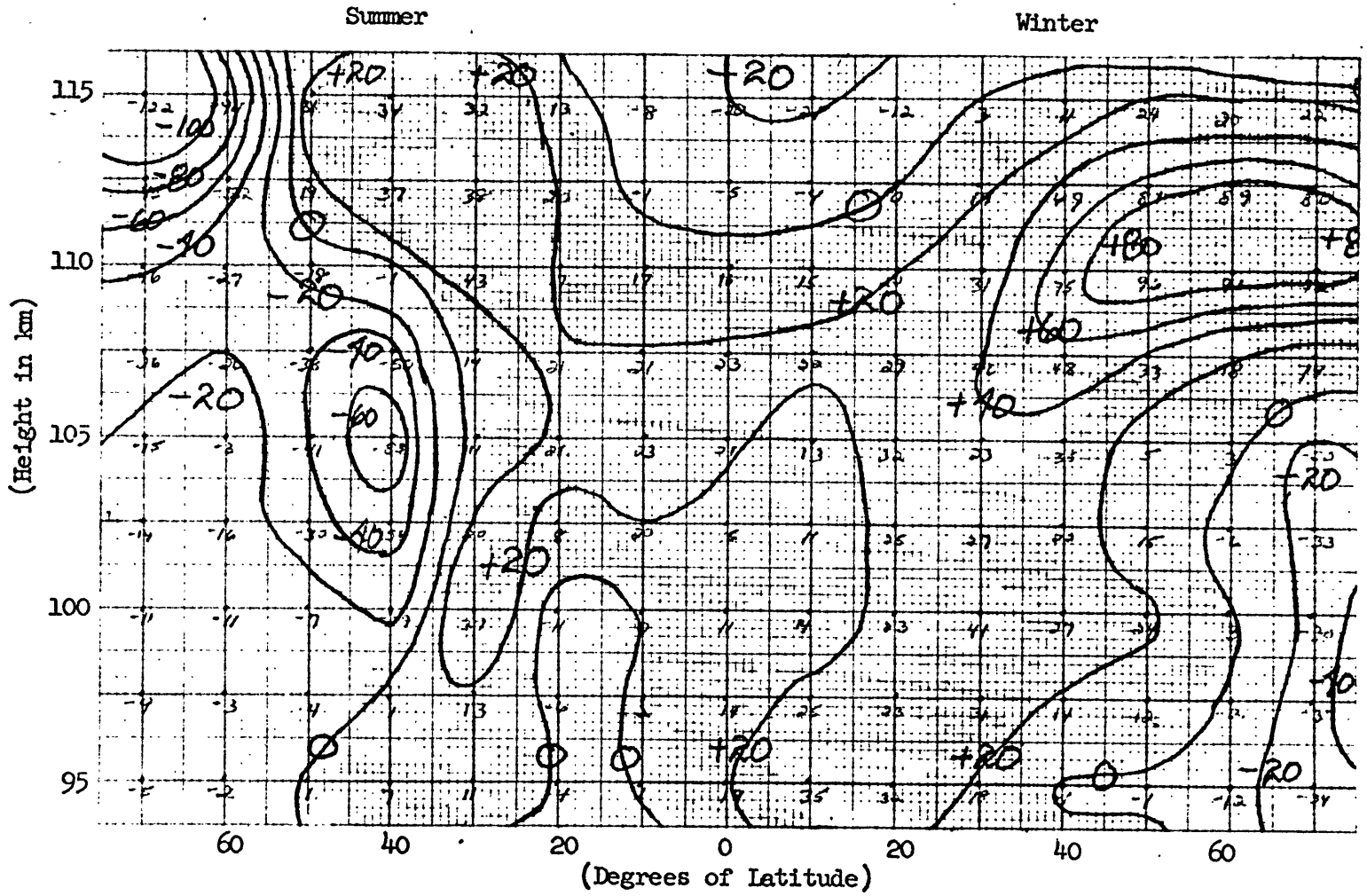

Figure 25f: Height Profile of the Zonal Wind Without the Prevailing Component at 2000 Local Time

E. Hemispheric Zonal and Meridional Prevailing Motion

Figures 26a and 26b show the hemispheric zonal prevailing wind in winter and summer. Figures 26c and 26d show the prevailing meridional wind for the same periods. The location of each station given in Table 1 is shown along with the number of observations and value of the motion. In addition, the results from Jodrell Bank (Greenhow and Neufeld, 1961) have also been placed on the figures. This has been labeled JB in the figures. It is seen in all figures that the results obtained from Jodrell Bank are in good agreement with the data analyzed in this thesis.

The general outline of the zonal prevailing wind is towards strong easterlies or weak westerlies in winter. The summer zonal motion becomes strong westerly or in some cases weak easterly where it had been strong easterly (Figure 26b). There was a certain amount of freedom in drawing the isolines. However, there is the appearance of standing waves in the figures. This is more true in Figures 26c and 26d, which show the meridional prevailing wind. The position of the standing wave remains consistent from winter to summer. The wave number may be one or two (or both).

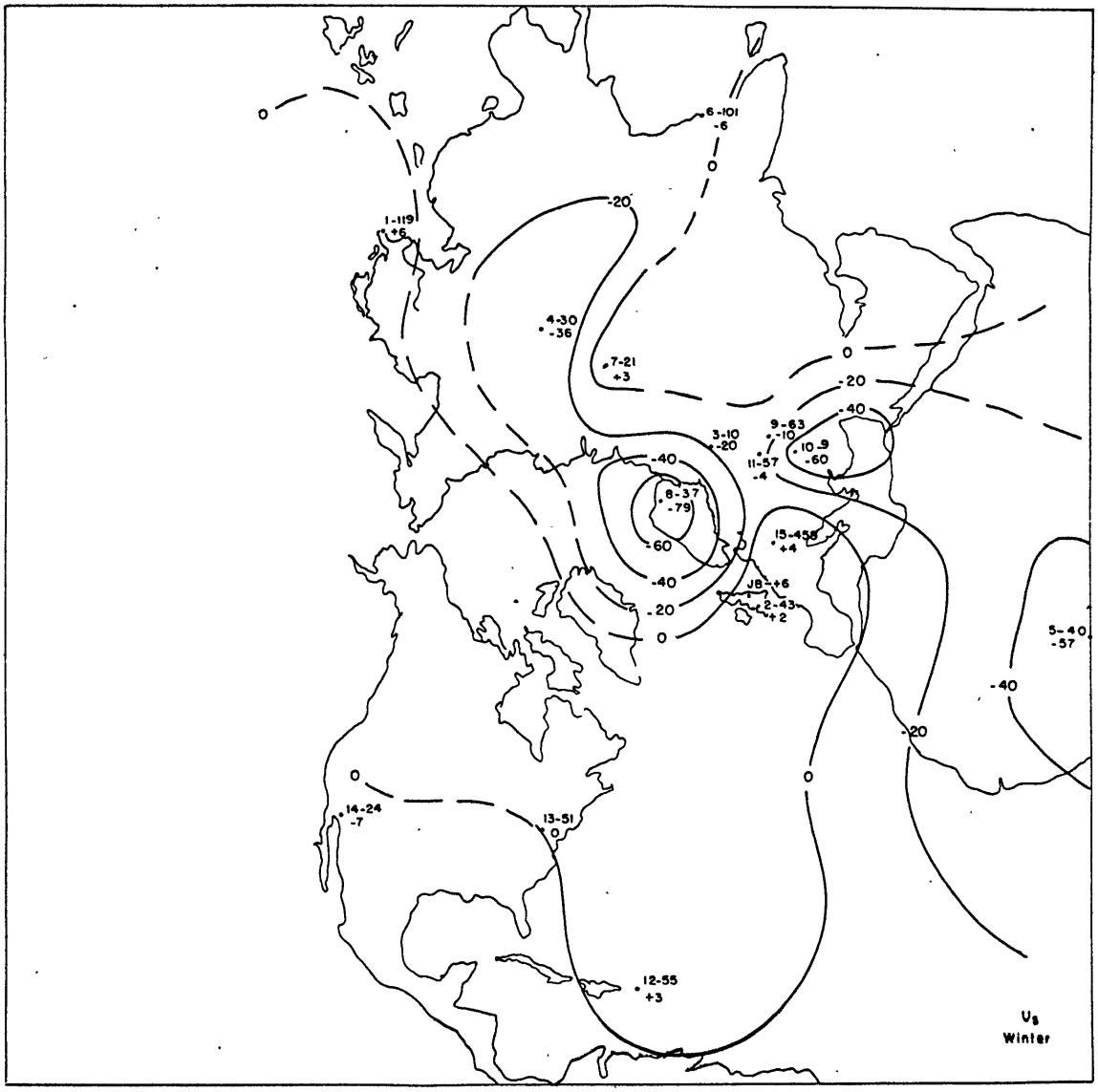

Figure 26a. Hemispheric Map of the Prevailing Zonal Winds in the Winter

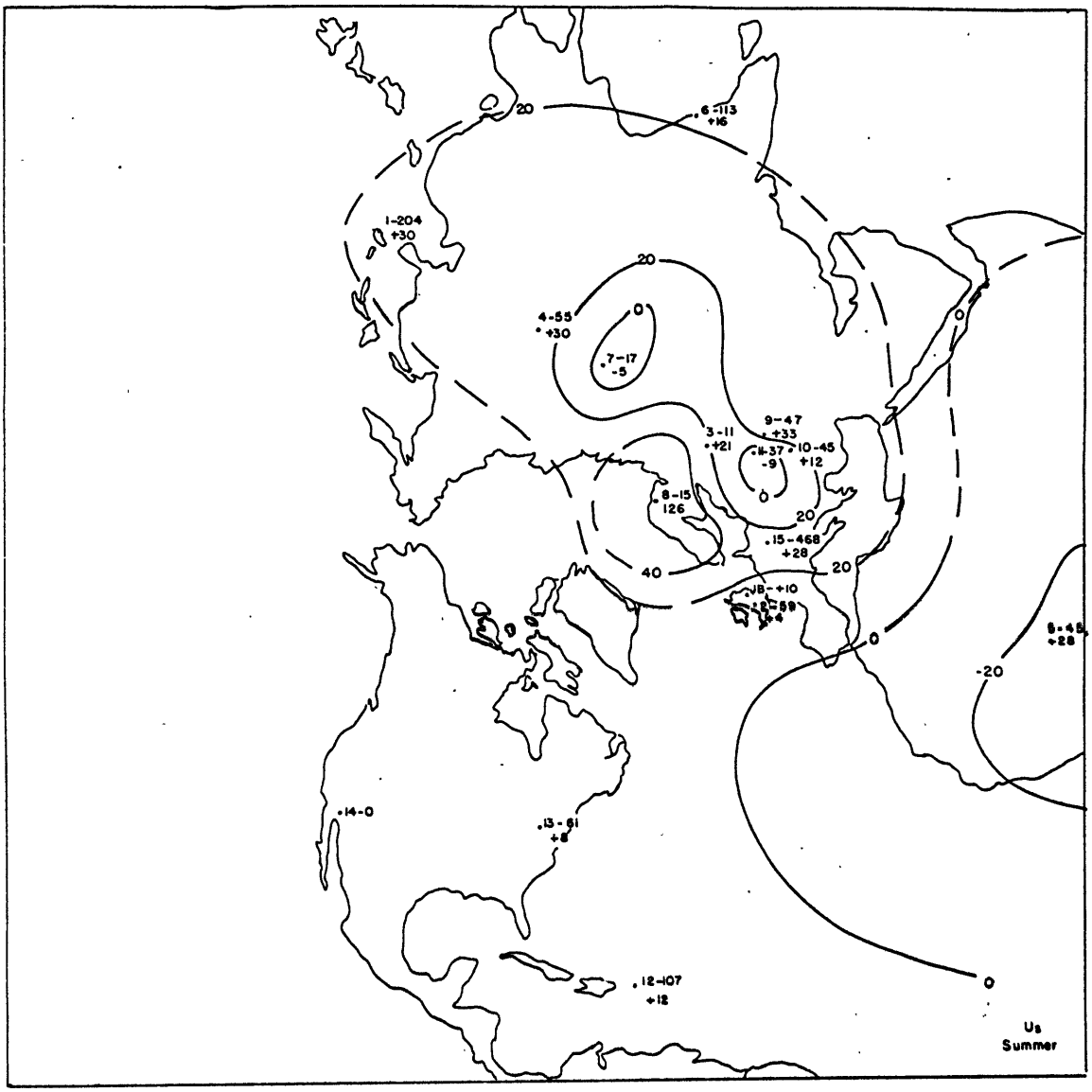

Figure 26b. Hemispheric Map of the Prevailing Zonal Winds in the Summer

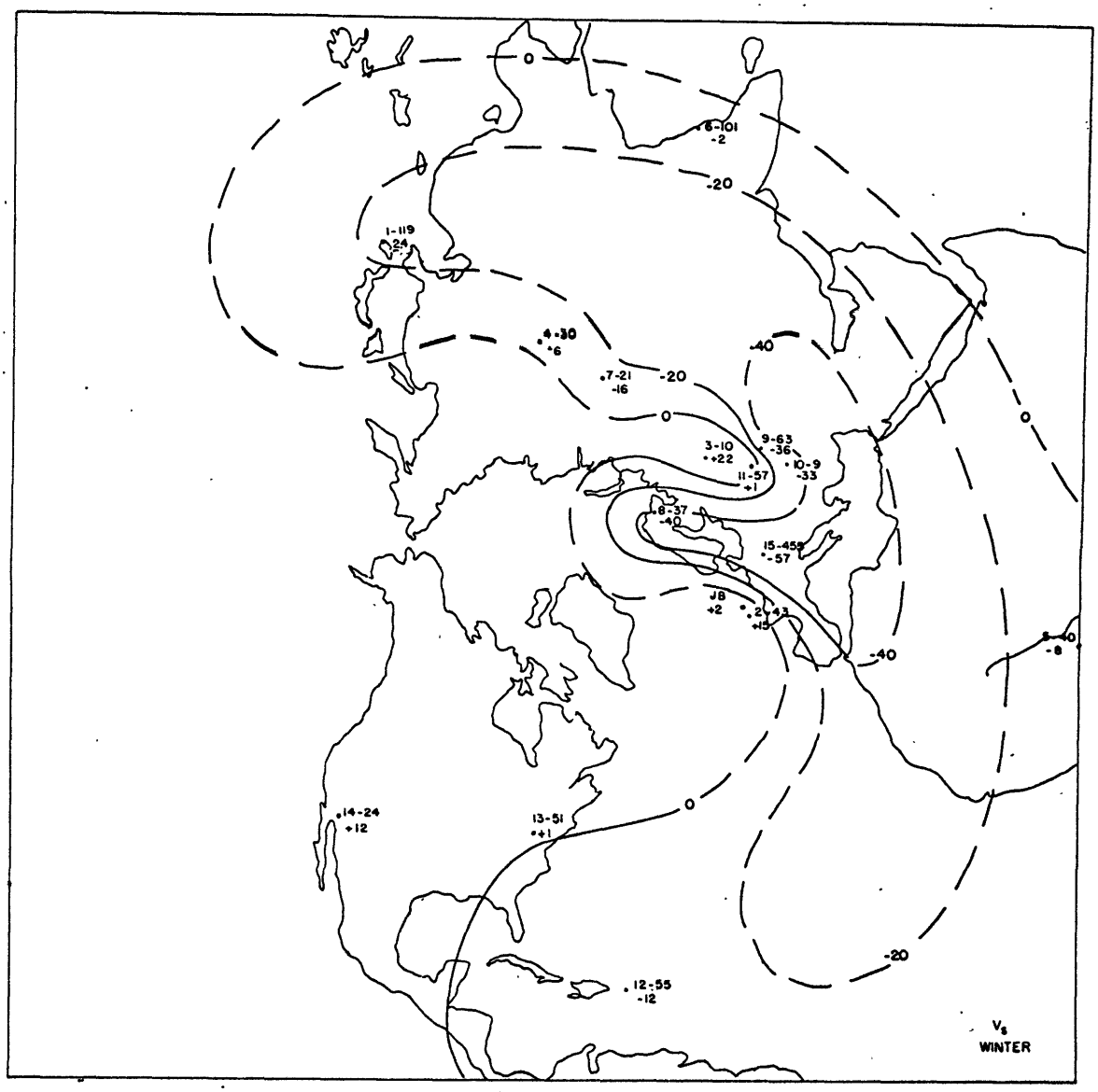

Figure 26c. Hemispheric Map of the Prevailing Meridional Winds in the Winter

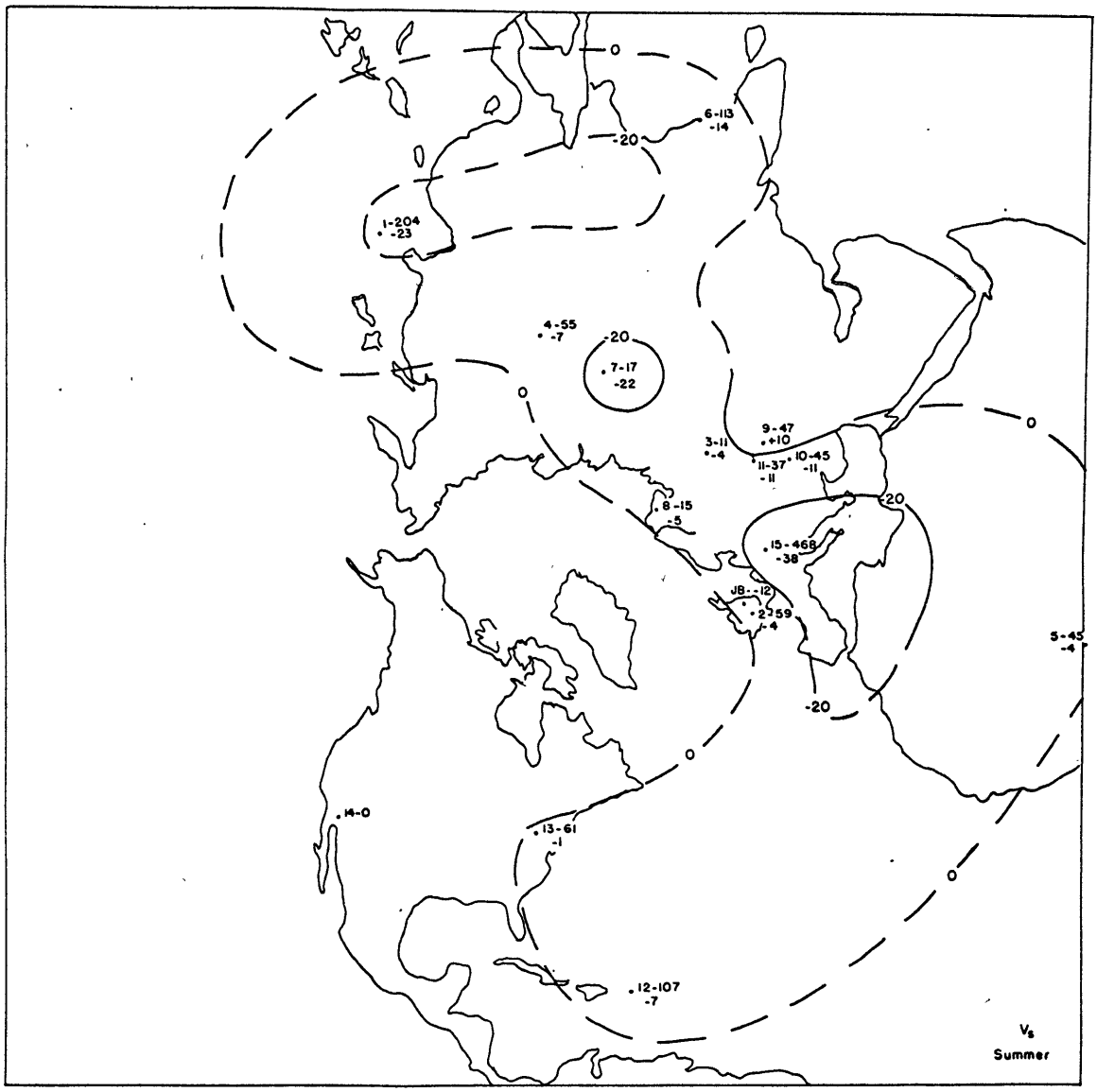

Figure 26d. Hemispheric Map of the Prevailing Meridional Winds in the Summer

CHAPTER IV. CONCLUSIONS

The data from fifteen ionospheric sounders has been used to determine the general circulation in the lower E-region. Evidence was presented to indicate that the motion determined by radio propagation techniques coincides with the neutral wind up to approximately 110 km.

The diurnal variations of the wind determined at selected stations show that the wind is fairly stable from day to day during the spring and autumn. There is considerable variability of the wind during the summer and winter. Strong tidal influence is implied from the data. A more complete analysis must be made, however, to determine the magnitude of this influence.

The height profiles of the wind show the variations with latitude throughout the day. Superimposed on the prevailing component of the zonal wind is motion that shows considerable variability throughout the day. These variable motions are the tidal oscillations. The prevailing zonal wind is generally westerly in the summer and easterly in the winter.

With due consideration for the number of stations, the hemispheric maps show the apparent existence of standing waves of low wave number in both summer and winter. The magnitude of the prevailing motion is generally greater in winter than in summer. The hemispheric maps also show that the prevailing wind is easterly in the winter and westerly in the summer.

This has been a preliminary study of the general circulation in the E-region. No definite statement may be made about the upward propagation of energy due to the limited number of observations available. Further studies are definitely needed. More observations at individual stations, such as obtained by Harnischmacher (1963), will allow the study of the momentum transports in this region, as Jones (1963) was able to do with the meteor wind data.

ACKNOWLEDGEMENTS

The writer would like to express his gratitude to Dr. K. Tsukamoto, Professor D. G. Yerg, Professor B. R. Rao, and Professor H. S. Lee for providing their data.

Special thanks are due to Professor R. E. Newell for his guidance and useful suggestions during the course of this study.

The writer would like to thank his wife, Jo-Anne Fedor, who reviewed and typed the manuscript.

BIBLIOGRAPHY

Aono, Y., K. Tsukamoto, and M. Ichinose, (Ed. Com.), 1961: IGY data of ionospheric drifts at Yamagawa in Japan. Nat. Committee for the Internat. Geophy. Coord. Sci. Coun. of Japan, December, 1961.

Axford, W. I., 1963: The formation and vertical movement of dense ionized layers in the ionosphere due to neutral wind shears. J. Geophy. Res., V. 68, 3, pp. 769-779.

Bowhill, S. A., 1956a: The fading of radio waves of frequencies between 16 and 2400 kc/s. J. Atmos. Terr. Phys., V. 8, pp. 129-145.

Bowhill, S. A., 1956b: The ionospheric irregularities causing fading of low-frequency radio waves. Scientific Report No. 89, Ionosphere Res. Lab., The Penn. St. U.

Briggs, B. H., G. J. Phillips, and D. H. Shinn, 1950: The analysis of observations on spaced receivers of the fading of radio signals. Proceed. of the Phys. Soc. of London Series B, V. 63, pp. 106-121.

Briggs, B.H., and M. Spencer, 1954: Horizontal movements in the ionosphere. Rep. on Prog. in Phys., V. 17, pp. 245-280.

Briggs, B. H., 1960: Survey of ionospheric drifts. URSI XII General Assembly, London, pp. 219-239.

Burke, M. J., and I. S. Jenkinson, 1957: Ionospheric drifts at Brisbane. Aust. J. Phys., V. 10, 3, pp. 378-386.

Charney, J. G., and P. G. Drazin, 1961: Propagation of planetary-scale disturbances from the lower into the upper atmosphere. J. Geophys. Res., V. 66, 1, pp. 83-109.

Fooks, G. F., and I. L. Jones, 1961: Correlation analysis of the fading of radio waves reflected vertically from the ionosphere. J. Atmos. Terr. Phys., V. 20, pp. 229-242.

Fooks, G. F., 1962: Ionospheric irregularities and the phase paths of radio waves. J. Atmos. Terr. Phys., V. 24, pp. 937-947.

Gossard, E. E., 1962: Vertical flux of energy into the lower ionosphere from internal gravity waves generated in the troposphere. J. Geophy. Res., V. 67, 2, pp. 745-757.

Gossard, E. E., and M. Paulson, 1964: The nighttime electron density profile through the D-region of the ionosphere in summer over the southwestern United States. Radio Science, J. Res. NBS/USNC-URSI, V. 68D, 3, pp. 265-273.

Greenhow, J. S., and E. L. Neufeld, 1961: Winds in the upper atmosphere. Quart. J. Roy. Met. Soc., V. 87, pp. 472-489.

Hargreaves, J. K., 1961: Random fluctuations in very low frequency signals reflected obliquely from the ionosphere. J. Atmos. Terr. Phys., V. 20, pp. 155-166.

Harnischmacher, E., 1963: Results of E-region drift measurements. Proceedings of the International Conference on the Ionosphere held at Imperial College, London, July, 1962, The Institute of Physics and the Physical Society, London, pp. 348-356.

Hines, C. O., 1960: Internal atmospheric gravity waves at ionospheric heights. Can. J. Phys., V. 38, pp. 1441-1481.

Hines, C. O., 1963: The upper atmosphere in motion. Quart. J. Roy. Met. Soc., V. 89, 379, pp. 1-42.

Jones, I. L., 1958: The height variation of drift in the E-region. J. Atmos. Terr. Phys., V. 12, pp. 68-76.

Jones, W. L., 1963: Energetics of the solar semidiurnal tide in the atmosphere. Scientific Report No. 2, Planet. Circ. Proj., Meteor. Dept., Mass. Inst. of Tech.

Kochanski, A., 1963: Circulation and temperatures at 70 to 100 kilometer height. J. Geophys. Res., V. 68, 1, pp. 213-226.

Lee, H. S., 1962: A statistical study of apparent horizontal ionospheric movements using 300 kc/s radio waves. Scientific Report No. 170, Ionosphere Res. Lab., The Penn. St. Univ.

Murgatroyd, R. J., 1957: Winds and temperatures between 20 km and 100 km - a review. Quart. J. Roy. Met. Soc., V. 83, 358, pp. 417-458.

Phillips, G. J., and M. Spencer, 1955: The effects of anisometric amplitude patterns in the measurement of ionospheric drifts. Proc. Phys. Soc. of London, Series B, V. 68, pp. 481-492.

Ratcliffe, J. A., 1959b: Ionizations and drifts in the ionosphere. J. Geophys. Res. V. 64, 12, pp. 2102-2111.

Ratcliffe, J. A., 1959a: The Magneto-Ionic Theory and its Applications to the Ionosphere. University Press, Cambridge.

Sales, G. S., 1960: Low frequency radio studies of apparent ionospheric motions. Scientific Report No. 131, Ionosphere Res. Lab., The Penn. St. Univ.

Sales, G. S., and S. A. Bowhill, 1962: Apparent ionospheric motion in the night-time D-region. J. Atmos. Terr. Phys., V. 24, pp. 451-465.

Teweles, S., 1963: Spectral aspects of the stratospheric circulation during the IGY. Report No. 8, 7 January 1963, Plan. Circ. Proj. Meteor. Dept., Mass. Inst. of Tech.

Yerg, D. G., 1959: An analysis of drifts of the signal pattern associated with ionospheric reflections. J. Geophys. Res., V. 64, 1, pp. 27-31.

Yerg, D. G., 1961a: Analysis of diffraction patterns on the ground caused by ionospheric irregularities. Scientific Report No. 1, Mich. College of Mining and Tech., March 1961.

Yerg, D. G., 1961b: Analysis of diffraction patterns on the ground caused by ionospheric irregularities. Scientific Report No. 2, Final Report, Mich. College of Mining and Tech., June 1961.